Electroanalysis and Raman Spectroscopy of Graphene-Modified Electrodes Influenced by the Synthesis and Transfer of the Two-Dimensional Nanomaterial

Dissertation

zur Erlangung des

Doktorgrades der Naturwissenschaften

(Dr. rer. nat.)

an der Fakultät Chemie und Pharmazie

der Universität Regensburg

Deutschland

vorgelegt von

Eva-Maria Kirchner

aus Regensburg

im Jahr 2020

Die vorgelegte Dissertation entstand in der Zeit von Februar 2016 bis Juni 2020 am Institut für Analytische Chemie, Chemo- und Biosensorik an der Universität Regensburg.

Die Arbeit wurde angeleitet von Prof. Antje J. Bäumner und Dr. Thomas Hirsch.

Promotionsgesuch eingereicht am: 10.06.2020

Prüfungsausschuss:

Vorsitzender: Prof. Dr. Oliver Tepner

Erstgutachterin: Prof. Dr. Antje J. Bäumner

Zweitgutachter: Prof. Dr. Frank-Michael Matysik

Drittprüfer: Prof. Dr. Werner Kunz

DANKSAGUNG

Table of Contents

Declaration of Collaborations

Thomas Hirsch (T.H.) and Antje Bäumner supervised the research. T.H. and the author conceived and designed this work. The author prepared all samples and performed all measurements, except those mentioned in detail. Data evaluation was carried out solely by the author. Some of the results were obtained together with other researchers. In accordance with § 8 Abs. 1 Satz 2 Punkt 7 of the "Ordnung zum Erwerb des akademischen Grades eines Doktors der Naturwissenschaften (Dr. rer. nat.) an der Universität Regensburg vom 18. Juni 2009", this section gives information about these collaborations.

(Chapter 1)

Together with T.H., the author conceived this review. The literature survey was performed by the author as well as writing the manuscript. T.H. revised the manuscript and is the corresponding author.

(Chapter 3)

This study was conceived and designed by T.H. and the authors. The experimental work was carried out by the author solely, with contributions from Korbinian Pürkhauer who performed AFM measurements and Christian Baumgartner who has done the SEM study. The manuscript was written by the author and revised by T.H., who is the corresponding author.

1. Recent Developments in Carbon-Based Two-Dimensional Materials: Synthesis and Modification Aspects for Electrochemical Sensors

1.1   Abstract

This review (162 references) focuses on two-dimensional carbon materials, which include graphene as well as its allotropes varying in size, number of layers and defects, for their application in electrochemical sensors. Many preparation methods are known to yield in two-dimensional carbon materials which are often simply addressed as graphene, but which show huge variations in their physical and chemical properties and therefore on the sensing performance. The first section briefly reviews the most promising as well as the latest achievements in graphene synthesis based on growth and delamination techniques, such as chemical vapor deposition, liquid phase exfoliation *via* sonication or mechanical forces, as well as oxidative procedures ranging from chemical to electrochemical exfoliation. Two-dimensional carbon materials are highly attractive to be integrated in a wide field of sensing applications. Here, graphene is examined as recognition layer in electrochemical sensors like field-effect transistors, chemiresistors, impedance-based devices as well as voltammetric and amperometric sensors. The sensor performance is evaluated from the material's perspective of view and revealed the impact of structure and defects of the 2D carbon materials in different transducing technologies. It is concluded that the performance of 2D carbon-based sensors is strongly related to the preparation method in combination with the electrical transduction technique. Future perspectives address challenges to transfer 2D carbon-based sensors from the lab to the market.
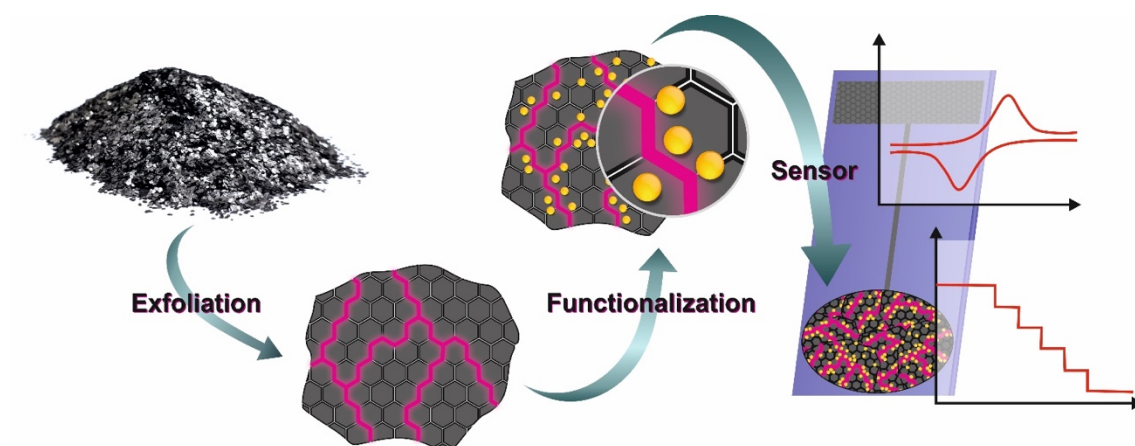
Figure 1.1: Schematic overview from synthesis and modification of two-dimensional carbon materials to sensor application.

This chapter has been published.

Kirchner EM, Hirsch T, (2020) Recent Developments in Carbon-Based Two-Dimensional Materials: Synthesis and Modification Aspects for Electrochemical Sensors, Microchim. Acta, 187, 441.

Author contributions:

This manuscript is authored by Eva-Maria Kirchner (EMK) and Thomas Hirsch (TH). TH and EMK conceived this review. The literature survey was performed by EMK as well as writing the manuscript. TH revised the manuscript and is the corresponding author.

1.2 Introduction

Ten years ago, J. Justin Gooding and Filip Braet have asked, "Should you use nanotubes or graphene as carbon nanomaterial in biosensors?" [1], motivated by numerous publications on carbon nanotubes in biosensing and the start of the graphene hype, which was discovered as a single flake about 15 years ago [2]. One decade ago, only a few papers using 2D carbon materials have been published and research on this topic was in the early stage where all those interesting properties coming with this material have been described; some of them even outperforming the ones known for carbon nanotubes (CNTs). Today, carbon-based nanomaterials have become one of the dominating materials in many sensor applications. A web-of-science survey revealed up to now more than 2.200 publications related to nanomaterial and sensing and roughly about 50% of them deal with carbon nanomaterials. On a closer look, about half of the carbon materials are from the so-called graphene family. These impressive numbers raise the question why 2D carbon nanomaterials got so popular in sensing that one finds almost three times more publications with this class of materials compared to CNTs. Graphene, ideally consisting of a honeycomb structured monolayer of sp^2-hybridized carbon atoms, is characterized as an almost transparent, chemically inert material, exhibiting high carrier mobility, as well as excellent electric and thermal conductivity [3,4]. These properties are often mentioned together with a high surface-to-volume ratio as motivation why 2D carbon nanomaterials are used in (bio)analytical applications, especially for sensor development where also costs of materials come into play. In electroanalytical applications, carbon-based electrodes outperform many other materials, such as noble metals, because they are less prone to surface fouling and they are known for a wider electrochemical potential window ranging from -1.5 to +1 V *vs.* Ag/AgCl [5-8].

For sensor development, it is desired that the electrode fabrication can be performed in an easy way, allowing mass production, which is not in coincidence with the preparation of individual graphene flakes from graphite by the famous scotch tape method [2]. Many other manufacturing methods have been developed, and it turned out by sophisticated material characterization processes that those two-dimensional carbon materials are

somehow similar to graphene, even when they contain many defects compared to an ideal graphene flake [2]. In the last years, the number of exfoliation protocols to obtain 2D carbon materials has risen, mostly motivated by the goal to produce a material, which comes as close as possible to a perfect graphene but to be accessible in large scale. It became clear, as for every nanomaterial, that intrinsic material properties with regard to the exfoliation process are differing a lot due to their flake morphology, which are varying in the size of the flakes, the amount of defects, the number of layers (mono-, bi-, few-, multilayers), and the doping ratios [9,10]. All the structural and chemical variations introduced during the processing of such materials change the intrinsic material properties. This leads to the question of how different exfoliation methods affect the properties of electrochemical sensors based on 2D carbon nanostructures, which is evaluated in this review.

1.3   Synthesis and Functionalization

Preparation techniques for 2D materials are often classified either bottom-up or top-down approaches which are capable to create nanomaterials with a varying distribution of lattice defects. These include vacancies, grain boundaries, oxygen functional groups, dangling bonds, and Stone-Wales defects resulting in a certain degree of functionalization. Excellent reviews are published on the high diversity of preparation methods to yield two-dimensional materials [10-14]. With regard to the preparation method, the intrinsic characteristics of 2D materials can be chosen, as well as parameters such as the potential for scale-up-synthesis and processability, which influence their use as sensor material [10,13,15-17]. In the following, the most important fabrication techniques and functionalization strategies are critically evaluated.

1.3.1. Chemical Exfoliation

The chemical synthesis is the widest distributed technique to obtain graphene, ensured by the simple instrumentation and the advantage to obtain aqueous dispersions of 2D carbon nanomaterials. Graphene oxide (GO) is synthesized by treating graphite with a strong acid and an oxidizing species, which delaminates the graphite crystal structure

introducing oxygen functional groups. This material can be reduced in many ways to reduced graphene oxide (rGO), which is widely applied as sensor layer. Brodie paved the way for the graphene oxide synthesis already in 1859 by oxidizing graphite with potassium chlorate and fuming nitric acid [18], followed by Staudenmayer around 40 years later who modified Brodie's synthetic route slightly by stepwise oxidation of the graphite in a mixture of sulfuric acid and nitric acid. Potassium chlorate was added in small portions to avoid explosive reactions in a more acidic environment [19]. In 1957 Hummers and Offeman established a safer production method for GO. Graphite was oxidized by the addition of $KMnO_4$ and $NaNO_3$ in concentrated sulfuric acid [20]. This synthetic route is still applied nowadays by slight modifications with additional amounts of oxidizing agents for an increased oxidation rate of the material [21,22]. The high degree of oxygen-containing functional groups distributed along the surface of the GO flake leads to an electrically insulating material. The interlayer spacing of the sheets is increased by the oxidation of graphite with oxidizing agents forming epoxy, hydroxy, and carboxyl groups [23]. Oxidative cleavage cause in-plane voids and cracks at the edges [24]. The subsequent reduction of GO eliminates the oxygen residues, restoring the sp^2 hybridized carbon system and its conductivity. Figure 1.2 indicates that the reduction step cannot remove structural defects of the material, which originate from the oxidation process [24]. Reduced graphene oxide is classified as highly defective material. The harsh oxidation and subsequent reduction process introduce structural defects as well as oxygen moieties [25].

Graphene oxide   **Reduced graphene oxide**
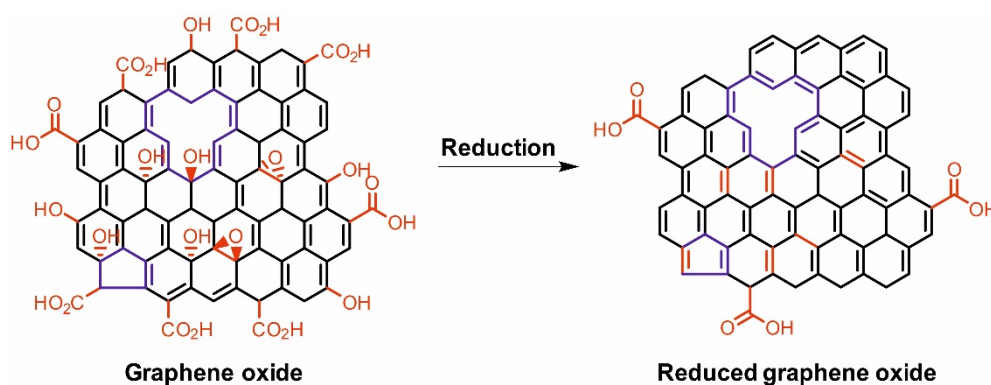
Figure 1.2: Chemical structure of highly defective graphene oxide. The reduction process leads to a restored sp^2 hybridized carbon lattice with oxygen moieties at the edges of the flakes. The elimination of structural defects within the material is not feasible.

The thermal treatment is the simplest way to reduce GO [26-28]. Many of the thermal reduction steps to form rGO are performed hydrothermally in an autoclave to reduce the precursor material under high temperature and pressure [22,29,30]. A chemical reduction, mainly by hydrazine, ascorbic acid, sodium citrate, hydroiodic acid, or sodium borohydrate is also quite common [29,31-33].

An advantage of the aqueous dispersed rGO compound is the facile transfer mechanism for chemically synthesized 2D materials [13,30,34-36]. Spin-casting requires an ink-formulation to ensure a fast evaporation of the solvent as well as the application of ideal processing parameters in order to form a coherent, homogeneous film [37]. Drop coating from aqueous dispersion seems easier but is challenging in resulting homogeneous films.

Chemical synthesis of 2D materials provides a large degree of freedom to adjust process parameters. So far, these options have not been fully exploited, *e.g.*, by the design of 2D materials with a controlled number of defects. Such materials might be of great interest in sensing applications. It is observed for surface functionalization by nanoparticle (NP) deposition that the structural irregularities act as nucleation sites for the particles [35]. Defects allow the introduction of bandgaps, which might be beneficial in field effect transistors [38].

In comparison to chemical synthesis, which needs in total several days to proceed, the exfoliation can be speeded up to hours by applying a strong electrical potential to graphite electrodes. Upon application of an electrical voltage, solvated ions of the electrolyte intercalate within the graphite working electrode, weakening the interlayer forces and driving the individual flakes apart, which are released into the electrolyte [39,40]. The application of a negative potential to the graphite electrode in organic medium force positively charged ions between the layers of the bulk material, which is called cathodic electrochemical exfoliation. The applied voltage, size of the anions, and the type of solvent do not only affect the intercalation process, but also have an impact on the quality of processed material. The cathodic electrochemical exfoliation is either carried out by intercalating Li$^+$ ions or quaternary ammonium salts in organic solvents [41-43]. Anodic exfoliation is performed in aqueous solution, where anions intercalate between the graphite layers upon electrolysis, triggering the delamination (Figure 1.3).

Parvez *et al.* extensively studied the exfoliation efficiency of various inorganic salts (NH_4Cl, Na_2SO_4, $(NH_4)_2SO_4$, $NaNO_3$, K_2SO_4 and $NaClO_4$). Sulfate yields large graphene flakes with a lateral size up to 44 µm (>85% with ≤3 layers) and no exfoliation was observed for ClO_4^-, Cl^- and NO_3^- [44].
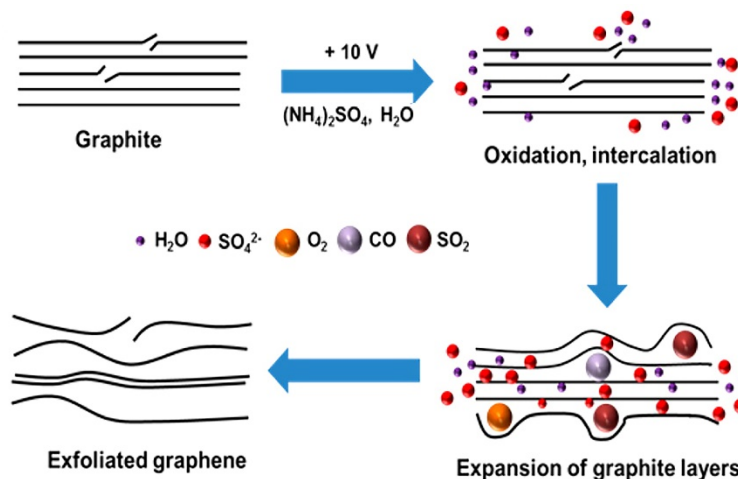
Figure 1.3: Scheme of an anodic electrochemical exfoliation process of graphite. Oxidation of water causes the formation of oxygen containing species attacking the edges and grain boundaries of graphite promoting the SO_4^{2-} intercalation and exfoliation of graphene layers. Reprinted with permission from [44]. Copyright 2014 American Chemical Society.

Raman spectroscopy, a versatile tool for non-destructive optical characterization of 2D materials, revealed that the material got oxidized during the exfoliation procedure exhibiting major structural defects [45]. The electrochemical exfoliation procedure is not that widely integrated into sensor preparation so far. A reason might be that this method was only recently developed. Several advantages such as less labor-intense, easier control of flake size, and defects by the ideal choice of intercalating salts and electrochemical potentials let one expect that electrochemical exfoliation might become more attractive in the future.

1.3.2. Chemical Vapor Deposition

Chemical vapor deposition (CVD) gained its popularity due to the possibility to grow large high-quality 2D carbon materials [46]. The growth mechanism of this bottom-up technique depends on the metallic catalyst triggering the layer deposition. There are two

prominent representatives of catalytic support, Ni and Cu, which differ in the deposition mechanism as highlighted in Figure 1.4. Generally, the growth of graphene on Ni is hardly controllable. The high solubility of C atoms in Ni can lead to the formation of CVD graphene (cvdG) domains with different thickness resulting in an inhomogeneous layer. In contrast to Ni, the growth on Cu bases on a self-limiting surface adsorption process, attributed to the low solubility of C atoms in Cu [47-49]. The decomposed carbon atom nucleates on top of the metallic surface forming ordered crystals subsequently growing a two- dimensional carbon layer [47,49,50]. The issue of multilayered cvdG grown on Ni seemed to be solved by cvdG on Cu substrates on the price of grain boundaries and wrinkles along its surface [49-51], which might affect the physical properties of the material and therefore the sensing performance.
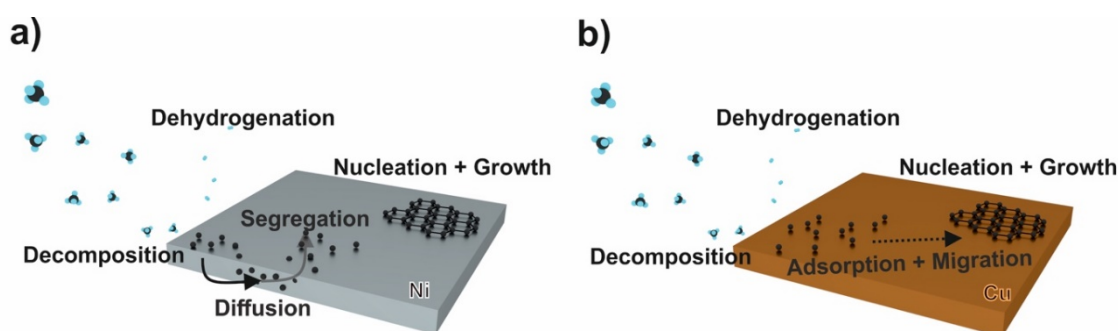
Figure 1.4: Schematic illustration of the cvdG growth process on a carbon soluble metal support (Ni) where the hydrocarbon molecules, *e.g.*, methane, decompose and the C atoms diffuse into the bulk of the metal. The C atoms segregate upon supersaturation, nucleate, and grow a carbon layer (a). On a Cu substrate, the hydrocarbons decompose, as carbon poorly segregates in copper. The adsorbed adatoms migrate along the surface, nucleate, and form the graphene layer (b). As depicted in detail by Muñoz and Gómez-Aleixandre [52].

Apart from the deposition, the layer transfer to a substrate of choice is still challenging for 2D carbon materials prepared by CVD. Etching of the metallic substrate increases the cost and introduces ionic impurities [49,53]. A post-introduction of defects can be caused by electrochemical or mechanical delamination [54]. The films are prone to the introduction of cracks and wrinkles, which lead to a deterioration of the physical properties [55]. In contrast, a systematic introduction of defects by transferring cvdG, specifically to form a wrinkled layer, was found to induce a bandgap [56]. Besides the transfer, also a modification might induce defects within the CVD grown layer. To

establish an NO_2 senor, a pulsed laser deposition of ZrO_2NPs- or AgNPs on cvdG did not only decorate the carbon layer but also introduce defects [57].

Even though, research aims for ongoing improvement of the growth mechanism to achieve large-area films of high-qualitative graphene material, mostly for optoelectronic applications such as displays, it became apparent that there is no need for the growth of large films in sensing applications, since most electrochemical sensors operate with small electrodes in the mm^2 range or even smaller. Moreover, the preparation method still is time-consuming and compensates a lot of energy due to the high operating temperature of around 1000 °C. To circumvent the need of a metallic catalyst requiring a subsequent transfer step as well as to reduce the deposition temperature, the growth of graphene on non-conductive materials, such as SiO_2, was developed [58]. Figure 1.5 schemes the growth procedure, which does not result in a horizontal growth of the carbon material, but deposits vertically oriented graphene flakes, which additionally enhances the surface area of the carbon layer. In terms of larger surface-to-volume ratio, such vertically aligned carbon 2D materials should outperform horizontally aligned carbon layers in sensor applications which rely on a large specific surface area.
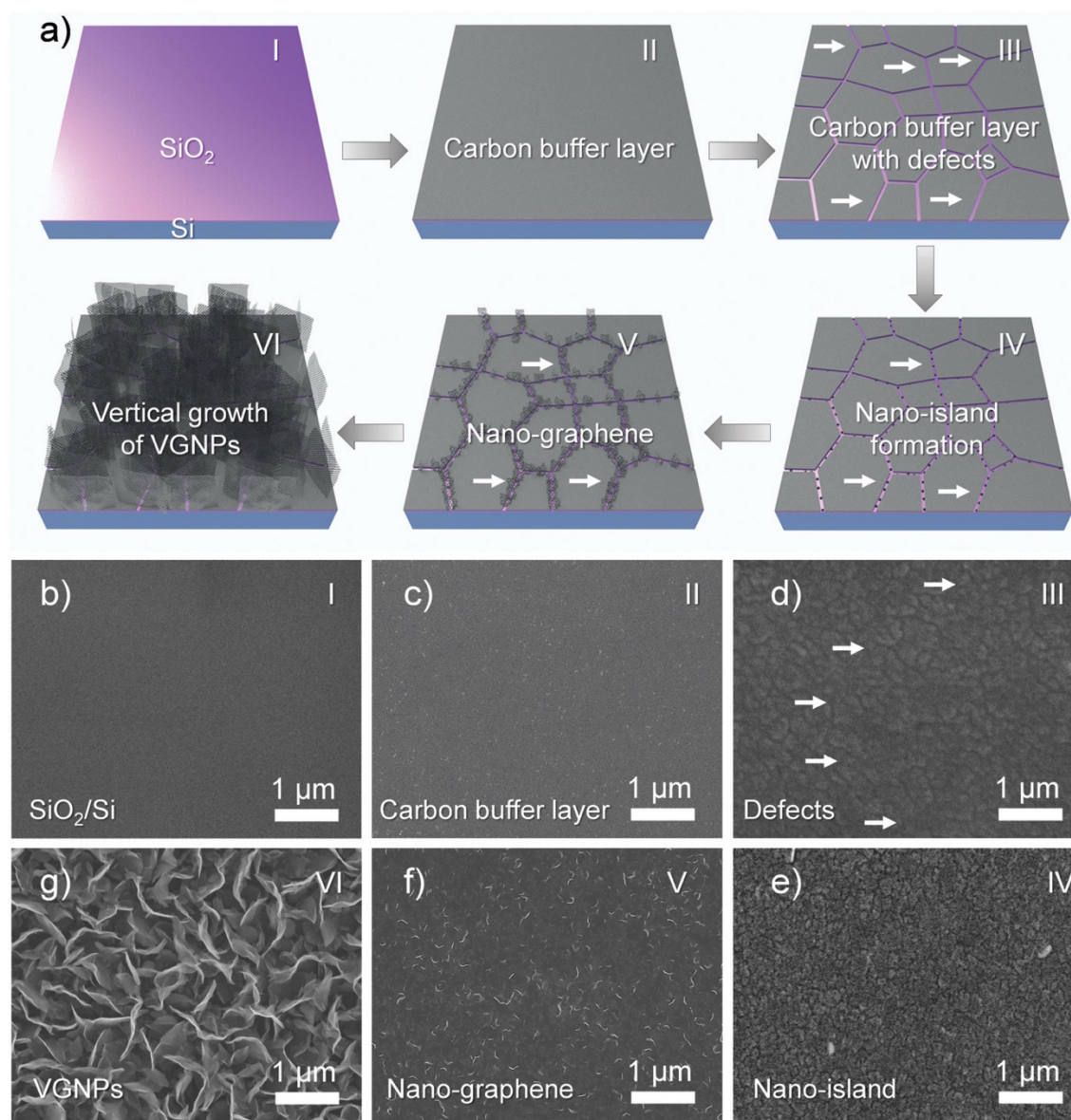
Figure 1.5: Illustration of the preparation process of graphene derived by plasma assisted CVD growth (a). The numbers (I-IV) scheme the corresponding SEM images (b-g). The SiO₂/Si support (I, b) was modified by depositing a carbon buffer layer (II, c), followed by the introduction of defects within the material (III, d) forming nano-islands (IV, e). At the edges of the nano-islands, the growth of graphene is initiated (V, f), resulting in the vertical growth of graphene flakes (VI, g). Reprinted from [58] with permission from The Royal Society of Chemistry.

1.3.3. Liquid Phase Exfoliation

An alternative synthesis routine was investigated to obtain high qualitative 2D materials dispersed in liquid medium. This method can be applied to numerous bulk crystals, yielding colloidal stable dispersions (Figure 1.6), which are supposed to facilitate the processability of the material and a scale-up in liter-sized batches is possible.
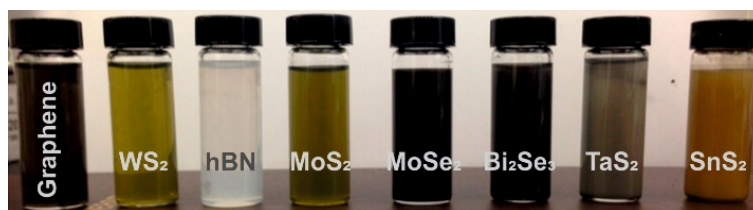
Figure 1.6: Variety of liquid-phase exfoliated 2D materials dispersed in appropriate solvent. Reprinted with permission from [59]. Copyright 2015 American Chemical Society.

In contrast to chemical synthesis, either by oxidizing graphite under harsh conditions yielding GO, the liquid phase exfoliation (LPE) takes advantage of a direct, mild exfoliation of the bulk material in liquid medium [60,61]. It yields materials free of defects within the basal plane. This method is solely based on the application of ultrasound or shear forces and does not need further sophisticated equipment. Liquid phase exfoliation imposes three steps. First, the weak interlayer van der Waals forces must be overcome by introducing energy during the exfoliation procedure. Second, the exfoliated nanosheets have to be stabilized against reaggregation by choosing an appropriate solvent or surfactant. Third, the purification and size selection of the obtained batch of exfoliated layered material. The last step is necessary to get rid of unexfoliated material as well as to distinguish fractions with a certain size and number of layers [62].

Coleman *et al.* pioneered the field of LPE [63]. The exfoliation base on sonication, which induces the formation of cavitation, generates micro jets and shock waves (Figure 1.7). The resulting tensile stress and shear stress cause the delamination and fragmentation of the bulk material [12,64,65]. It is reported that the material preparation based on shear forces induced by rotating blade mixers is more applicable in industrial-scale production compared to ultrasound [66]. The exfoliation time for sonication requires a few hours, whereas shear exfoliation consumes more time to yield the same amount of 2D material. Nevertheless, larger volumes in liter-range can be produced by shear exfoliation contrary to ultrasound, which yields fractions of less than 0.5 L [62].
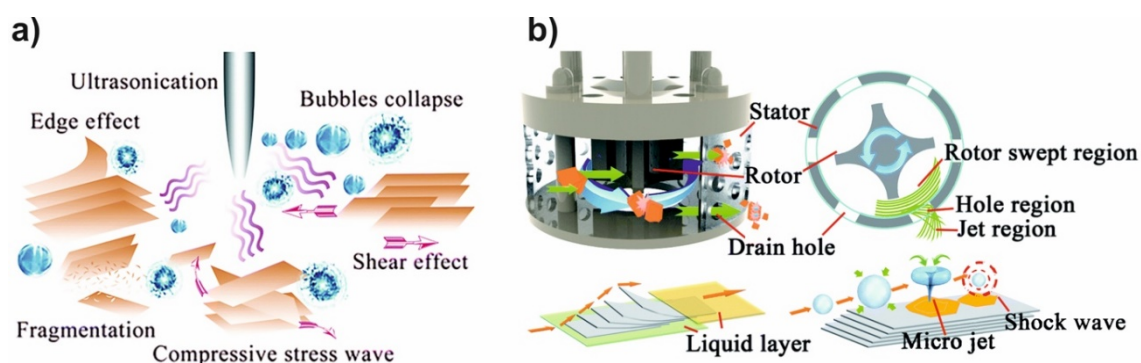
Figure 1.7: Scheme of liquid phase exfoliation strategies based on ultrasound (a) [64] or shear forces (b) [65]. Reproduced from [64] with permission from the PCCP Owner Societies. Adapted from [65] with permission from The Royal Society of Chemistry.

The choice of the solvent is the key in terms of production. Apart from the effective delamination of the material, it is mandatory to keep the dispersion colloidal stable. This can be achieved when the solvent and delaminated material match in surface energies and possess similar Hansen solubility parameters [67,68]. High boiling point solvents like N,N-dimethylformamide (DMF) and N-methyl-1-pyrrolidone (NMP) were found to be versatile dispersants [69-71]. One might assume that the simple LPE exfoliation is an excellent method to produce almost defect-free 2D materials without any additional impurities, but this comes for the price of delaminated flakes with inhomogeneous morphology. A reproducible preparation of defined mono- to multi-layered flakes with varying flake size is challenging.

Liquid-phase exfoliation is gaining more interest due to the timesaving, up-scalable exfoliation, which yield materials mostly unchanged in their chemical structure ranging from dispersed monolayers to few-layers [72]. So far, only a very limited number of sensor application make use of 2D materials prepared by LPE. One reason might be that the solvents which warrant colloidal stability are hardly removed by washing steps or thermal treatment [73], which may cause a deterioration of electronics and sensing devices.

In contrast to many noble metal, 2D carbon materials have been reported as stable against electrode fouling. This was demonstrated by copper electrodes which were partly covered by cvdG. Even for inner sphere redox couples, no apparent fouling was observed [74].

1.3.4. Functionalization

The high surface-to-volume ratio and large sp² hybridized carbon system are key properties of 2D carbon materials to be integrated into a sensor device. Analyte interaction can take place *via* π-interaction of the extended aromatic carbon system or by hydrogen bonding with the oxygen residues present within and at the edge-planes of the graphene flakes. The introduction of additional recognition elements is highly desired to enhance the sensitivity and selectivity of the carbon material. Georgakilas *et al.* published detailed reviews on the functionalization of graphene, covalently and non-covalently [75,76]. Therefore, the most common modification routines are only briefly introduced, with emphasis on their use in electrochemical sensors. Non-covalent modifications take place *via* π-stacking, van der Waals forces, ionic interactions as well as due to hydrogen bonds [76]. These functionalization strategies are less selective, but the sp² hybridized carbon lattice remains intact. Intermolecular interactions with materials exhibiting a π-system are feasible [75,77-79]. Especially porphyrins are promising, as they exhibit a metallic core, which can mimic enzymatic-like reactions or induce a change in the physical properties of graphene resulting in an opened bandgap, potentially tuning its intrinsic characteristics [80,81]. One has to be cautious as there is no bandgap control upon non-covalent functionalization, which might be used in maximizing the detection sensitivity by minimizing the electrical noise [76]. Pyrene derivatives have been reported as non-covalent linker between graphene and other (bio-)molecules, which act either as probe or as target [32,82,83]. The π-interaction of graphene with carbon nanotubes enables the processability of the former hydrophobic carbon wires in aqueous solution [84]. The carbon surface is decorated by deposition of metallic nanoparticles, *i.e.*, noble metals. Preferably, defective graphene materials are used as support, as it provides numerous nucleation sites for the deposition of the metallic nucleus growing to a particle [30,35,84-87]. Covalent modifications were initiated by anodization of graphene layers to introduce more oxygen functionalities or by a radical reaction, forming a diazonium salt that attacks the sp² hybridized carbon lattice [71,88]. Oxygen functionalities present at the surface of defective graphene compounds offer binding sites for linkage *via* carbodiimide coupling [77]. The covalent attempt is often found for biomolecular modified graphene compounds, as the amide bonds

combine with the oxygen residues of graphene. Ultra-high pressures allow to tune the doping ratio of graphene surfaces [89]. The reactivity towards oxygen was shown to be enhanced by charge-doping under photothermal heating applying either positive or negative pulsed back gate voltages causing either electron doping or hole doping. Back gating without photothermal treatment did not result in a doping effect. The charge-doped-increased reactivity poses as an alternative to chemical-based catalysis, which can potentially enhance and control the chemical reactivity of a material [90]. A non-destructive functionalization technique is the creation of stacked van der Waals heterostructures. Structural relatives of two-dimensional graphene, *e.g.*, transition metal dichalcogenides or hexagonal boron nitride, act as building blocks to tremendous possibilities of material design tuning the physical properties of the materialistic compounds [91,92].

1.4   Sensors

The direct interaction of graphene-like materials with analytes or ease of functionalization as well as the tenability to obtain materials either of metallic, semiconducting, or insulating character is highly attractive for electrochemical sensors. Excellent reviews focus on the sensing capabilities of 2D carbon materials towards numerous analytes [93-97]. A critical evaluation of the effect and requirements for 2D carbon materials in different types of electrochemical sensors is missing so far and presented in the following.

1.4.1. Field-Effect-Transistors and Chemiresistors

In field-effect-transistors (FET), semiconducting 2D carbon materials act as channel between source and drain electrode applying a potential of the gate electrode. Two sensing types are accomplished, either back-gating or top-gating, also known as solution-gating. The interaction of the analyte with the 2D carbon material changes its charge carrier density due to electric charge distribution making this technology capable to develop rapid, miniaturized sensors [98]. A chemiresistor is similar to the FET. The detection principle remains the same, but it omits the gate electrode. The slightly more

complex electronics of FETs compared to chemiresistors enable better sensitivity by tuning the conductance of the material by controlling the gate voltage. Both techniques can easily be adapted for commercialization. 2D carbon nanomaterials are preferably used due to excellent chemical stability and electric field sensitivity (Figure 1.8) [98].
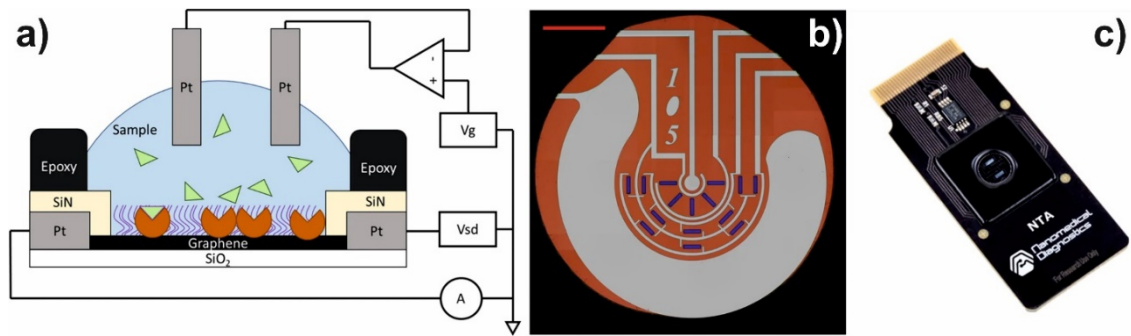
Figure 1.8: Scheme of a graphene field effect transistor with symbolized proteins linked to the 2D carbon material (a). The entire sensor surface of a commercial sensor showing five sensing spots with a red scale bar of 1 mm is depicted in (b). A photograph of the fully integrated graphene-based senor chip from Nanomedical Diagnostics is shown in (c). Adapted from [98]. Copyright (2019) Springer Nature.

In a graphene FET (GFET), the material is accessible to surface functionalization as the channel is partially integrated into the device and the electrical double layer allows operation at low gate voltage with high conductivity. Monolayer graphene may be superior compared to multi-layered graphene as the conductance is improved. This is demonstrated by a DNA sensor, where the probe DNA was coupled to monolayer graphene *via* a pyrene butyric N-hydroxysuccinimide ester showing an outstanding limit of detection (LOD) of 25 aM for 24 mer target DNA [82]. A FET targeting at DNA, based on multi-layer graphene, was found to detect a 42 mer target DNA down to 10 fM. Here, graphene exfoliated by ultrasonication in DMF was used as channel material. The fabrication of the transistor is rather complicated. The substrate needs to be modified by glutaraldehyde and LPE graphene was drop-coated on top of the surface. The formation of a continuous film of carbon 2D material required a two times repetition [99]. To enhance the surface area, rGO was drop-casted onto a substrate to be used as channel material, providing a rough carbon layer. A peptide nucleic acid (PNA) – DNA hybridization FET was accomplished, by attaching the PNA by π–interaction of a pyrene-linker to the rGO. At constant bias voltage (V_{ds} = 0.1 V) the highly selective sensor

showed a LOD of 100 fM for a 22 mer DNA strand [32]. These three examples in DNA sensing based on FET transduction show that a lower number of defects and a lower number of layers achieve slightly better detection limits. The superior conductivity of the material outperforms the enlarged surface area by improved signal-to-noise ratios.

On the other hand, defects are reported to enhance the sensitivity. This was demonstrated for a glucose sensor by fabricating a graphene mesh *via* CVD on a copper foil where certain areas were blocked by silica spheres [100]. The edge defects can be used to link the enzyme glucose oxidase (GOx) to the carbon material improving the charge transfer. Compared to the same sensor with cvdG, the sensitivity was enhanced from -0.37 mV mM^{-1} to -0.53 mV mM^{-1} for the graphene mesh. A similar effect was reported, when it was discovered that certain graphene-based pH sensors can exceed the theoretical maximum Nernst limit of 59 mV pH^{-1} in sensitivity. This was also attributed to defects, which allow in addition to the electrostatic gating effect a direct transfer of the charge carriers to the 2D carbon material [101].

Disease-related small marker molecules like glucose [100], dopamine [87], urea [102] or environmental-related parameters such as 17β-estradiol [103], pH [104], heavy metal ions [105], or chlorine [106] have also be determined by GFETs. Selectivity can be achieved by using a differential measurement of two differently modified GFETs as it is illustrated in Figure 1.9. This can easily be realized without complicating the fabrication process and due to the miniaturized size of GFETs, this does not affect the total size, the sample consumption, or the need of any complex electronics.
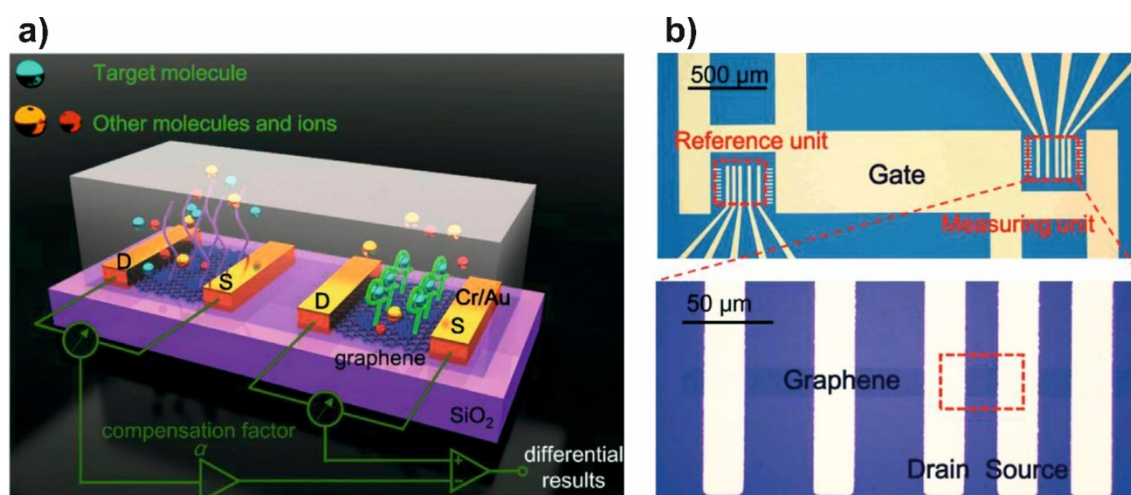
Figure 1.9: Scheme of a combination of two aptamer modified GFETs allowing *via* differential measurement to distinguish between analyte binding and non-specific binding (a). Microscopic image of the electrode layout (b). Reprinted with permission from [103]. Copyright (2019) Elsevier.

In general, cvdG is the material of choice in terms of miniaturization and mass production. Even when mass production still suffers from defects, originating of polymer contamination, affecting 44.2% of all chips [98], this material is easier to handle compared to carbon nanotubes or solvent dispersed carbon 2D materials in small dimensions. Transferred monolayers can be further etched by using masks in combination with oxygen plasma.

One of the rare exceptions of using rGO in FETs was reported by the group of Wolfgang Knoll. They report on a layer-by-layer (LbL) assembly of urease and polyethyleneimine on rGO and exploit the pH dependency of liquid-gated GFETs when detecting urea [102]. The LbL technique was chosen to neither disrupt the functionality of the biomolecule [107] nor to damage the sp^2-hybridization of the graphene lattice [108]. Reduced GO is advantageous for pH sensing due to its defective structure, which allows a change in the surface charge density and the electric double layer when pH is changing, causing additional electrostatic gating effects [109].

Graphene FETs have also been reported as a platform for immunosensors, *e.g.* to determine emerging pathogens such as coronavirus 2 (SARS-CoV-2) (Figure 1.10). Graphene, as supporting layer, equips the FET with a highly conductive material providing a large surface area to enable low-noise detection of the virus. A SARS-CoV-2 spike

antibody modified with a pyrene linker was assembled to cvdG by π-stacking. The sensor was highly sensitive for SARS-CoV-2 in clinical samples as well as selective compared to Middle East respiratory syndrome coronavirus (MERS-CoV). The detection limit is 1 fg mL^{-1} for the SARS-CoV-2 antigen protein. The sensor proved to be successfully applied in clinical diagnosis as nasopharyngeal swab specimen from COVID19-patients and healthy persons were investigated [110].
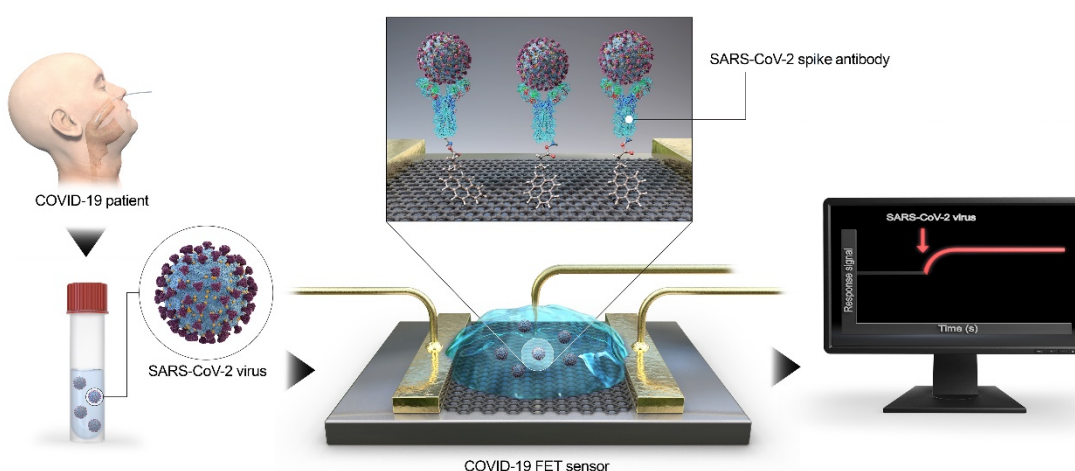
Figure 1.10: Schematic operation procedure of the COVID-19 FET using graphene as channel material, modified by 1-pyrenebutyric acid N-hydroxysuccinimide ester *via* π-stacking, coupling the SARS-CoV-2 spike antibody. Reprinted with permission from [110]. Copyright (2020) American Chemical Society.

Chemiresistors are extremely popular in gas sensing. Here 2D carbon materials can add additional value by their high affinity to gasses, together with excellent conductivity and catalytic effects. Figure 1.11 shows a measurement device with an array of chemiresistors recording the change of conductance in presence of $(NH_3)_{gas}$ under different environmental conditions, which is enhanced by the recognition elements, cobalt meso-arylporphyrins [111].
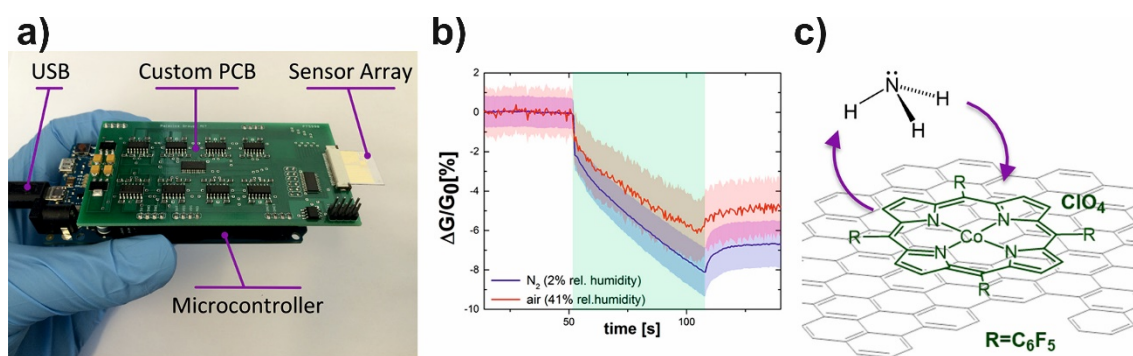
Figure 1.11: A measurement device with implemented sensor array (a), recording the change of conductivity upon exposure to gaseous NH_3 under varying environmental conditions (b). The sensitivity is enhanced by graphene functionalized with cobalt meso-arylporphyrins, which interact with the analyte (c). Reprinted with permission from [111]. Copyright (2018) American Chemical Society.

The high operating temperatures (often >200 °C) are one of the major drawbacks in gas sensing with semiconducting metal oxides, which can be overcome. Ammonia is one of the most frequently studied analytes, as it is harmful to humans already at very low concentrations. The threshold concentration is 25 ppm for an exposure time of 8 h [112]. Besides safety issues, ammonia is also known as health marker in breath or to monitor food quality [113]. Graphene oxide reacts to ammonia with functional groups, accompanied by a decrease in its conductivity, which is usually attributed to p-doping of physically adsorbed oxygen. To introduce selectivity, several functionalization strategies have been studied. The most promising are phthalocyanines, especially with Cu as central metal, to be used in breath analysis [114]. A high selectivity was found for many volatile organic compounds (VOCs) and what is more, the combination of GO with Cu tetra-β-amine-phthalocyanines strongly reduces the cross-sensitivity to humidity. Humidity is one of the major interfering substances when it comes to the quantification of gases at room temperature. For low relative humidity (r.h.) (<30%), water adsorbs on the 2D material's surface and acts as an electron acceptor, which increases the electrical conductivity. When r.h. gets larger, the water molecules adsorbed on the sensor surface can be ionized, H_3O^+ is formed, which acts as charge carrier. In such cases, both electrical and ionic conductivity will be enhanced, and the sensor is interfered. Therefore, the choice of the 2D carbon material has an impact on sensitivity as well as on selectivity. The complexity in the surface chemistry of 2D materials decreases in the order of GO < rGO < LPE graphene < cvdG. In the same order, the conductivity of the material

increases. A large variety in surface chemistry might be attributed to many binding sites, either for adsorption of the gas itself or for easy modification with metal or metal oxide nanoparticles, which further increase the surface area, number of binding sites, binding affinities, or even may introduce electrocatalytic effects. Table 1.1 summarizes the recent achievement of ammonia sensors operated at room temperature in the order of the carbon materials used. A remarkable short response and recovery time of few seconds only was found when using rGO in combination with silver nanoparticles [115] or SnO_2 nanorods [116]. This might be ascribed to the catalytic effects of Ag_2O and the SnO_2 surface of the particles/rods with generated radicals, which are known for a fast reaction. In comparison of silver nanoparticle modified 2D carbon materials, a huge difference in the range of detection is found for cvdG [117] and rGO [115]. This can be attributed to the smaller metallic particles (50 nm in size) on rGO compared to 200 nm sized particles on cvdG. A reason for the bigger nanocrystals on the less defective carbon 2D material could be that defects act as nucleation sites, which allow better control of the reduction step. An outstanding low LOD in the ppt range was achieved by a vertical alignment of cvdG [58]. The authors highly attributed the hydrophobicity (water contact angle: 137°), the ultra-high specific surface area, exposed sharp edges, and the unique non-stacking three-dimensional geometry to be beneficial in reaching such high sensitivity. The drawback of this method is to be found in the device fabrication, which is rather time-consuming. For other gaseous analytes, the choice of the 2D material and the functionalization strategies can easily be derived from the examples shown for ammonia.

Table 1.1: Chemiresistive transducers based on differently fabricated 2D carbon materials for quantification and determination of ammonia at room temperature. PPy: polypyrrole, EA: ethyl acetate.

Material	Modification	LOD	Range / ppm	Response / recovery	r.h. / %	Selectivity	Comment	Reference
cvdG	-	-	(0.1 - 1) 10^{-4}	4 min / few min (-)	-	-	vertically aligned cvdG	[58]
cvdG	Co *meso*-arylporphyrins	-	20 – 160	60 s / - (-)	41	VOCs	FET	[111]
cvdG	Ag NPs	-	(0.05 - 1.2) 10^4	120 s / 70 s (-)	30	VOCs	-	[117]
ecG	ZnO nanowires	-	0.5 - 50	6s / 36 s (0.5 ppm)	-	VOCs, benzene, nitrobenzene, nitrotoluene	-	[118]
rGO	Ag NPs	1.2 ppb	0.1 - 15	5s / 6s (0.1 ppm)	25	H_2, CO	-	[115]
rGO	In_2O_3 nanofibers	44 ppb	1 - 60	17 s / 214 s (-)	30	Organic solvents, nitrogenated compounds	impedance at 10 kHz	[119]
rGO	mesoporous PPy layer	200 ppb	10 - 40	5 min / 10 min (-)	-	VOCs, acetonitrile, chloro-benzene, EA, toluene	no influence on humidity	[120]
rGO	MXene	-	10 - 50	-	-	VOCs, H_2S, SO_2, xylene, benzene	-	[121]
rGO	SnO_2 nanorods	20 ppm	20 - 3000	8 s / 13 s (200 ppm)	45	VOCs, NO, CO, H_2S	no influence on humidity	[116]
GO	fluorinated	6 ppb	0.1 - 0.5	86 s / 116 s (-)	-	VOCs, NO_2, H_2, toluene	-	[122]
GO	Cu tetra-β-amine-phthalocyanine	-	0.8	- / 350 s (-)	-	VOCs, NO_2	no influence on humidity	[114]

1.4.2. Impedimetric, Amperometric, and Voltammetric Sensors

Graphene modified electrodes as impedimetric sensors are popular in determination of biomolecules, biomarker, proteins, or DNA. Mostly, the sensing mechanism depends on the blocking of the electrode upon analyte binding, which inhibits the interaction of the

electrode with a redox marker present in the electrolyte. Table 1.2 presents graphene-based sensors to determine proteins or clinically relevant biomarkers by electrochemical impedance spectroscopy.

Table 1.2: Selection of various graphene modified impedimetric sensors to quantify proteins and disease-relevant biomarkers. BSA: bovine serum albumin, CEA: carcinoembryonic antigen, (MW/SW)CNT: multi-walled/single-walled carbon nanotubes, CRP: c reactive protein, CTnI: cardiac troponin I, CytC: cytochrome C, (B)Hb: (bovine) hemoglobin, HER2: human epidermal growth factor, HSA: human serum albumin, β-LG: β-lactoglobulin, Mb: myoglobin, PSA: prostate specific antigen.

Material	Modification	Analyte	Linear Range	LOD	Selectivity	Reference
rGO	MWCNT-Au NPs-chitosan	lysozyme	0.02 - 250 pM	9 fM	BSA, HSA, Hb, thrombin, IgG, CytC, PSA, enzymes	[123]
rGO	MWCNT-Au NPs	PSA	5 - 0.1 µg mL^{-1}	1 pg mL^{-1}	BSA, Hb, thrombin, IgG, lysozyme	[124]
rGO	SWCNT-Au NPs-aptamer	HER2	0.1 pg mL^{-1} - 1 ng mL^{-1}	50 fg·mL^{-1}	BSA, BHb, thrombin, IgG, lysozyme, PSA	[125]
cvdG	anti-OVA	Ovalbumin	1 - 0.1 pg mL^{-1}	0.9 pg mL^{-1}	β-LG, lysozyme	[88]
cvdG	anti-CEA	CEA	1.0 - 25.0 ng mL^{-1}	0.23 ng mL^{-1}	KCl, CYFRA-21-1, CTnI	[83]
cvdG	anti-IgG	IgG	0.1 – 100 µg mL^{-1}	0.136 µg mL^{-1}	BSA, Hb, avidin	[78]

An impedimetric immunosensor was established by using cvdG. The protocol forsakes a physical adsorption of the antibody towards rabbit immunoglobulin G (IgG) onto a multi-layered cvdG, grown on nickel [78]. Edges and wrinkles became present within the layered carbon material. The physical adsorption of anti-IgG is followed by a blocking step with BSA. Compared to the introduction of linker molecules, the non-destructive physical adsorption appeared to be superior as it leaves the sp²-hybridized structure of graphene intact, retaining the physical properties. Electrochemical impedance spectroscopy revealed an increase in the charge transfer resistance (R_{CT}) from bare cvdG *via* an anti-IgG/cvdG to a BSA/anti-IgG/cvdG assembly (Figure 1.12). The incubation with rabbit-IgG led to an even more enhanced R_{CT}, capable to determine the analyte with a

LOD of 0.136 µg mL^{-1} IgG. Only after 7 days of storage, the signal response of this sensor drops to 48%. This demonstrates a drawback of the physical adsorption of biomolecules in receptor design on 2D carbon materials.
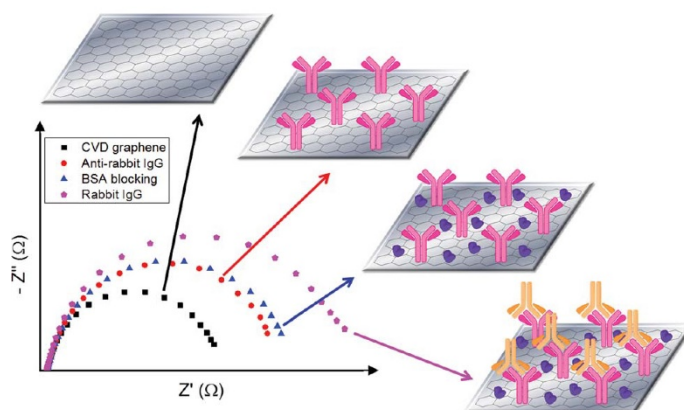
Figure 1.12: Impedance behavior in the presence of a redox marker for cvdG (black), anti-IgG/cvdG (red), BSA/anti-IgG/cvdG (blue) and IgG/BSA/anti-IgG/cvdG (pink), respectively. Reproduced from [78] by permission of The Royal Chemical Society.

Better stability can be achieved by attaching a receptor covalently. This is difficult for cvdG as it exhibits only functionalities upon an imperfect handling. A straightforward approach was developed by electrografting of 4-aminobenzoic acid on cvdG to design a sensor for the determination of ovalbumin (OVA) [88]. Even though cvdG was supposed to convince with the exceptional electrical properties of a low-defective material, it was not taken into consideration that a covalent functionalization routine destructs the sp^2-hybridized carbon lattice, changing the electronic properties of the material, *i.e.*, by opening a bandgap. The LOD was 0.9 pg mL^{-1} OVA in a linear range of 1 pg mL^{-1} to 100 ng mL^{-1}.

A comparison of electrochemically reduced graphene oxide and untreated graphene oxide was drawn to investigate the ability to improve the sensing performance towards DNA upon label-free electrical and enzymatic signal amplification [79]. The non-covalent modification of graphene layers with probe DNA increases the R$_{CT}$ value between redox marker and electrode surface due to electrostatic repulsion. Upon hybridization with the

target DNA, the resistance increases even more. The enzyme exonuclease III recycles the
sensor layer upon cleavage of the dsDNA (Figure 1.13).
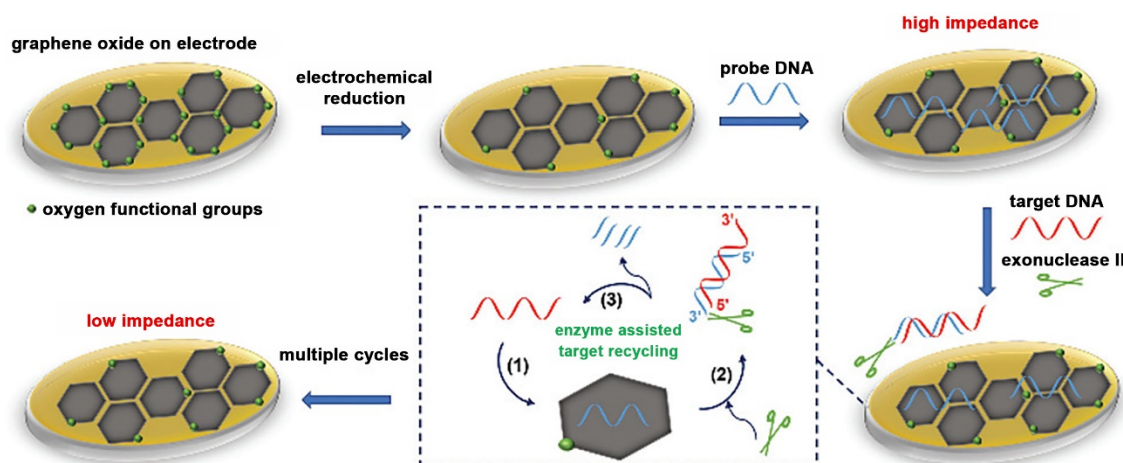
Figure 1.13: Scheme of an impedimetric sensor based on rGO, which is modified by adsorption of probe DNA. The
determination of complementary target DNA is accompanied by enzyme-assisted sensor recycling. Reproduced
from [79] by permission of The Royal Society of Chemistry.

Investigations on DNA with various concentrations were performed for either GO
modified electrodes (10 fM - 1 nM ssDNA) or rGO modified electrodes (5 aM - 1 nM
ssDNA). The GO modified electrode revealed a LOD of 50 fM DNA, whereas the LOD is
significantly decreased to 10 aM for rGO modified electrodes. Compared to GO which is
almost an insulating material due to the enormous structural irregularities, highly
conductive rGO is sensitive towards surface processes resulting in an enhanced change
of R_{CT} upon blocking and regeneration of the electrode material. A regenerated sensor
layer did not suffer a loss of performance, whereas it became apparent that upon
increased incubation time of the enzyme, artifacts regarding matrix adsorption as well as
spontaneous enzyme deactivation might take place [79].

In contrast to glassy carbon (GC), rGO provides a high affinity to aromatic molecules as
demonstrated by porphyrins, which easily attach to rGO by π stacking. A metallic
porphyrin-modified rGO impedimetric sensor was prepared to capture hepatitis C-DNA
by a complementary ssDNA, which is linked to manganese(III) tetraphenylporphyrin
(MnTPP) [80]. The non-covalent modification left the sp²-hybridized carbon lattice intact,
maintaining high conductivity. In contrast to pyrene groups, porphyrins are able to

incorporate an electrochemically active metal ion. The manganese ion served to monitor the stability of the porphyrin linker attached to the electrode during electrochemical measurements. The use of rGO as supporting material prevented the MnTPP from detaching, in contrast to a glassy carbon electrode (GCE). An increased electron transfer attributed to graphene's high surface area as well as the short distance between graphene and porphyrin result in a sufficient sensor performance [80].

Table 1.3 presents impedimetric graphene modified sensors that determine DNA strands, potentially applicable in clinical diagnosis to identify viruses, bacteria, as well as relevant biomarkers. Many allotropes from the pool of graphene materials can be found as sensor material, but the reduced graphene oxide is the most frequently used compound, due to the well-established fabrication protocols. The functional groups present at the material's surface enable easy functionalization by deposition of conductive polymers [126,127], liposomes [128], metallic nanoparticles [129-132] or porphyrins [80] to pave the way for enhanced analysis strategies.

Table 1.3: Impedimetric graphene modified sensors to determine ssDNA. Every sensor layer is additionally modified with a specific capture probe DNA. APTMS: (3-aminopropyl)trimethoxysilane, PABA: 4-aminobenzoic acid, PANI: polyaniline (emeraldine salt), non-compl.: non-complementary.

Material	Modification	Nucleotides	Linear Range	LOD	Selectivity	Reference
GO	Chitosan	21	10 fM - 10 nM	3.6 fM	mismatched	[133]
carboxylated graphene-nanoflakes	APTMS-ZnO	17	0.1 fM - 1 μM	0.1 fM	mismatched, non-compl.	[134]
rGO	Exonuclease III	23	50 aM - 1 nM	10.0 aM	mismatched	[79]
rGO	liposome	24	1 μM - 1 fM	10.0 aM	mismatched, non-compl.	[128]
rGO	Au NPs-PABA	20	0.1 fM - 10 nM	37 aM	mismatched	[129]
rGO	PANI	23	0.5 fM - 0.1 nM	0.1 fM	mismatched, non-compl.	[126]
rGO	PPy-CO$_2$H	19	10 fM - 10 nM	3 fM	mismatched, non-compl.	[127]
rGO	ZrO$_2$-hairpin probe DNA	22	10 fM - 0.1 nM	4.3 fM	mismatched, non-compl.	[135]
rGO	Nafion	-	0.1 pM - 0.1 nM	23 fM	mismatched	[136]
rGO	Au NPs	30	0.1 pM - 0.1 μM	36 fM	mismatched, non-compl.	[130]
rGO	MnTPP	25	0.1 fM - 10 pM	61 fM	mismatched, non-compl.	[80]
rGO	Au NPs	18	10 nM - 20 μM	0.18 nM	non-compl.	[131]
cvdG	oxygenated	15	2 aM - 1 pM	1.0 aM	mismatched, non-compl.	[137]
ecG	-	-	0.2 - 5 pg mL^{-1}	0.68 pg mL^{-1}	-	[138]
ultrasound exfoliated graphene	ZnO	25	10 pM - 1 μM	4.3 pM	mismatched, non-compl.	[132]

In contrast to frequency-dependent impedance spectroscopy, which monitors binding events in an equilibrium, time-dependent sensing techniques, *e.g.*, voltammetry and amperometry, are attractive to investigate induced electrochemical reactions.

Numerous exfoliation protocols strive for the preparation of graphene materials with a low number of defects to come close to the ideal graphene. For time-dependent electrochemical sensing techniques, the presence and number of defects within the

graphene affects their electrochemical activity. The defect-dependent sensing capability of the 2D carbon compounds generated by sonication was investigated upon the determination of phenolic compounds. The quality of the carbon materials ranges from a low number of defects present within the structure to graphene compounds, which were anodized to provide additional functional groups [71]. NMP-dispersed-graphite powder was exfoliated in a sonication bath (40 kHz, 100 W) for 48 h yielding graphene sheets. For a comparative study, GO was synthesized by a modified Hummers' method. Glassy carbon electrodes were modified by drop-casting of graphene and drying under an infrared lamp. The LPE graphene-modified electrodes were anodized (1.8 V for 2 min) in acetate buffer (pH 5.6). Atomic force microscopy revealed the roughest surface for sonication-derived graphene-modified GCE, potentially exhibiting the highest number of active sites. Differential pulse voltammetry (DPV) for all phenolic compounds revealed none or very weak oxidation peaks for GCE and GO-modified electrodes. The oxidation peaks are enhanced and shifted to more negative potentials for graphene/GCE and anodized graphene/GCE. The LODs are calculated to be 12 nM, 15 nM, 10 nM and 40 nM for hydroquinone, catechol, 4-chlorophenol, and 4-nitrophenol, respectively [71]. The electrochemical sensor performance of differently prepared graphene compounds was examined for a wide range of electrochemically active analytes like biomolecules, synthetic colorants, and phenolic compounds (4-chlorophenol, 4-nitrophenol)) using DPV. The plain GCE was not able to determine the analytes at low concentrations, but as the amount of defects increased within the graphene materials, the oxidation current of the different analytes increases [70]. Although the addition of salts might enhance the exfoliation efficiency of graphene *via* LPE, one of the advantages of fabrication by ultrasound is the possibility to prepare 2D materials in appropriate medium without the need of any additives, potentially influencing the physical behavior of the material. Comparing the detection limits of salt-assisted exfoliated graphene to sonicated graphene subsequently anodized, the LOD for 4-chlorophenol and 4-nitrophenol was increased by a factor of two and of six, respectively. The extended sonication time seems to be a promising alternative to prepare graphene compounds, instead of using additives, potentially influencing the material.

Electrochemical graphite exfoliation is predestined for simplification as the preparation procedure and material functionalization can be combined to one step, which was proved for a graphene-porphyrin compound. Graphite was exfoliated electrochemically with porphyrin as intercalant, simultaneously functionalizing graphene flakes by π-interaction, introducing an oxidizing agent for catechol [81]. Apparently, the material exfoliated by means of additional salts weakens the performance of the established electrochemical sensor with regard to liquid-phase exfoliation of graphene derived solely by exfoliation in appropriate solvent. The generation of 2D-based heterostructures incorporating catalytically active compounds is required to improve the performance of sensors towards analyte determination.

The design of improved electrochemical sensors envisions the hybridization of electrocatalytic active groups with graphene substrates. Besides the functionalization of graphene with carbon allotropes by π-stacking, highly attractive became the decoration with electrocatalytic active metallic nanoparticles (NPs). They provide a suitable substitute to natural enzymes, as they are more stable and are less prone to operation and environmental conditions. Metallic nanoparticles combine easily with carbon materials upon hydrothermal route or by direct electrodeposition onto the substrate of choice [86,124,125,129,132,134,139-143]. For successful analyte determination upon catalytic reaction, the achievement of homogeneously distributed small metallic NPs exhibiting a large electrical active surface is crucial. Nevertheless, it became apparent that deposited NPs tend to agglomerate on polycrystalline materials, *i.e.*, GC due to inhomogeneous charge distribution. This drawback is targeted by using graphene as supporting material, which prevent the particles from agglomeration resulting in homogeneously distributed monodisperse NPs creating an electrochemical synergy of the carbon-metal-interface [144].

The diameter of nanoparticles is crucial towards the electrocatalytic behavior, as the potentials of redox reactions can be shifted by the nanoparticle's size and shape. The size of the particles can be either modulated by applied deposition voltage or deposition time, as shown in Figure 1.14.
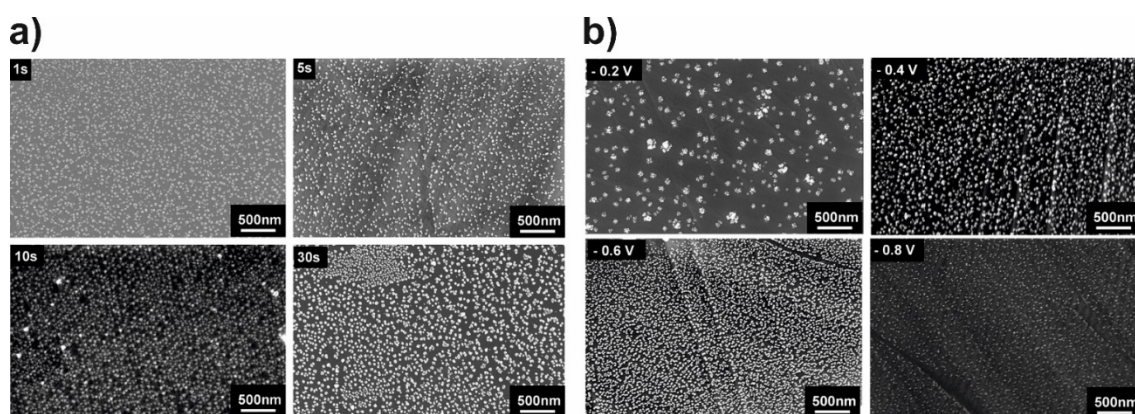
Figure 1.14: SEM images of AgNPs modified cvdG for 1 s, 5 s, 10 s, and 30 s in 0.2 M KNO_3 containing 0.7 mM $AgNO_3$ stepping the potential from 0 V to -0.4 V (a). AgNPs were deposited on cvdG at potentials of -0.2 V, -0.4 V, -0.6 V and -0.8 V, respectively, for 30 s (b). All potentials are given *vs*. Ag/AgCl. Adapted from [141] with permission from The Royal Society of Chemistry.

Table 1.4 and Table 1.5 provide an overview of graphene modified electrodes targeting hydrogen peroxide or glucose, both frequently determined in bioanalysis. To enhance the sensitivity and selectivity, catalytically active metals replaced enzymes almost completely influencing the operation potential. An amperometric gold-GO-based sensor was prepared by simultaneous electrodeposition of GO containing $HAuCl_4$, forming a AuNPs modified rGO hybrid [86]. Gold nanoparticles were chosen as catalyst due to its stability and operation in neutral medium. An aqueous dispersion of GO was electrodeposited on gold electrodes by application of a potential of -30 V for 20 min, reducing GO. The graphene support is necessary to stabilize AuNPs, which tend to agglomerate otherwise. Additionally, graphene enhances the glucose oxidation process. Amperometric measurements were performed in phosphate buffer (pH 7.4) at a potential of 0 V *vs*. Ag/AgCl, subsequently adding glucose with increasing concentration, exhibiting a LOD of 12 µM.

Table 1.4: Amperometric sensors based on graphene modified electrodes to determine glucose. All potentials were measured against Ag/AgCl when not stated otherwise. AA: ascorbic acid, AP: 4-acetamidophenol, DA: dopamine, Fru: fructose, Gal: galactose, Lac: lactose, LIG: laser-induced graphene, PANI: polyaniline (emeraldine salt), Suc: sucrose, UA: uric acid.

Material	Modification	Potential / V	Linear Range	LOD / μM	Selectivity	Reference
LIG	Cu NPs	-0.4 (SCE)	1 - 4.54 μM	0.35	AA, UA, DA, AP, Fru, Lac, Suc	[145]
N-rGO	Cu NPs	0.6	0.01 - 100 μM	0.01	AA, UA, DA, Fru, Lac, Suc	[146]
N-rGO	Ni(OH)$_2$ nanorods	0.45	0.5 - 11.5 μM; 11.5 - 240 μM	0.12	AA, UA, DA, Fru, Lac, Suc	[147]
rGO	Cu NPs-PANI	0.5 (SCE)	1 μM - 0.96 mM	0.27	AA, UA, DA, Lac, Suc	[148]
rGO	Cu nanoflower	0.6	2 μM - 2 mM; 2 - 13 mM	0.5	AA, UA, DA, NaNO$_3$	[143]
rGO	Ag-CuO NPs	0.6	0.01 - 28 mM	0.76	AA, UA, DA, Gal, Lac, Suc	[139]
rGO	Ni doped MoS$_2$ NPs	0.55	0.005 - 8.2 mM	2.7	AA, UA, DA, AP	[149]
rGO	PtAu NPs -GOx-chitosan	0.45	0.005 - 2.4 mM	5	AA, UA, AP	[142]
rGO	Au NPs	0	0.05 - 14 mM; 14 - 42 mM	12	AA, UA, DA, urea	[86]
CVD	Au NPs	0	6 μM - 28.5 mM	1		[150]
oxygenated-CVD	GOx-Nafion	-0.5	0.4 - 2 mM	124.2		[151]

Recent Developments in Carbon-Based Two-Dimensional Materials: Synthesis and Modification Aspects for Electrochemical Sensors

31

A ternary hybrid composed of graphene, AgNPs and Nafion, targets the determination of H_2O_2 [30]. The combination of material enhances the surface area, the conductivity, and leads to stable compounds. Silver pose electrocatalytic activity but tend to oxidation, which requires the protective Nafion layer. The hydrothermal synthesis of the heterostructure was accomplished by a one-pot approach, mixing the precursor materials, GO dispersion, Nafion solution, and $AgNO_3$. Glassy carbon electrodes were modified by drop casting of rGO-Nafion-AgNPs. Cyclic voltammetric studies showed that an excessive AgNPs decoration led to the deterioration of the reduction ability of the sensor, as the aggregation of AgNPs reduces the electrocatalytic active sites of the material. Amperometric sensing was performed by applying a potential of -0.65 V revealing a LOD of 0.53 µM H_2O_2, with a high selectivity for H_2O_2 compared to the five times increased concentration of urea, glucose, dopamine, uric acid, and ascorbic acid [30]. In contrast, a H_2O_2 sensor was prepared consisting of a heterostructure, decorated by microspheres of noble metals, Au and Pt, supported by rGO [35]. Reduced graphene oxide convinced as support due to higher conductivity and better stability. Furthermore, the lattice defects and functional groups pose attractive sites for deposition of metallic particles, which prevent them from aggregation. The solutions of GO, H_2PtCl_6 and $HAuCl_4$ were mixed in equal molar ratio adding $NaBH_4$ to trigger the reduction reaction. A GC electrode was drop-coated with rGO/Au/Pt. To detect H_2O_2 amperometrically, a potential of 80 mV *vs*. Ag/AgCl was applied, subsequently injecting the analyte into PBS (pH 7) resulting in a low LOD of 0.008 µM [35]. Apparently, even though noble metals are more expensive, they provide an enhanced electrocatalytic behavior in combination with graphene due to synergistic effects.

Table 1.5: Amperometric sensors based on graphene modified electrodes to determine hydrogen peroxide. All potentials were measured against Ag/AgCl, when not stated otherwise. AA: ascorbic acid, AP: 4-acetamidophenol, Cys: cysteine, DA: dopamine, Fru: fructose, GOx: glucose oxidase, GSH: glutathione, Lac: lactose, LIG: laser-induced graphene, nAPAMS: nano Au and Pt alloy microsphere, PANI: polyaniline (emeraldine salt), Suc: sucrose, UA: uric acid.

Material	Modification	Potential / V	Linear Range	LOD / μM	Selectivity	Reference
LIG	Ag NPs	-0.5	0.1 - 10 mM	7.9	AA, Glu,	[152]
3D-N-doped rGO	$NiCo_2O_4$ nanoflowers	0.5	1 - 510 μM	0.136	AA, UA, DA	[153]
rGO	nAPAMSs	-0.5	0.005 - 4 mM	0.008	AA, UA, AP, Glu	[35]
rGO	Fe NPs	-0.5	0.1 μM - 2.15 mM	0.056	AA, UA, DA, CT, Glu	[154]
rGO	Ferumoxytol-Pt NPs	0.1	0.4 - 10 μM; 0.0075 - 4.3 mM; 4.9 - 10.8 mM	0.38	AA, DA, Cys, GSH, Fru	[155]
rGO	Cu_2O-PANI	-0.2 (SCE)	0.8 μM - 12.78 mM	0.5	AA, UA, Glu	[140]
rGO	Nafion-Ag NPs	-0.6 (SCE)	1 - 30 mM	0.54	AA, UA, DA, Glu, urea	[30]
CVD	Au NPs	0.5	25 nM - 1.5 mM	0.01	-	[156]
CVD	Pd NPs	-0.12	4 μM - 13.5 mM	1.5	-	[157]
CVD	Fe_3O_4 NPs	0.7	12.5 - 112.5 μM	4.4	-	[158]
sono-ecG	-	-0.4	0.02 - 2.9 mM	2.67	AA, UA	[159]

1.5   Conclusion

Two-dimensional carbon materials have been intensively studied regarding synthesis, fabrication and their implementation in electrochemical sensors. The fact that this class of nanomaterial is much more than a sp^2-hybridized honeycomb-lattice of carbon atoms becomes vivid, when investigating the physical and chemical properties of the material, depending on the exfoliation technique. It can be stated that the preparation method guides the performance of the sensor material due the different intrinsic characteristics.

The variances originate from defects distributed within the carbon lattice, layer inconsistencies, oxygen functional groups and adatoms. The still ongoing development of fabrication methods for 2D carbon materials in the last years aims for a high yield production with a reproducible quality. Overcoming the weak interlayer van-der-Waals forces results in the delamination of the bulk material, yielding robust and flexible nanomaterial flakes due to strong intralayer forces [40,160].

In 2018, the group of Castro-Neto has investigated the quality of graphene supplied from 60 different producers with the result that the quality of these materials is rather poor, and this is claimed as one of the key issues for the slow development of applications [161]. Especially for liquid-dispersed graphene, it is difficult to produce these batches with high reproducibility in quality. There is also information missing on the aging of such dispersions restacking of the material. In contrast to dispersions, cvdG shows better reproducibility. It is expected that challenges in reproducibility can be overcome by better characterization techniques [161].

The modification of the 2D materials are easily achieved either by covalent or non-covalent functionalization to improve the selectivity of the sensor [75,76]. On the one hand, covalent modifications are reported to damage the sp^2-hybridized carbon system of graphene. On the other hand, the linkage of active biomolecules might become an issue as the natural structure of the biomolecule can be disrupted followed by a loss of activity [102].

Numerous sensors were reported for an enormous variety of analytes based on 2D materials beyond the scope of this review. Different exfoliation techniques yield 2D

carbon materials of a diverse structure, which consequently exhibits altered physical properties. Graphene, derived by CVD, is rather integrated in FETs or chemiresistors, as these sensors base on the change of the intrinsic electrical characteristics of the sensing layer upon analyte adsorption. The advantage of this material is claimed to be the intact sp^2-hybridized carbon lattice, but for most electrochemical sensors, this is not a limitation so far. It is to point out that cvdG is prone to an unintentional introduction of non-reproducible defects, *i.e.*, smallest variations of the processing parameters, complex transfer protocols inducing ionic impurities, and structural defects, deteriorating the physical and chemical properties. Besides the rather high-quality cvdG, synthetically derived rGO is widest applied as sensor layer since it is either produced in an ordinary laboratory or purchased from the growing market of suppliers offering graphene materials up to a liter-range. A large defect density is distributed along the material's basal planes. Even though this term has a negative connotation, those structural defects do not pose a drawback when it comes to sensing applications. Quite the contrary, the defects are resembled as active functional groups, preferably interacting with a potential analyte, when applied as sensor surface. Not any other material was used as frequently as reduced graphene oxide in sensor design, due to the simplicity of the material and its physicochemical properties. Additionally, the oxygen moieties enable the dispersibility of rGO in water.

In terms of easily derived, low-cost, liquid processable material, one has to keep in mind the LPE-process of graphite. The exfoliation *via* sonication or shear exfoliation is widely performed either in toxic, high-boiling point, organic solvents with a matching surface tension to the material or in aqueous solution with a stabilizing surfactant. Two-dimensional materials are obtained without a chemical change in the basal plane of their structure, but with varying flake size and number of layers from mono- to multi-layered compounds. The diverse surface chemistry often affects the physical properties in a non-reproducible way. The mechanical exfoliation process may not introduce structural irregularities within the carbon layer, yet the number of defects increase upon formation of smaller flakes dominated by edge-planes. Electrochemical exfoliation is performed in aqueous solution using inorganic salts as intercalating species upon application of a high voltage. A bonus is the possibility of direct functionalization during exfoliation. Many

reports exist on how to exfoliate 2D materials, but little is derived on the sensing behavior, especially when the morphology of the materials changes upon variation of the delamination process. Nevertheless, the reported LPE-derived materials applied in impedimetric or amperometric sensors revealed promising results. Future trends envision the use of all carbon-fabricated wearable electrochemical sensors. For a direct application on the skin, deeper understanding of the toxicity of each class of 2D carbon materials is still needed. The sustainability of the preparation procedures is barely addressed even though the growing demand of production and processing procedures result in an enhanced consumption of resources.

A deeper understanding of the electrochemical properties of the 2D carbon materials has to be obtained to unravel the question, whether a graphene material suits the requirements of the potential sensor. As stated before, the widest applied materials for sensor development were contrary materials, cvdG and rGO, known for either high-quality or defective graphene. Instead of implementing the materials according to their unique features, it was found that the intact sp^2-hybridized carbon system of cvdG was intentionally destructed by introduction of sp^3-hybridized functionalities. To become an essential part in mass produced electrochemical sensors, the system integration must be compatible to already existing complementary metal-oxide-semiconductor (CMOS) technologies [162]. It is vital to understand which material will meet the sensor's need to improve its performance. The electrochemical features have to be explored and further correlated to the chemical structure of the material. The obtained fundamental knowledge of physical and chemical correlations might be the key to tune the material's properties directly to the special requirements, which would lead to much smarter sensors in the future.

1.6 References

[1] Yang W, Ratinac KR, Ringer SP, Thordarson P, Gooding JJ, Braet F (2010) Carbon nanomaterials in biosensors: should you use nanotubes or graphene? Angew. Chem., Int. Ed. 49:2114–2138.

[2] Novoselov KS, Geim AK, Morozov SV, Jiang D, Zhang Y, Dubonos SV, Grigorieva IV, Firsov AA (2004) Electric field effect in atomically thin carbon films. Science 306:666–669.

[3] Ferrari AC, Bonaccorso F, Fal'ko V, Novoselov KS, Roche S, Bøggild P, Borini S, Koppens FHL, Palermo V, Pugno N, Garrido JA, Sordan R, Bianco A, Ballerini L, Prato M, Lidorikis E, Kivioja J, Marinelli C, Ryhänen T, Morpurgo A, Coleman JN, Nicolosi V, Colombo L, Fert A, Garcia-Hernandez M, Bachtold A, Schneider GF, Guinea F, Dekker C, Barbone M, Sun Z, Galiotis C, Grigorenko AN, Konstantatos G, Kis A, Katsnelson M, Vandersypen L, Loiseau A, Morandi V, Neumaier D, Treossi E, Pellegrini V, Polini M, Tredicucci A, Williams GM, Hong BH, Ahn J-H, Kim JM, Zirath H, van Wees BJ, van der Zant H, Occhipinti L, Di Matteo A, Kinloch IA, Seyller T, Quesnel E, Feng X, Teo K, Rupesinghe N, Hakonen P, Neil SRT, Tannock Q, Löfwander T, Kinaret J (2015) Science and technology roadmap for graphene, related two-dimensional crystals, and hybrid systems. Nanoscale 7:4598–4810.

[4] Zhang H, Chhowalla M, Liu Z (2018) 2D Nanomaterials: Graphene and transition metal dichalcogenides. Chem. Soc. Rev. 47:3015–3017.

[5] Benck JD, Pinaud BA, Gorlin Y, Jaramillo TF (2014) Substrate selection for fundamental studies of electrocatalysts and photoelectrodes: inert potential windows in acidic, neutral, and basic electrolyte. PloS One 9:e107942.

[6] Zhou M, Zhai Y, Dong S (2009) Electrochemical sensing and biosensing platform based on chemically reduced graphene oxide. Anal. Chem. 81:5603–5613.

[7] Ferreira M, Varela H, Torresi RM, Tremiliosi-Filho G (2006) Electrode passivation caused by polymerization of different phenolic compounds. Electrochim. Acta 52:434–442.

[8] Sha R, Puttapati SK, Srikanth VV, Badhulika S (2017) Ultra-sensitive phenol sensor based on overcoming surface fouling of reduced graphene oxide-zinc oxide composite electrode. J. Electroanal. Chem. 785:26–32.

[9] Zheng D, Hu H, Liu X, Hu S (2015) Application of graphene in electrochemical sensing. Curr. Opin. Colloid Interface Sci. 20:383–405.

[10] Backes C, Abdelkader AM, Alonso C, Andrieux-Ledier A, Arenal R, Azpeitia J, Balakrishnan N, Banszerus L, Barjon J, Bartali R, Bellani S, Berger C, Berger R, Ortega MMB, Bernard C, Beton PH, Beyer A, Bianco A, Bøggild P, Bonaccorso F, Barin GB, Botas C, Bueno RA, Carriazo D, Castellanos-Gomez A, Christian M, Ciesielski A, Ciuk T, Cole MT, Coleman J, Coletti C, Crema L, Cun H, Dasler D, Fazio D de, Díez N, Drieschner S, Duesberg GS, Fasel R, Feng X, Fina A, Forti S, Galiotis C, Garberoglio G, García JM, Garrido JA, Gibertini M, Gölzhäuser A, Gómez J, Greber T, Hauke F, Hemmi A, Hernandez-Rodriguez I, Hirsch A, Hodge SA, Huttel Y, Jepsen PU, Jimenez I, Kaiser U, Kaplas T, Kim H, Kis A, Papagelis K, Kostarelos K, Krajewska A, Lee K, Li C, Lipsanen H, Liscio A, Lohe MR, Loiseau A, Lombardi L, Francisca López M, Martin O, Martín C, Martínez L, Martin-Gago JA, Ignacio Martínez J, Marzari N, Mayoral Á, McManus J, Melucci M, Méndez J, Merino C, Merino P, Meyer AP, Miniussi E, Miseikis V, Mishra N, Morandi V, Munuera C, Muñoz R, Nolan H, Ortolani L, Ott AK, Palacio I, Palermo V, Parthenios J, Pasternak I, Patane A, Prato M, Prevost H, Prudkovskiy V, Pugno N, Rojo T, Rossi A, Ruffieux P, Samorì P, Schué L, Setijadi E, Seyller T, Speranza G, Stampfer C, Stenger I, Strupinski W, Svirko Y, Taioli S, Teo KBK, Testi M, Tomarchio F, Tortello M, Treossi E, Turchanin A,

Vazquez E, Villaro E, Whelan PR, Xia Z, Yakimova R, Yang S, Yazdi GR, Yim C, Yoon D, Zhang X, Zhuang X, Colombo L, Ferrari AC, Garcia-Hernandez M (2020) Production and processing of graphene and related materials. J. Phys.: Condens. Matter 7:22001.

[11] Tan C, Cao X, Wu X-J, He Q, Yang J, Zhang X, Chen J, Zhao W, Han S, Nam G-H, Sindoro M, Zhang H (2017) Recent advances in ultrathin two-dimensional nanomaterials. Chem. Rev. 117:6225–6331.

[12] Bonaccorso F, Bartolotta A, Coleman JN, Backes C (2016) 2D-crystal-based functional inks. Adv. Mater. 28:6136–6166.

[13] Bonaccorso F, Lombardo A, Hasan T, Sun Z, Colombo L, Ferrari AC (2012) Production and processing of graphene and 2D crystals. Mater. Today 15:564–589.

[14] Gupta A, Sakthivel T, Seal S (2015) Recent development in 2D materials beyond graphene. Prog. Mater. Sci. 73:44–126.

[15] Anichini C, Czepa W, Pakulski D, Aliprandi A, Ciesielski A, Samorì P (2018) Chemical sensing with 2D materials. Chem. Soc. Rev. 47:4860–4908.

[16] Reina G, González-Domínguez JM, Criado A, Vázquez E, Bianco A, Prato M (2017) Promises, facts and challenges for graphene in biomedical applications. Chem. Soc. Rev 46:4400–4416.

[17] Yadav N, Lochab B (2019) A comparative study of graphene oxide: Hummers, intermediate and improved method. FlatChem 13:40–49.

[18] Brodie BC (1859) XIII. On the atomic weight of graphite. Philos. Trans. R. Soc. London 149:249–259.

[19] Staudenmaier L (1898) Verfahren zur Darstellung der Graphitsäure. Ber. Dtsch. Chem. Ges. 31:1481–1487.

[20] Hummers WS, Offeman RE (1958) Preparation of graphitic oxide. J. Am. Chem. Soc. 80:1339.

[21] Botas C, Álvarez P, Blanco P, Granda M, Blanco C, Santamaría R, Romasanta LJ, Verdejo R, López-Manchado MA, Menéndez R (2013) Graphene materials with different structures prepared from the same graphite by the Hummers and Brodie methods. Carbon 65:156–164.

[22] Kong F-Y, Li R-F, Yao L, Wang Z-X, Li H-Y, Lv W-X, Wang W (2019) Voltammetric simultaneous determination of catechol and hydroquinone using a glassy carbon electrode modified with a ternary hybrid material composed of reduced graphene oxide, magnetite nanoparticles and gold nanoparticles. Microchim. Acta 186:177.

[23] Kang JH, Kim T, Choi J, Park J, Kim YS, Chang MS, Jung H, Park KT, Yang SJ, Park CR (2016) Hidden second oxidation step of Hummers method. Chem. Mater. 28:756–764.

[24] Stankovich S, Dikin DA, Dommett GHB, Kohlhaas KM, Zimney EJ, Stach EA, Piner RD, Nguyen ST, Ruoff RS (2006) Graphene-based composite materials. Nature 442:282–286.

[25] Eigler S, Enzelberger-Heim M, Grimm S, Hofmann P, Kroener W, Geworski A, Dotzer C, Röckert M, Xiao J, Papp C, Lytken O, Steinrück H-P, Müller P, Hirsch A (2013) Wet chemical synthesis of graphene. Adv. Mater. 25:3583–3587.

[26] Ghosh R, Nayak AK, Santra S, Pradhan D, Guha PK (2015) Enhanced ammonia sensing at room temperature with reduced graphene oxide/tin oxide hybrid films. RSC Adv. 5:50165–50173.

[27] Wang X, Gu D, Li X, Lin S, Zhao S, Rumyantseva MN, Gaskov AM (2019) Reduced graphene oxide hybridized with WS_2 nanoflakes based heterojunctions for selective ammonia sensors at room temperature. Sens. Actuators, B 282:290–299.

[28] Yoo SS, Kim SY, Kim KS, Hong S, Oh MJ, Nam MG, Kim W-J, Park J, Chung C-H, Choe W-S, Yoo PJ (2020) Controlling inter-sheet-distance in reduced graphene oxide electrodes for highly sensitive electrochemical impedimetric sensing of myoglobin. Sens. Actuators, B 305:127477.

[29] Wang Z, Sackmann A, Gao S, Weimar U, Lu G, Liu S, Zhang T, Barsan N (2019) Study on highly selective sensing behavior of ppb-level oxidizing gas sensors based on Zn_2SnO_4 nanoparticles immobilized on reduced graphene oxide under humidity conditions. Sens. Actuators, B 285:590–600.

[30] Yusoff N, Rameshkumar P, Mehmood MS, Pandikumar A, Lee HW, Huang NM (2017) Ternary nanohybrid of reduced graphene oxide-nafion@silver nanoparticles for boosting the sensor performance in non-enzymatic amperometric detection of hydrogen peroxide. Biosens. Bioelectron. 87:1020–1028.

[31] Pei S, Cheng H-M (2012) The reduction of graphene oxide. Carbon 50:3210–3228.

[32] Cai B, Wang S, Le Huang, Ning Y, Zhang Z, Zhang G-J (2014) Ultrasensitive label-free detection of PNA-DNA hybridization by reduced graphene oxide field-effect transistor biosensor. ACS Nano 8:2632–2638.

[33] Chua CK, Pumera M (2014) Chemical reduction of graphene oxide: a synthetic chemistry viewpoint. Chem. Soc. Rev. 43:291–312.

[34] Becerril HA, Mao J, Liu Z, Stoltenberg RM, Bao Z, Chen Y (2008) Evaluation of solution-processed reduced graphene oxide films as transparent conductors. ACS Nano 2:463–470.

[35] Bai Z, Dong W, Ren Y, Zhang C, Chen Q (2018) Preparation of nano Au and Pt Alloy microspheres decorated with reduced graphene oxide for nonenzymatic hydrogen peroxide sensing. Langmuir 34:2235–2244.

[36] Chen D, Feng H, Li J (2012) Graphene oxide: preparation, functionalization, and electrochemical applications. Chem. Rev. 112:6027–6053.

[37] Zöpfl A, Lemberger M-M, König M, Ruhl G, Matysik F-M, Hirsch T (2014) Reduced graphene oxide and graphene composite materials for improved gas sensing at low temperature. Faraday Discuss. 173:403–414.

[38] Xu X, Liu C, Sun Z, Cao T, Zhang Z, Wang E, Liu Z, Liu K (2018) Interfacial engineering in graphene bandgap. Chem. Soc. Rev. 47:3059–3099.

[39] Yang Y, Hou H, Zou G, Shi W, Shuai H, Li J, Ji X (2018) Electrochemical exfoliation of graphene-like two-dimensional nanomaterials. Nanoscale 11:16–33.

[40] Ambrosi A, Pumera M (2018) Exfoliation of layered materials using electrochemistry. Chem. Soc. Rev. 47:7213–7224.

[41] Zeng Z, Yin Z, Huang X, Li H, He Q, Lu G, Boey F, Zhang H (2011) Single-layer semiconducting nanosheets: high-yield preparation and device fabrication. Angew. Chem., Int. Ed. Engl. 50:11093–11097.

[42] Wang J, Manga KK, Bao Q, Loh KP (2011) High-yield synthesis of few-layer graphene flakes through electrochemical expansion of graphite in propylene carbonate electrolyte. J. Am. Chem. Soc. 133:8888–8891.

[43] Lin Z, Liu Y, Halim U, Ding M, Liu Y, Wang Y, Jia C, Chen P, Duan X, Wang C, Song F, Li M, Wan C, Huang Y, Duan X (2018) Solution-processable 2D semiconductors for high-performance large-area electronics. Nature 562:254–258.

[44] Parvez K, Wu Z-S, Li R, Liu X, Graf R, Feng X, Müllen K (2014) Exfoliation of graphite into graphene in aqueous solutions of inorganic salts. J. Am. Chem. Soc. 136:6083–6091.

[45] Ambrosi A, Pumera M (2016) Electrochemically exfoliated graphene and graphene oxide for energy storage and electrochemistry applications. Chem. - Eur. J. 22:153–159.

[46] Deng B, Liu Z, Peng H (2019) Toward mass production of CVD graphene films. Adv. Mater. 31:e1800996.

[47] Li X, Colombo L, Ruoff RS (2016) Synthesis of graphene films on copper foils by chemical vapor deposition. Adv. Mater. 28:6247–6252.

[48] Chen X, Zhang L, Chen S (2015) Large area CVD growth of graphene. Synth. Met. 210:95–108.

[49] Seah C-M, Chai S-P, Mohamed AR (2014) Mechanisms of graphene growth by chemical vapour deposition on transition metals. Carbon 70:1–21.

[50] Miseikis V, Convertino D, Mishra N, Gemmi M, Mashoff T, Heun S, Haghighian N, Bisio F, Canepa M, Piazza V, Coletti C (2015) Rapid CVD growth of millimetre-sized single crystal graphene using a cold-wall reactor. 2D Mater. 2:14006.

[51] Lee E, Baek J, Park JS, Kim J, Yuk JM, Jeon S (2019) Effect of nucleation density on the crystallinity of graphene grown from mobile hot-wire-assisted CVD. 2D Mater. 6:11001.

[52] Muñoz R, Gómez-Aleixandre C (2013) Review of CVD synthesis of graphene. Chem. Vap. Deposition 19:297–322.

[53] Gao L, Ren W, Xu H, Jin L, Wang Z, Ma T, Ma L-P, Zhang Z, Fu Q, Peng L-M, Bao X, Cheng H-M (2012) Repeated growth and bubbling transfer of graphene with millimetre-size single-crystal grains using platinum. Nat. Commun. 3:699.

[54] Chen Y, Gong X-L, Gai J-G (2016) Progress and challenges in transfer of large-area graphene films. Adv. Sci. 3:1500343.

[55] Deng S, Berry V (2016) Wrinkled, rippled and crumpled graphene: an overview of formation mechanism, electronic properties, and applications. Mater. Today 19:197–212.

[56] Hwang MT, Heiranian M, Kim Y, You S, Leem J, Taqieddin A, Faramarzi V, Jing Y, Park I, van der Zande AM, Nam S, Aluru NR, Bashir R (2020) Ultrasensitive detection of nucleic acids using deformed graphene channel field effect biosensors. Nat. Commun. 11:1543.

[57] Kodu M, Berholts A, Kahro T, Avarmaa T, Kasikov A, Niilisk A, Alles H, Jaaniso R (2016) Highly sensitive NO_2 sensors by pulsed laser deposition on graphene. Appl. Phys. Lett. 109:113108.

[58] Li J, Liu Z, Guo Q, Yang S, Xu A, Wang Z, Wang G, Wang Y, Chen D, Ding G (2019) Controllable growth of vertically oriented graphene for high sensitivity gas detection. J. Mater. Chem. C 7:5995–6003.

[59] Shen J, He Y, Wu J, Gao C, Keyshar K, Zhang X, Yang Y, Ye M, Vajtai R, Lou J, Ajayan PM (2015) Liquid phase exfoliation of two-dimensional materials by directly probing and matching surface tension components. Nano Lett. 15:5449–5454.

[60] Paton KR, Varrla E, Backes C, Smith RJ, Khan U, O'Neill A, Boland C, Lotya M, Istrate OM, King P, Higgins T, Barwich S, May P, Puczkarski P, Ahmed I, Moebius M, Pettersson H, Long E, Coelho J, O'Brien SE, McGuire EK, Sanchez BM, Duesberg GS, McEvoy N, Pennycook TJ, Downing C, Crossley A, Nicolosi V, Coleman JN (2014) Scalable production of large quantities of defect-free few-layer graphene by shear exfoliation in liquids. Nat. Mater. 13:624–630.

[61] Ciesielski A, Samorì P (2014) Graphene via sonication assisted liquid-phase exfoliation. Chem. Soc. Rev. 43:381–398.

[62]   Backes C, Higgins TM, Kelly A, Boland C, Harvey A, Hanlon D, Coleman JN (2017) Guidelines for exfoliation, characterization and processing of layered materials produced by liquid exfoliation. Chem. Mater. 29:243–255.

[63]   Hernandez Y, Nicolosi V, Lotya M, Blighe FM, Sun Z, De S, McGovern IT, Holland B, Byrne M, Gun'Ko YK, Boland JJ, Niraj P, Duesberg G, Krishnamurthy S, Goodhue R, Hutchison J, Scardaci V, Ferrari AC, Coleman JN (2008) High-yield production of graphene by liquid-phase exfoliation of graphite. Nat Nanotechnol. 3:563–568.

[64]   Tao H, Zhang Y, Gao Y, Sun Z, Yan C, Texter J (2017) Scalable exfoliation and dispersion of two-dimensional materials - an update. Phys. Chem. Chem. Phys 19:921–960.

[65]   Liu L, Shen Z, Yi M, Zhang X, Ma S (2014) A green, rapid and size-controlled production of high-quality graphene sheets by hydrodynamic forces. RSC Adv. 4:36464–36470.

[66]   Biccai S, Barwich S, Boland D, Harvey A, Hanlon D, McEvoy N, Coleman JN (2019) Exfoliation of 2D materials by high shear mixing. 2D Mater. 6:15008.

[67]   Coleman JN (2013) Liquid exfoliation of defect-free graphene. Acc. Chem. Res. 46:14–22.

[68]   Hu G, Kang J, Ng LWT, Zhu X, Howe RCT, Jones CG, Hersam MC, Hasan T (2018) Functional inks and printing of two-dimensional materials. Chem. Soc. Rev. 47:3265–3300.

[69]   Kang J, Sangwan VK, Wood JD, Hersam MC (2017) Solution-based processing of monodisperse two-dimensional nanomaterials. Acc. Chem. Res. 50:943–951.

[70]   Wei P, Shen J, Wu K, Yang N (2019) Defect-dependent electrochemistry of exfoliated graphene layers. Carbon 154:125–131.

[71]   Wu C, Cheng Q, Wu K (2015) Electrochemical functionalization of N-methyl-2-pyrrolidone-exfoliated graphene nanosheets as highly sensitive analytical platform for phenols. Anal. Chem. 87:3294–3299.

[72]   Niu L, Coleman JN, Zhang H, Shin H, Chhowalla M, Zheng Z (2016) Production of two-dimensional nanomaterials via liquid-based direct exfoliation. Small 12:272–293.

[73]   Lotya M, Hernandez Y, King PJ, Smith RJ, Nicolosi V, Karlsson LS, Blighe FM, De S, Wang Z, McGovern IT, Duesberg GS, Coleman JN (2009) Liquid phase production of graphene by exfoliation of graphite in surfactant/water solutions. J. Am. Chem. Soc. 131:3611–3620.

[74]   Bosch-Navarro C, Laker ZPL, Rourke JP, Wilson NR (2015) Reproducible, stable and fast electrochemical activity from easy to make graphene on copper electrodes. Phys. Chem. Chem. Phys. 17:29628-29636.

[75]   Georgakilas V, Otyepka M, Bourlinos AB, Chandra V, Kim N, Kemp KC, Hobza P, Zboril R, Kim KS (2012) Functionalization of graphene: covalent and non-covalent approaches, derivatives and applications. Chem. Rev. 112:6156–6214.

[76]   Georgakilas V, Tiwari JN, Kemp KC, Perman JA, Bourlinos AB, Kim KS, Zboril R (2016) Noncovalent functionalization of graphene and graphene oxide for energy materials, biosensing, catalytic, and biomedical applications. Chem. Rev. 116:5464–5519.

[77]   Shin DH, Kim W, Jun J, Lee JS, Kim JH, Jang J (2018) Highly selective FET-type glucose sensor based on shape-controlled palladium nanoflower-decorated graphene. Sens. Actuators, B 264:216–223.

[78]   Loo AH, Ambrosi A, Bonanni A, Pumera M (2014) CVD graphene based immunosensor. RSC Adv. 4:23952–23956.

[79] Cao S-H, Li L-H, Wei W-Y, Feng Y, Jiang W-L, Wang J-L, Zhang X-P, Cai S-H, Chen Z (2019) A label-free
      and ultrasensitive DNA impedimetric sensor with enzymatic and electrical dual-amplification. Analyst
      144:4175–4179.

[80] Wang Y, Sauriat-Dorizon H, Korri-Youssoufi H (2017) Direct electrochemical DNA biosensor based on
      reduced graphene oxide and metalloporphyrin nanocomposite. Sens. Actuators, B 251:40–48.

[81] Coroş M, Pogăcean F, Măgeruşan L, Roşu M-C, Porav AS, Socaci C, Bende A, Stefan-van Staden R-I,
      Pruneanu S (2018) Graphene-porphyrin composite synthesis through graphite exfoliation: the
      electrochemical sensing of catechol. Sens. Actuators, B 256:665–673.

[82] Campos R, Borme J, Guerreiro JR, Machado G, Cerqueira MF, Petrovykh DY, Alpuim P (2019) Attomolar
      label-free detection of DNA hybridization with electrolyte-gated graphene field-effect transistors. ACS Sens.
      4:286–293.

[83] Singh VK, Kumar S, Pandey SK, Srivastava S, Mishra M, Gupta G, Malhotra BD, Tiwari RS, Srivastava A (2018)
      Fabrication of sensitive bioelectrode based on atomically thin CVD grown graphene for cancer biomarker
      detection. Biosens. Bioelectron. 105:173–181.

[84] Luo Y, Kong F-Y, Li C, Shi J-J, Lv W-X, Wang W (2016) One-pot preparation of reduced graphene oxide-
      carbon nanotube decorated with Au nanoparticles based on protein for non-enzymatic electrochemical
      sensing of glucose. Sens. Actuators, B 234:625–632.

[85] Pogacean F, Coros M, Magerusan L, Rosu M-C, Socaci C, Gergely S, van Staden R-IS, Moldovan M, Sarosi C,
      Pruneanu S (2018) Sensitive detection of hydroquinone using exfoliated graphene-Au/glassy carbon
      modified electrode. Nanotechnology 29:95501.

[86] He C, Wang J, Gao N, He H, Zou K, Ma M, Zhou Y, Cai Z, Chang G, He Y (2019) A gold electrode modified
      with a gold-graphene oxide nanocomposite for non-enzymatic sensing of glucose at near-neutral pH
      values. Microchim. Acta 186:722.

[87] Oh J, Lee JS, Jun J, Kim SG, Jang J (2017) Ultrasensitive and selective organic FET-type nonenzymatic
      dopamine sensor based on platinum nanoparticles-decorated reduced graphene oxide. ACS Appl. Mater.
      Interfaces 9:39526–39533.

[88] Eissa S, Jimenez GC, Mahvash F, Guermoune A, Tlili C, Szkopek T, Zourob M, Siaj M (2015) Functionalized
      CVD monolayer graphene for label-free impedimetric biosensing. Nano Res. 8:1698–1709.

[89] Ares P, Pisarra M, Segovia P, Díaz C, Martín F, Michel EG, Zamora F, Gómez-Navarro C, Gómez-Herrero J
      (2019) Tunable graphene electronics with local ultrahigh pressure. Adv. Funct. Mater. 29:1806715.

[90] Kim MA, Qiu N, Li Z, Huang Q, Chai Z, Du S, Liu H (2020) Electric field effect on the reactivity of solid state
      materials: the case of single layer graphene. Adv. Funct. Mater. 30:1909269.

[91] Liu Y, Huang Y, Duan X (2019) Van der Waals integration before and beyond two-dimensional materials.
      Nature 567:323–333.

[92] Azadmanjiri J, Srivastava VK, Kumar P, Sofer Z, Min J, Gong J (2020) Graphene-supported 2D transition
      metal dichalcogenide van der waals heterostructures. Appl. Mater. Today 19:100600.

[93] Sanati A, Jalali M, Raeissi K, Karimzadeh F, Kharaziha M, Mahshid SS, Mahshid S (2019) A review on recent
      advancements in electrochemical biosensing using carbonaceous nanomaterials. Microchim. Acta 186:773.

[94] Xu J, Wang Y, Hu S (2017) Nanocomposites of graphene and graphene oxides: synthesis, molecular
      functionalization and application in electrochemical sensors and biosensors. A review. Microchim. Acta
      184:1–44.

[95] Fu W, Jiang L, van Geest EP, Lima LMC, Schneider GF (2017) Sensing at the surface of graphene field-effect transistors. Adv. Mater. 29:1603610.

[96] Bobrinetskiy II, Knezevic NZ (2018) Graphene-based biosensors for on-site detection of contaminants in food. Anal. Methods 10:5061–5070.

[97] Gan T, Hu S (2011) Electrochemical sensors based on graphene materials. Microchim. Acta 175:1–19.

[98] Goldsmith BR, Locascio L, Gao Y, Lerner M, Walker A, Lerner J, Kyaw J, Shue A, Afsahi S, Pan D, Nokes J, Barron F (2019) Digital biosensing by foundry-fabricated graphene sensors. Sci. Rep. 9:434.

[99] Wang Z, Jia Y (2018) Graphene solution-gated field effect transistor DNA sensor fabricated by liquid exfoliation and double glutaraldehyde cross-linking. Carbon 130:758–767.

[100] Kwon SS, Shin JH, Choi J, Nam S, Park WI (2017) Defect-mediated molecular interaction and charge transfer in graphene mesh-glucose sensors. ACS Appl. Mater. Interfaces 9:14216–14221.

[101] Ang PK, Chen W, Wee ATS, Loh KP (2008) Solution-gated epitaxial graphene as pH sensor. J. Am. Chem. Soc. 130:14392–14393.

[102] Piccinini E, Bliem C, Reiner-Rozman C, Battaglini F, Azzaroni O, Knoll W (2017) Enzyme-polyelectrolyte multilayer assemblies on reduced graphene oxide field-effect transistors for biosensing applications. Biosens. Bioelectron. 92:661–667.

[103] Li Y, Zhu Y, Wang C, He M, Lin Q (2019) Selective detection of water pollutants using a differential aptamer-based graphene biosensor. Biosens. Bioelectron. 126:59–67.

[104] Kwon SS, Yi J, Lee WW, Shin JH, Kim SH, Cho SH, Nam S, Park WI (2016) Reversible and irreversible responses of defect engineered graphene-based electrolyte-gated pH sensors. ACS Appl. Mater. Interfaces 8:834–839.

[105] Li Y, Wang C, Zhu Y, Zhou X, Xiang Y, He M, Zeng S (2017) Fully integrated graphene electronic biosensor for label-free detection of lead (II) ion based on G-quadruplex structure-switching. Biosens. Bioelectron. 89:758–763.

[106] Xiong C, Zhang T, Di Wang, Lin Y, Qu H, Chen W, Luo L, Wang Y, Zheng L, Fu L (2018) Highly sensitive solution-gated graphene transistor based sensor for continuous and real-time detection of free chlorine. Anal. Chim. Acta 1033:65–72.

[107] Sheldon RA, van Pelt S (2013) Enzyme immobilisation in biocatalysis: why, what and how. Chem. Soc. Rev. 42:6223–6235.

[108] Niyogi S, Bekyarova E, Itkis ME, Zhang H, Shepperd K, Hicks J, Sprinkle M, Berger C, Lau CN, deHeer WA, Conrad EH, Haddon RC (2010) Spectroscopy of covalently functionalized graphene. Nano Lett. 10:4061–4066.

[109] Reiner-Rozman C, Larisika M, Nowak C, Knoll W (2015) Graphene-based liquid-gated field effect transistor for biosensing: Theory and experiments. Biosens. Bioelectron. 70:21–27.

[110] Seo G, Lee G, Kim MJ, Baek S-H, Choi M, Ku KB, Lee C-S, Jun S, Park D, Kim HG, Kim S-J, Lee J-O, Kim BT, Park EC, Kim SI (2020) Rapid detection of COVID-19 causative virus (SARS-CoV-2) in human nasopharyngeal swab specimens using field-effect transistor-based biosensor. ACS Nano. https://pubs.acs.org/doi/10.1021/acsnano.0c02823

[111] Mackin C, Schroeder V, Zurutuza A, Su C, Kong J, Swager TM, Palacios T (2018) Chemiresistive graphene sensors for ammonia detection. ACS Appl. Mater. Interfaces 10:16169–16176.

[112] Luengas A, Barona A, Hort C, Gallastegui G, Platel V, Elias A (2015) A review of indoor air treatment technologies. Rev Environ Sci Biotechnol 14:499–522.

[113] Di Rosa AR, Leone F, Cheli F, Chiofalo V (2017) Fusion of electronic nose, electronic tongue and computer vision for animal source food authentication and quality assessment – A review. J. Food Eng. 210:62–75.

[114] Li Y, Wang B, Yu Z, Zhou X, Di Kang, Wu Y, Chen Z, He C, Zhou X (2017) The effects of central metals on ammonia sensing of metallophthalocyanines covalently bonded to graphene oxide hybrids. RSC Adv. 7:34215–34225.

[115] Karaduman I, Er E, Çelikkan H, Erk N, Acar S (2017) Room-temperature ammonia gas sensor based on reduced graphene oxide nanocomposites decorated by Ag, Au and Pt nanoparticles. J. Alloys Compd. 722:569–578.

[116] Chen Y, Zhang W, Wu Q (2017) A highly sensitive room-temperature sensing material for NH_3: SnO_2-nanorods coupled by rGO. Sens. Actuators, B 242:1216–1226.

[117] Song H, Li X, Cui P, Guo S, Liu W, Wang X (2017) Morphology optimization of CVD graphene decorated with Ag nanoparticles as ammonia sensor. Sens. Actuators, B 244:124–130.

[118] Kampara RK, Rai PK, Jeyaprakash BG (2018) Highly sensitive graphene oxide functionalized ZnO nanowires for ammonia vapour detection at ambient temperature. Sens. Actuators, B 255:1064–1071.

[119] Andre RS, Mercante LA, Facure MHM, Mattoso LHC, Correa DS (2019) Enhanced and selective ammonia detection using In_2O_3/reduced graphene oxide hybrid nanofibers. Appl. Surf. Sci. 473:133–140.

[120] Qin J, Gao J, Shi X, Chang J, Dong Y, Zheng S, Wang X, Feng L, Wu Z-S (2020) Hierarchical ordered dual-mesoporous polypyrrole/graphene nanosheets as bi-functional active materials for high-performance planar integrated system of micro-supercapacitor and gas sensor. Adv. Funct. Mater. 30:1909756.

[121] Lee SH, Eom W, Shin H, Ambade RB, Bang JH, Kim HW, Han TH (2020) Room-temperature, highly durable $Ti_3C_2T_x$ MXene/graphene hybrid fibers for NH_3 gas sensing. ACS Appl. Mater. Interfaces 12:10434–10442.

[122] Kim YH, Park JS, Choi Y-R, Park SY, Lee SY, Sohn W, Shim Y-S, Lee J-H, Park CR, Choi YS, Hong BH, Lee JH, Lee WH, Lee D, Jang HW (2017) Chemically fluorinated graphene oxide for room temperature ammonia detection at ppb levels. J. Mater. Chem. A 5:19116–19125.

[123] Heydari-Bafrooei E, Askari S (2017) Ultrasensitive aptasensing of lysozyme by exploiting the synergistic effect of gold nanoparticle-modified reduced graphene oxide and MWCNTs in a chitosan matrix. Microchim. Acta 184:3405–3413.

[124] Heydari-Bafrooei E, Shamszadeh NS (2017) Electrochemical bioassay development for ultrasensitive aptasensing of prostate specific antigen. Biosens. Bioelectron. 91:284–292.

[125] Rostamabadi PF, Heydari-Bafrooei E (2019) Impedimetric aptasensing of the breast cancer biomarker HER2 using a glassy carbon electrode modified with gold nanoparticles in a composite consisting of electrochemically reduced graphene oxide and single-walled carbon nanotubes. Microchim. Acta 186:495.

[126] Gong Q, Han H, Yang H, Zhang M, Sun X, Liang Y, Liu Z, Zhang W, Qiao J (2019) Sensitive electrochemical DNA sensor for the detection of HIV based on a polyaniline/graphene nanocomposite. J. Materiomics 5:313–319.

[127] Shahrokhian S, Salimian R (2018) Ultrasensitive detection of cancer biomarkers using conducting polymer/electrochemically reduced graphene oxide-based biosensor: application toward BRCA1 sensing. Sens. Actuators, B 266:160–169.

[128] Imran H, Manikandan PN, Dharuman V (2018) Graphene oxide supported liposomes for efficient label free electrochemical DNA biosensing. Sens. Actuators, B 260:841–851.

[129] Shamsipur M, Samandari L, Taherpour AA, Pashabadi A (2019) Sub-femtomolar detection of HIV-1 gene using DNA immobilized on composite platform reinforced by a conductive polymer sandwiched between two nanostructured layers: A solid signal-amplification strategy. Anal. Chim. Acta 1055:7–16.

[130] Jayakumar K, Camarada MB, Dharuman V, Ju H, Dey RS, Wen Y (2018) One-step coelectrodeposition-assisted layer-by-layer assembly of gold nanoparticles and reduced graphene oxide and its self-healing three-dimensional nanohybrid for an ultrasensitive DNA sensor. Nanoscale 10:1196–1206.

[131] Nagar B, Balsells M, La Escosura-Muñiz A de, Gomez-Romero P, Merkoçi A (2019) Fully printed one-step biosensing device using graphene/AuNPs composite. Biosens. Bioelectron. 129:238–244.

[132] Low SS, Loh H-S, Boey JS, Khiew PS, Chiu WS, Tan MTT (2017) Sensitivity enhancement of graphene/zinc oxide nanocomposite-based electrochemical impedance genosensor for single stranded RNA detection. Biosens. Bioelectron. 94:365–373.

[133] Xu S (2017) Electrochemical DNA biosensor based on graphene oxide- chitosan hybrid nanocomposites for detection of Escherichia Coli O157:H7. Int. J. Electrochem. Sci.:3443–3458.

[134] Jaiswal N, Pandey CM, Solanki S, Tiwari I, Malhotra BD (2019) An impedimetric biosensor based on electrophoretically assembled ZnO nanorods and carboxylated graphene nanoflakes on an indium tin oxide electrode for detection of the DNA of Escherichia coli O157:H7. Microchim. Acta 187:1.

[135] Zhang K, Zhang N, Zhang L, Wang H, Shi H, Liu Q (2018) Label-free impedimetric sensing platform for microRNA-21 based on ZrO_2 -reduced graphene oxide nanohybrids coupled with catalytic hairpin assembly amplification. RSC Adv. 8:16146–16151.

[136] Gong Q, Wang Y, Yang H (2017) A sensitive impedimetric DNA biosensor for the determination of the HIV gene based on graphene-Nafion composite film. Biosens. Bioelectron. 89:565–569.

[137] Benvidi A, Saucedo NM, Ramnani P, Villarreal C, Mulchandani A, Tezerjani MD, Jahanbani S (2018) Electro-oxidized monolayer CVD graphene film transducer for ultrasensitive impedimetric DNA biosensor. Electroanalysis 30:1791–1800.

[138] Mohanraj J, Durgalakshmi D, Rakkesh RA, Balakumar S, Rajendran S, Karimi-Maleh H (2020) Facile synthesis of paper based graphene electrodes for point of care devices: a double stranded DNA (dsDNA) biosensor. J. Colloid Interface Sci. 566:463–472.

[139] Xu D, Zhu C, Meng X, Chen Z, Li Y, Di Zhang, Zhu S (2018) Design and fabrication of Ag-CuO nanoparticles on reduced graphene oxide for nonenzymatic detection of glucose. Sens. Actuators, B 265:435–442.

[140] Liu J, Yang C, Shang Y, Zhang P, Liu J, Zheng J (2018) Preparation of a nanocomposite material consisting of cuprous oxide, polyaniline and reduced graphene oxide, and its application to the electrochemical determination of hydrogen peroxide. Microchim. Acta 185:172.

[141] Bosch-Navarro C, Rourke JP, Wilson NR (2016) Controlled electrochemical and electroless deposition of noble metal nanoparticles on graphene. RSC Adv. 6:73790–73796.

[142] Xuan X, Yoon HS, Park JY (2018) A wearable electrochemical glucose sensor based on simple and low-cost fabrication supported micro-patterned reduced graphene oxide nanocomposite electrode on flexible substrate. Biosens. Bioelectron. 109:75–82.

[143] Wang B, Wu Y, Chen Y, Weng B, Li C (2017) Flexible paper sensor fabricated via in situ growth of Cu nanoflower on RGO sheets towards amperometrically non-enzymatic detection of glucose. Sens. Actuators, B 238:802–808.

[144] Lee C-S, Yu SH, Kim TH (2017) One-step electrochemical fabrication of reduced graphene oxide/gold nanoparticles nanocomposite-modified electrode for simultaneous detection of dopamine, ascorbic acid, and uric acid. Nanomaterials 8.

[145] Lin S, Feng W, Miao X, Zhang X, Chen S, Chen Y, Wang W, Zhang Y (2018) A flexible and highly sensitive nonenzymatic glucose sensor based on DVD-laser scribed graphene substrate. Biosens. Bioelectron. 110:89–96.

[146] Shabnam L, Faisal SN, Roy AK, Haque E, Minett AI, Gomes VG (2017) Doped graphene/Cu nanocomposite: a high sensitivity non-enzymatic glucose sensor for food. Food Chem. 221:751–759.

[147] Zhang Y, Lei W, Wu Q, Xia X, Hao Q (2017) Amperometric nonenzymatic determination of glucose via a glassy carbon electrode modified with nickel hydroxide and N-doped reduced graphene oxide. Microchim. Acta 184:3103–3111.

[148] Zheng W, Hu L, Lee LYS, Wong K-Y (2016) Copper nanoparticles/polyaniline/graphene composite as a highly sensitive electrochemical glucose sensor. J. Electroanal. Chem. 781:155–160.

[149] Di Geng, Bo X, Guo L (2017) Ni-doped molybdenum disulfide nanoparticles anchored on reduced graphene oxide as novel electroactive material for a non-enzymatic glucose sensor. Sens. Actuators, B 244:131–141.

[150] Thanh TD, Balamurugan J, Hwang JY, Kim NH, Lee JH (2016) In situ synthesis of graphene-encapsulated gold nanoparticle hybrid electrodes for non-enzymatic glucose sensing. Carbon 98:90–98.

[151] Wei S, Hao Y, Ying Z, Xu C, Wei Q, Xue S, Cheng H-M, Ren W, Ma L-P, Zeng Y (2020) Transfer-free CVD graphene for highly sensitive glucose sensors. J. Mater. Sci. Nanotechnol. 37:71–76.

[152] Aparicio-Martínez E, Ibarra A, Estrada-Moreno IA, Osuna V, Dominguez RB (2019) Flexible electrochemical sensor based on laser scribed graphene/Ag nanoparticles for non-enzymatic hydrogen peroxide detection. Sens. Actuators, B 301:127101.

[153] Lu Z, Wu L, Zhang J, Dai W, Mo G, Ye J (2019) Bifunctional and highly sensitive electrochemical non-enzymatic glucose and hydrogen peroxide biosensor based on $NiCo_2O_4$ nanoflowers decorated 3D nitrogen doped holey graphene hydrogel. Mater. Sci. Eng., C 102:708–717.

[154] Amanulla B, Palanisamy S, Chen S-M, Velusamy V, Chiu T-W, Chen T-W, Ramaraj SK (2017) A non-enzymatic amperometric hydrogen peroxide sensor based on iron nanoparticles decorated reduced graphene oxide nanocomposite. J. Colloid Interface Sci. 487:370–377.

[155] Zhang Y, Duan Y, Shao Z, Chen C, Yang M, Lu G, Xu W, Liao X (2019) Amperometric hydrogen peroxide sensor using a glassy carbon electrode modified with a nanocomposite prepared from ferumoxytol and reduced graphene oxide decorated with platinum nanoparticles. Microchim. Acta 186:386.

[156] Yuan Y, Zheng Y, Liu J, Wang H, Hou S (2017) Non-enzymatic amperometric hydrogen peroxide sensor using a glassy carbon electrode modified with gold nanoparticles deposited on CVD-grown graphene. Microchim. Acta 184:4723–4729.

[157] Wang J, Sun H-b, Pan H-y, Ding Y-y, Wan J-g, Wang G-h, Han M (2016) Detection of hydrogen peroxide at a palladium nanoparticle-bilayer graphene hybrid-modified electrode. Sens. Actuators, B 230:690–696.

[158] Dau TNN, Vu VH, Cao TT, van Nguyen C, Ly CT, Tran DL, Pham TTN, Loc NT, Piro B, Vu TT (2019) In-situ electrochemically deposited Fe_3O_4 nanoparticles onto graphene nanosheets as amperometric amplifier for electrochemical biosensing applications. Sens. Actuators, B 283:52–60.

[159] Hsu S-Y, Lee C-L (2017) Sonoelectrochemical exfoliation of highly oriented pyrolytic graphite for preparing defective few-layered graphene with promising activity for non-enzymatic H_2O_2 sensors. Microchim. Acta 184:2489–2496.

[160] Velický M, Toth PS (2017) From two-dimensional materials to their heterostructures: an electrochemist's perspective. Appl. Mater. Today 8:68–103.

[161] Kauling AP, Seefeldt AT, Pisoni DP, Pradeep RC, Bentini R, Oliveira RV, Novoselov KS, Castro Neto AH (2018) The worldwide graphene flake production. Adv. Mater. 44:1803784.

[162] Batra G, Santhanam N, Surana K (2018) Graphene: The next S-curve for semiconductors? https://www.mckinsey.com/industries/semiconductors/our-insights/graphene-the-next-s-curve-for-semiconductors. Accessed June 02 2020

2. Aim of the work

Graphene is on a remarkable journey ever since it has found its way into science around 15 years ago. Principally, "a single carbon layer of the graphite structure, describing its nature by analogy to a polycyclic aromatic hydrocarbon of quasi infinite size" [1], has made a name for itself, due to the prosperity of exceptional physicochemical properties, combined in one material. It even reached the stage that the European Community funded the Graphene Flagship in 2013, with over 150 partners in 23 countries sharing a budget of 1 billion € for 10 years. The mission is proclaimed to "take technologies based on graphene and related materials from the laboratory to commercial applications" [2].

The consortium of the Graphene Flagship proposed that biosensors would be one of the first applications, which reach the market at an expected date of 2018. Up to now, this goal was not reached so far despite the fact there are already many publications reporting on electrochemical biosensors based on graphene, demonstrating the outstanding potential of this material. Nevertheless, there are still major hurdles on the way to an application: a) the fabrication of the material in a defined quality still is challenging; b) characterization techniques and standardization need to be improved to make work comparable; c) the transfer of the material on any substrate is still in its infancy.

Motivated by this, this thesis investigates graphene prepared by different methods, transferred to semiconductor substrates, as electrode material. As flake size, defects, and topography of the electrode surface plays a crucial role a thorough characterization of the interface is needed with the aim to get a better understanding of the electrolyte-graphene interface for the development of electrochemical sensors.

2.1   References

[1] Fitzer E, Kochling KH, Boehm HP, Marsh H, (1995) Recommended terminology for the description of carbon as a solid (IUPAC Recommendations 1995). Pure & Appl. Chem., 67:473-506.

[2] Fodgen S, Waters R, (2018) Graphene Flagship Annual Report 2018 https://graphene-flagship.eu/SiteCollectionDocuments/Admin/Annual%20report/Graphene%20Flagship%20Annual%20Report%202018.pdf Accessed May 29 2020

3. Control of the Graphene Electrode by the Synthesis and Transfer of the 2D Carbon Material

3.1   Abstract

The numerous exfoliation techniques available to fabricate graphene lead to materials, which significantly differ in their physical properties due to structural variations derived from the preparation method. A comparison of chemical vapor deposited graphene (cvdG), mechanically exfoliated graphene (meG), electrochemically exfoliated graphene (ecG) and chemically synthesized reduced graphene oxide (rGO) on their performance in their electrochemistry derived in a trend in their classification, which is in accordance to the characteristics of such materials in Raman spectroscopy. Cyclic voltammetry studies as well as electrochemical impedance spectroscopy provide an understanding about the heterogeneous electron transfer between the electrode-analyte interface as well as the charge transfer resistance of the graphene compounds. An anisotropic effect in the in- and out-of-plane charge decelerate the electrochemical properties of multilayered non-defective two-dimensional materials. The fast electron transfer with a peak separation of (143 ± 19) mV between analyte and electrode material as well as the low charge transfer resistance (R_{CT} = 0.051 ± 0.011) kΩ cm^2 reveal hydrophilic reduced graphene oxide as best applicable material for electrode-analyte interaction in aqueous environment.
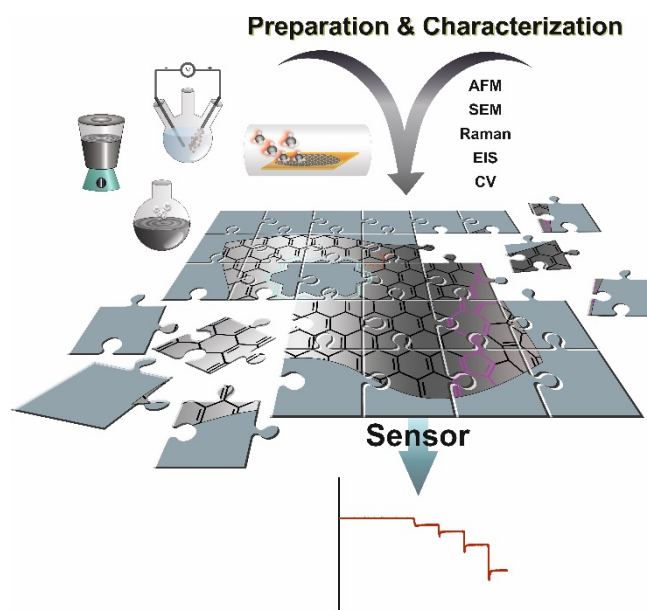
Figure 3.1: Graphical abstract for the impact of graphene structure on analyte-electrode mediated electrochemical applications in aqueous medium.

This chapter was submitted on June 7th, 2020 to Advanced Materials Interface (WILEY-VCH, Weinheim).

Author contributions

This manuscript was authored by Eva-Maria Kirchner (EMK) and Thomas Hirsch (TH). This study was conceived and designed by TH and EMK. Most of the experimental work was carried out by EMK. The manuscript was written by EMK and revised by TH, who is the corresponding author.

3.2   Introduction

Two primarily goals are dominating the development of chemical and biosensors: sensitivity and selectivity. Electrochemical sensors which allow cheap transduction, simple miniaturization or easy handling, rely on fully understanding the interface between transducer and the real world containing the analyte, where the analytical signal is generated. Therefore, tremendous research is attributed to the development of electrodes providing highly sensitivity and selectivity but also with resistance against surface fouling, possibilities for functionalization, chemical stability and reversibility [1-4]. Carbon materials are outstanding in many of these needs, especially the 2D materials, due to high surface area, rapid heterogeneous electron transfer, wide potential windows, and plethora of functionalization strategies [5-9]. In nano-dimensions, the classification of a material becomes complicated attributed to the fact that number of layers, flake size, defects, or impurities, have a massive impact on the properties of graphene materials [10]. Common disorders are oxygen residues, structural disorders like holes, vacancies and grain boundaries, depicted in Figure 3.2. In almost all practical applications not dealing with a single graphene flake obtained by the scotch-tape method [11], the structure of the obtained materials is quite different to the theoretically quasi-infinite, monocrystalline, one-atom thick carbon layer of "graphene" [12].
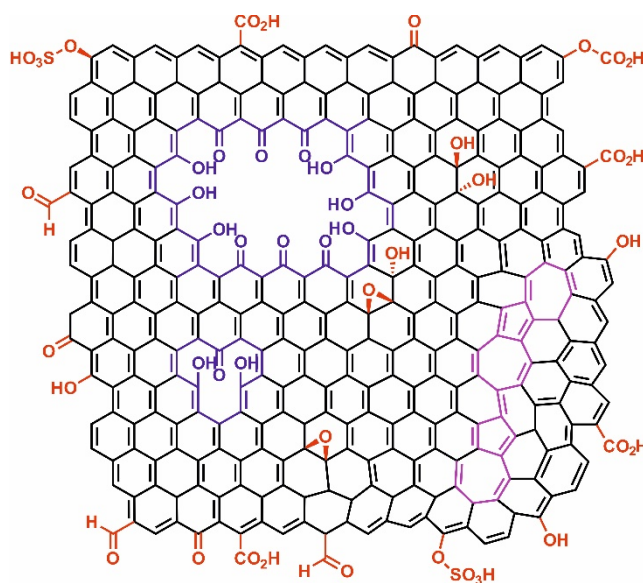

Figure 3.2: Chemical structure of a graphene with oxygen defects (red), Structural defects (blue), *i.e.* vacancies and holes as well as grain boundaries (pink).

This results in a subcategorization of two-dimensional carbon materials to their numerous exfoliation routines, either based on bottom-up synthesis, where small units form larger constructs, *i.e.* chemical vapor deposition, or top-down approach, where graphene is produced by decomposition of graphite into its individual flakes in liquid dispersion, *i.e.* chemical synthesis, electrochemically or by mechanical exfoliation in dispersion [13,14]. The variety of growth and delamination processes lead to highly divergent graphene allotropes [15]. These are in a range from monocrystalline and non-defective materials to polycrystalline, highly defective materials. Graphene's electrochemical properties are highly affected by its surface chemistry with present defects, induced intentionally or unintentionally, which are advantageous compared to high quality carbon materials. Nevertheless, variations on the electrochemical behavior can be expected according to different experimental procedures applied during material preparation [15,16]. So far only limited attention is attributed in sensor development to the fact that differently prepared and transferred graphene may result in different properties, most often only the excellent properties of an individual perfect single graphene are highlighted as motivation. This is often far away from the real situation as there are tremendous differences. The high-quality representatives, such as graphene prepared by chemical vapor deposition (cvdG) requires a complicated transfer which is prone to post-introduction of defects [17]. In contrast, top-down exfoliated materials seem to be processed easier as they can be formulated in stable dispersions but are suffering from small flake sizes and numerous of defects. Such differences in quality and structure demand a good understanding and characterization of 2D carbon materials. So far, a fast and powerful way to structurally characterize the material is statistical Raman analysis, which clearly distinguishes between the number of layers and number of defects of graphene materials [18-20]. This is a promising way to evaluate, compare and classify the members of the graphene-like materials. On the other hand, for electrochemical applications not only structural parameters are important and therefore the question arises if the sensing-related electrochemical properties can be aligned to the structural analysis given by the statistical Raman microscopy.

Motivated by the numerous of different possibilities to synthesize 2D carbon materials, this work intends to complete the picture of the structure related electrochemical properties of graphene materials. Electrodes fabricated from dispersions of 2D carbon materials prepared by chemical, electrochemical, and mechanical exfoliation have been thoroughly compared in their electrochemical properties to electrodes modified by monolayer graphene transferred *via* a wet etching process from cvdG grown on copper. The electrochemical results correlate with the defects of the material, surface roughness and wettability of the modified electrodes as confirmed by Raman spectroscopy, AFM and contact angle measurements. As a consequence, in amperometric determination of hydrogen peroxide, an endogenously produced molecule, which plays a key role in many biological processes, electrodes modified with different graphene materials show different performance. From the data obtained from the thorough characterization of the electrode interface one can conclude that it is of great importance how the electrode material was prepared and transferred. On a wider perspective this knowledge of the contribution of physicochemical features of the electrode surface enables a control of the electrode properties which fit best to an analytical application.

3.3   Results and Discussion

3.3.1 Mechanically Exfoliated Graphene

Mechanically exfoliated graphene (meG) is prepared by shear exfoliation of graphite, which stresses the graphite flakes upon the formation and implosion of micro jets and the random collision [21]. One of the challenges for this method is the choice of an appropriate solvent to successfully delaminate graphene flakes from graphite precursor material and to stabilize the exfoliated flakes. N-methyl-2-pyrrolidone (NMP) has been chosen as dispersant, as its surface tension of around 40 mJ m^{-2} matches almost perfectly the surface energy of graphene [22]. Mechanical exfoliation does not introduce lattice defects or oxygen moieties into the carbon lattice [23,24]. Dynamic light scattering was applied to obtain the flake size from the Brownian motion of the flakes in a water-NMP mixture. Especially for 2D materials one has to keep in mind that the hydrodynamic diameter obtained by such measurements represents the size of a sphere showing the same diffusion properties compared to the investigated object. Therefore, the hydrodynamic diameter should not be correlated as an exact flake size but gives a good measure to compare dispersed 2D carbon materials fabricated by different techniques [25]. Mechanically exfoliated graphene exhibits an average hydrodynamic diameter of (202 ± 3) nm with a polydispersity index (PDI) of 0.23 ± 0.04 as shown in Figure 3.3. In a 9:1 (v:v) mixture of NMP and water meG is negatively charged as displayed by a ζ-potential of (-16.9 ± 0.9) mV.

3.3.2 Electrochemically Exfoliated Graphene

The electrochemical exfoliation of graphite is performed by dipping two graphite rods into aqueous $(NH_4)_2SO_4$ (0.1 M). A potential of 10 V applied to the graphite rods causes the oxidation of water, forming hydroxyl and oxygen ions and radicals, which oxidize edge-planes and grain boundaries of the graphite anode [26,27]. The expansion of layers facilitates the intercalation of SO_4^{2-} ions and water molecules. A gas evolution indicates the formation of SO_2 and O_2 applying force on the graphite layers tearing weakly bonded layers apart [26,27]. A dispersion of ecG exhibits a ζ-potential of (-17.9 ± 0.4) mV and an average size of (363 ± 5) nm with a PdI = 0.25 ± 0.005 (Figure 3.3). The average flake size

of ecG is slightly larger compared to meG, yet the ζ-potential is nearly the same. The comparison of one single flake of ecG to meG, assumes that a larger flake exposes a higher total number of carbon atoms located at the border. The almost identical ζ-potentials of both types of graphene at identical mass concentrations implies that more oxygen-containing moieties should be present at meG [28]. As a consequence, it seems that only a low number of oxygen-containing groups would be introduced into ecG during exfoliation, which is consistent with literature data as Parvez *et al.* reported a C/O ratio of 12.3-17.2 for ecG and a C/O-ratio of ≈ 8 for shear exfoliated graphene [26,27,29].

3.3.3 Chemically Exfoliated Graphene

Chemically exfoliated graphene was prepared by the chemical reduction of graphene oxide obtained by a modified Hummers method. A dispersion of rGO in water shows a negative surface charge of -33 ± 0.4 mV attributed to negatively charged groups attached to the surface. The average hydrodynamic diameter of (196 ± 4) nm (PdI = 0.21 ± 0.01) (Figure 3.3) is almost identical compared to meG but the surface charge is double that negative. Mechanically exfoliated graphene is of a similar size as rGO.
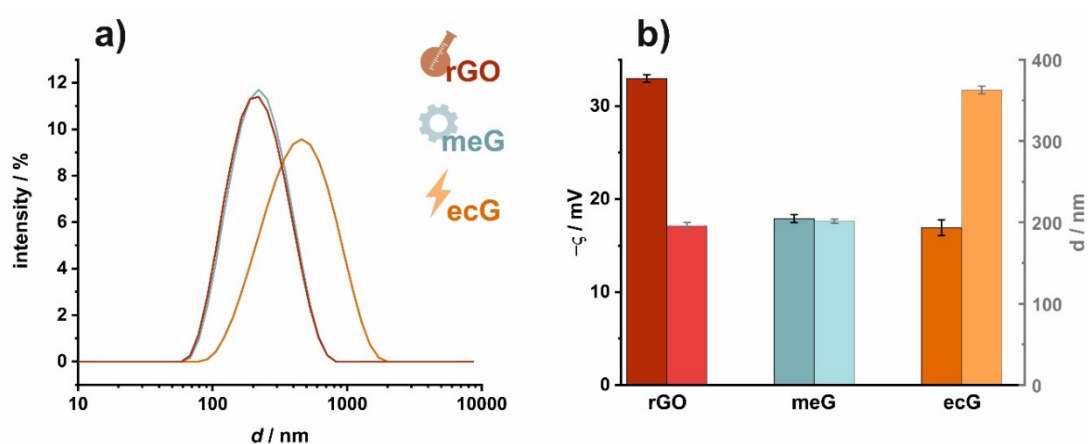

Figure 3.3: Intensity weighted particle size distribution for rGO (red, 0.05 mg mL^{-1}), meG (green, 0.01 mg mL^{-1}) and ecG (orange, 0.01 mg mL^{-1}) measured by dynamic light scattering of the graphene dispersions in a water-NMP mixture (9:1)$_{v/v}$ (a) (n=3). The flake size distribution of rGO and meG is almost identical. A larger particle size distribution with increased averaged size was found for ecG. Column diagram of the zeta potential (darker shading) and particle size distribution (lighter shading) of rGO, meG and ecG (b).

3.3.4 Electrode Fabrication

The negative ζ-potentials of aqueous meG, ecG and rGO dispersions indicate sufficient colloidal stability of all aqueous dispersions. This is an important prerequisite for the development of reproducible methods to apply 2D carbon nanomaterials onto a substrate, which can further be used as an electrode in bioanalytical applications. The deposition of the different carbon nanomaterials as a homogeneous thin film onto the electrodes is still challenging. Simple drop-casting or spin-coating processes does not result in reproducible coherent layers of for meG and ecG, therefore alternative deposition strategies have been developed for those materials (Figure 3.4).
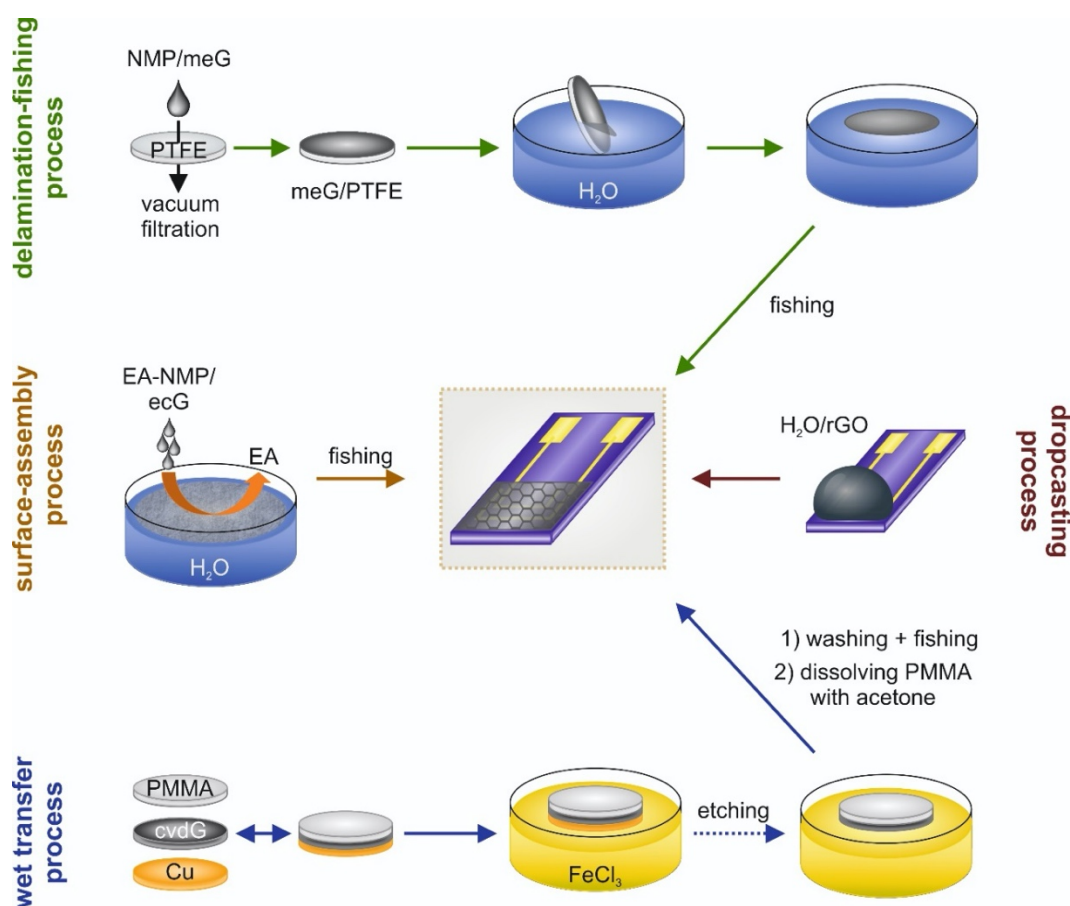

Figure 3.4: Overview of the deposition schemes applied in this work to generate electrodes of 2D carbon materials. The delamination-fishing-process describes the transfer of meG via a polytetrafluoroethylene (PTFE) membrane. The meG/PTFE is placed on a thin solid support, immersed perpendicularly into a water bath, causing a delamination of a meG layer due to weak adhesion. The floating meG layer is fished by the substrate of choice. The surface-assembly forsakes an ethyl acetate (EA)/NMP-ecG dispersion to spread across the water surface forming a self-assembled-graphene film, which can be fished off by the electrode. A drop-casting of an aqueous rGO dispersion is followed by solvent evaporation. For the wet transfer of cvdG, an aqueous FeCl$_3$ solution etches the copper support. The cvdG/poly(methyl methacrylate) (PMMA) layer was fished by the substrate, followed by a dissolution of PMMA in acetone.

An established wet transfer was applied to deposit cvdG on the substrate [30]. First, the copper layer needs to be removed before the material can be deposited to a new substrate. Poly(methyl methacrylate) (PMMA) is deposited on the graphene to allow an etching of the copper in an acidic solution of $FeCl_3$ without destroying the graphene sheet. Thorough washing is necessary to avoid any contamination with iron adatoms as well as ionic impurities of the metallic support [30]. Raman microscopy revealed that the wet transfer technique results in cvdG modified substrates free from cracks within the carbon structure. Yet, formation of wrinkles within the structure cannot be avoided [17]. Drop casting of NMP-dispersed materials form inhomogeneous layers upon slow solvent evaporation for meG and ecG (Figure 3.5a).
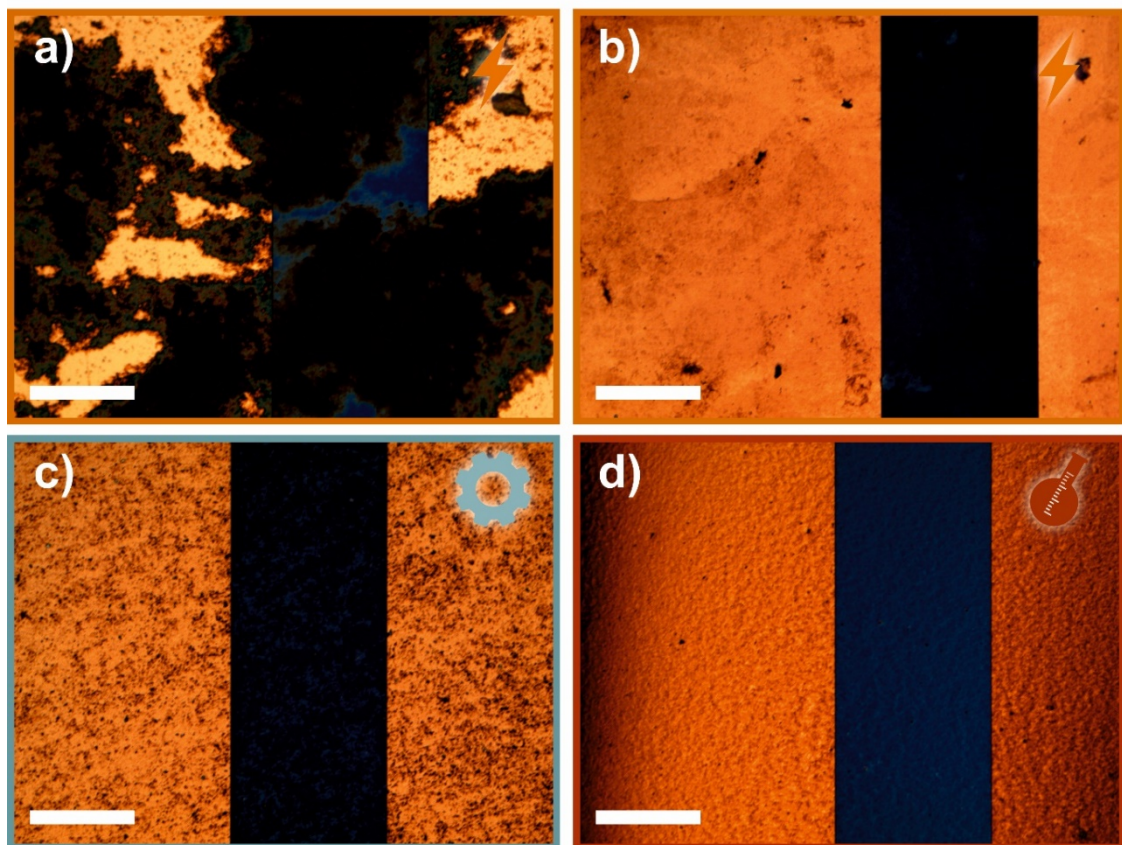

Figure 3.5: Light microscopy images of drop casted ecG deposited onto a Au/SiO₂-electrode (a). Besides a thin layer deposition, aggregates formed upon solvent evaporation. The alternative surface-assembly techniques overcome the aggregation of graphene forming a coherent ecG layer (b). Comparison to liquid-processed meG (c) and rGO (d) deposited via deposition-fishing and drop-casting, respectively. Scale bars are 100 μm.

Instead of optimizing the slow evaporation process by using different solvent mixtures, temperatures, etc., a pre-deposition step stabilizing the graphene layer on a temporary

substrate was applied. The meG/NMP dispersion is filtrated through a solvent-resistant PTFE membrane to generate a graphene film, which delaminates upon vertical immersion in water forming a floating graphene film, which is fished off by the substrate used as electrode. The transfer of ecG requires an alternative deposition process. Upon delamination of the graphene film into the water bath, no uniform layer is observed. The graphene film broke apart into small pieces, which is assumed to correlate to the lower amount of oxygen functionalities present at the edges of ecG, which would favor a superimposition of the flakes. Ethyl acetate was added to the NMP dispersion ($(1:2)_{v/v}$) and carefully dropped onto the water surface until a homogeneous carbon layer is formed upon solvent spreading as ethyl acetate is moderately miscible with water forming a thin sublayer [31]. The aqueous dispersion of rGO is simply drop-casted to form a coherent carbon layer on interdigitated gold electrodes on a silicon wafer.

3.3.5 Electrode Characterization

The topography of graphene-covered electrodes was investigated by scanning electron microscopy (SEM) (Figure 3.6). Electrodes modified by cvdG do not exhibit any edges or cracks over a wide range, which indicate a successful transfer of a graphene monolayer. Mechanically exfoliated graphene shows small, individual sharp edge terminated flakes, covering completely the surface. In contrast, the ecG smoothly cover the substrate with large flakes, which tend to fold upon deposition. Reduced graphene oxide forms a dense packed layer of numerous small flakes.
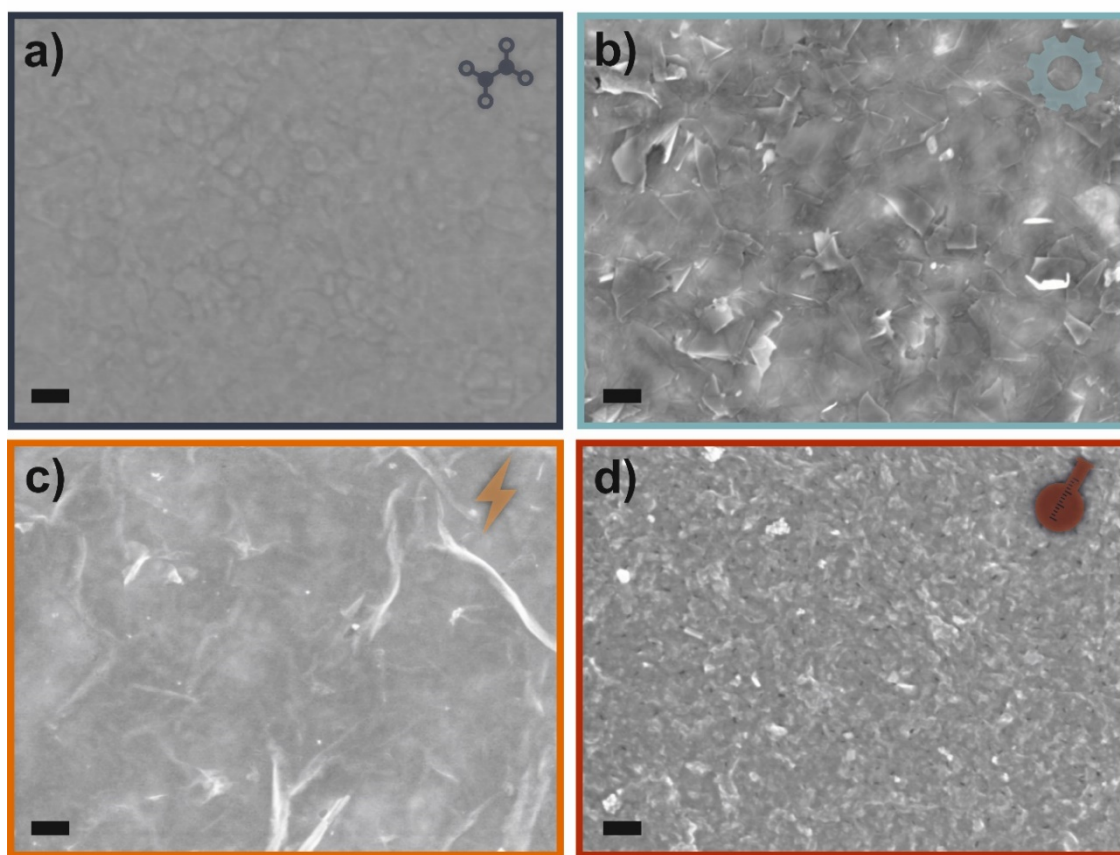
Figure 3.6: Scanning electron microscope images of cvdG (a), meG (b), ecG (c), and rGO (d) modified gold microelectrodes to investigate the surface morphology. Scale bars are 200 nm.

A more detailed insight to the morphology of the electrode surface was achieved by atomic force microscopy. The results complete the picture to the expectations from the characterization of the dispersions by DLS. Even if it is impossible to observe individual flakes due to the roughness of the polycrystalline gold electrode, which dealt as substrate, the deviations in the height of the individual electrodes reveal a smooth surface for cvdG (Figure 3.7). The height fluctuation, estimated from three individual line scans of each sample for the bare gold film of the electrode with a roughness, calculated as arithmetic mean of the absolute vertical distances from the mean line, is $R_a = (2.7 \pm 0.4)$ nm. This value increases only slightly to $R_a = (3.2 \pm 1.5)$ nm for cvdG. The further increase from ecG ($R_a = (6.3 \pm 1.3)$ nm) *via* meG ($R_a = (14.2 \pm 4.3)$ nm) to rGO ($R_a = (14.4 \pm 4.5)$ nm) resembles the decrease in the individual flake sizes.
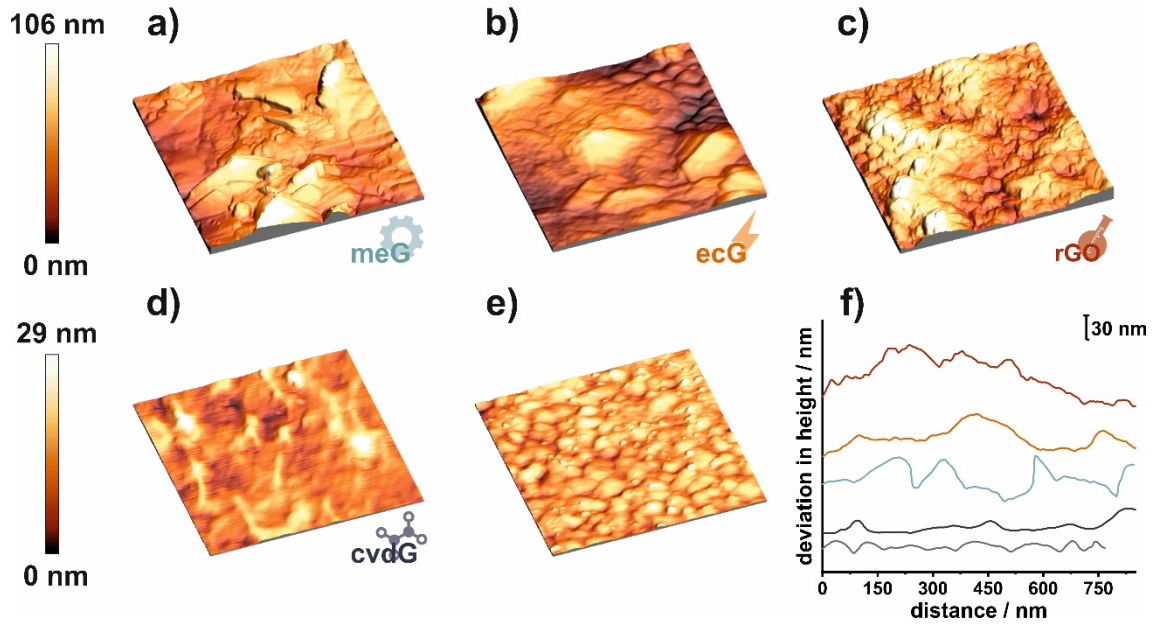
Figure 3.7: Atomic force microscopy images of meG (a), ecG (b), rGO (c), cvdG (d), modified gold electrodes and the unmodified gold electrode (e, grey), to investigate the surface morphology with corresponding changes in the height over a distance of about 800 nm shown exemplarily for one line scan (f).

It is observed that cvdG keeps a relatively flat surface with some wrinkles. In contrast, dispersed graphene samples form rougher carbon layers attributed to a multiple flake arrangement. A closer look to the images exhibits sharp edges for meG, whereas ecG distributes softer edges upon transfer procedure. Characteristics of many height fluctuations with only small amplitude are in accordance to the small flakes for rGO-modified surfaces.

Raman spectroscopy gives a deeper insight to the materials as there are in-plane vibrations, shear modes and layer-breathing modes, which are very characteristic for this class of materials [32,33]. Qualitatively, the height of the D/G peak ratio correlates with the number of defects within the structure of the nanomaterial. The intensity of the 2D peak provides information on the number of stacked carbon layers, whereas the full width at half maximum of the 2D peak is assigned to the amount of structural disorder [18]. The I_D/I_G-peak ratio and full width at half maximum of the 2D peak ($FWHM_{2D}$) resembles the relative amount of lattice defects, *i.e.* point defects, vacancies, grain boundaries, edge sites etc. [34].

Figure 3.8 compares the Raman spectra of cvdG, meG, ecG and rGO modified electrodes. The intensity ratios of D/G-peak and 2D/G-peak, the half width at full maximum of the 2D-peak, the correlating crystallite sizes, and defect distribution of each carbon compound are summarized in Table 3.1. Two distinct and narrow peaks, the G- and 2D-peaks are present in the Raman spectrum of cvdG. The corresponding values of the I_D/I_G-peak ratio is 0.073 ± 0.025 and the full width at half maximum of the 2D peak (FWHM$_{2D}$) is (37.7 ± 3.8) cm^{-1}. This indicates that the cvdG layer is nearly free from structural defects. The intense 2D-peak proves cvdG graphene as a monolayer lacking structural defects and active-edge sites. In the Raman spectrum for meG, the D-peak appeared, leading to an increase in the peak ratio of I_D/I_G = 0.51 ± 0.01. The intensity of the 2D-peak decreased accompanied by a peak broadening indicated by FWHM$_{2D}$ = (75.5 ± 1.32) cm^{-1}. Shear forces stress the graphite precursor during the mechanical exfoliation process, introducing defects within the material upon delamination to a few-layered graphene material. The D/G-peak ratio of 1.35 ± 0.014 and a FWHM$_{2D}$ of (98.9 ± 1.98) cm^{-1} indicates that electrochemical exfoliation yields few-layered graphene, with a high number of defects distributed along its surface. The weak peak at 1135 cm^{-1}, solely apparent in ecG, can be attributed to trans-polyacetylene segments at grain boundaries of carbon surfaces [35].

Reduced graphene oxide exhibits a Raman spectrum with obviously broadened peaks, a peak ratio of I_D/I_G = 1.14 ± 0.005 and broad FWHM$_{2D}$ = (218 ± 4.9) cm^{-1}. The almost vanished 2D-peak for rGO can be ascribed to multilayer. The change of the spectrum's shape is attributed to the defects, *e.g.* structural irregularities stabilized by oxygen moieties. Equation 3.1 and Equation 3.2 determine the crystallite size L$_a$ and the defect density n$_D$ [36,37].

$$L_a[nm] = 2.4 \cdot 10^{10} \cdot \lambda_{laser}^4 \cdot \frac{I_G}{I_D} \qquad (3.1)$$

$$n_D\,[cm^{-2}] = \frac{(1.8 \pm 0.5) \cdot 10^{22}}{\lambda_{laser}^4} \cdot \frac{I_D}{I_G} \qquad (3.2)$$

The low number of structural irregularities found for the monolayer of cvdG in Raman spectroscopy is in accordance to the findings for AFM and SEM, as the materials exhibits a smooth, transparent surface. With the decrease of the flake size from a large, single-layer of graphene, to smaller few-layered to multi-layered flakes, deposited as a compact, rough film onto the substrate as revealed by microscopy imaging, the I_D/I_G ratio increased and 2D peak intensity decreased for meG, ecG and rGO. Raman examinations of rGO revealed it the most defective material compared to its graphene allotropes, which is coherent to the lowest Zeta potential, induced by charged oxygen functionalities. Apparently, the introduction of defects is inevitable by an exfoliation procedure of graphene in liquid phase. The crystallite size decreases, and the defect distribution increases by a factor of 7 for meG and 16 to 20 for rGO and ecG compared to cvdG. Solely considering the D/G-peak ratio, the model to describe the crystallite size and defect distribution may not be well adapted for rGO. Apparently, with exceeding number of defects, the intensity of D-peak starts to decrease accompanied by peak broadening, as displayed by the Raman spectrum of rGO. The impact of the surface topology and chemical structure upon the wettability of the carbon nanomaterials was investigated by sessile drop contact angle measurements using phosphate buffer, which resembles a typical electrolyte solution used for electroanalytical studies. The smooth cvdG graphene dominated by non-polar carbon lattice shows the highest value of $(114 \pm 6.8)°$ demonstrating its hydrophobicity. The contact angle decreased for more defective materials. Mechanically derived graphene exhibits a lower contact angle of $(89.2 \pm 1.0)°$. The edge-defects contain polar oxygen moieties leading to a better wettability of meG but the hydrophobic sp^2-carbon domains still outweigh the polar groups located at the edges of meG resulting in a high contact angle. A more hydrophilic behavior is shown for structural deteriorated materials like ecG $(74.6 \pm 3.2)°$ and rGO $(69.6 \pm 10.3)°$ (Figure 3.8b).
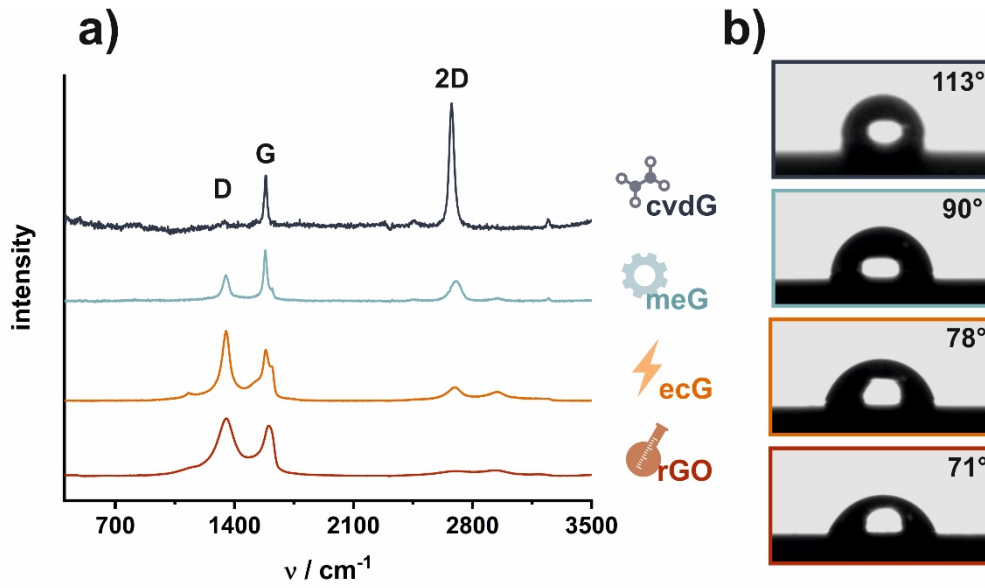
Figure 3.8: Raman spectra recorded at 532 nm for rGO (red), ecG (orange), meG (turquoise), and cvdG (blue) modified electrodes normalized to the intensity of their G-peak, respectively (a). Corresponding images of contact angle measurements depositing 0.2 µL phosphate buffer (10 mM Na_2HPO_4 / NaH_2PO_4, 0.1 M NaCl, pH 7.4) (b).

Table 3.1: D/G peak- and 2D/G peak- ratios, the full width at half maximum of the 2D peak and topological properties of the graphene materials investigated by Raman spectroscopy with regard to the crystallite size L_a and defect density n_D. Raman spectroscopy was performed using a 532 nm laser excitation with a power of 8 mW and a 50 µm slit (n = 24). Equations 3.1 and 3.2 have been used for the calculation of the crystallite size L_a and defect density n_D.

	I_D/I_G	I_{2D}/I_G	$FWHM_{2D}$ [cm^{-1}]	L_a [nm]	$n_D \cdot 10^{10}$ [cm^{-2}]
rGO	1.14 ± 0.005	0.09 ± 0.006	218 ± 4.70	17 ± 0.073	26 ± 0.1
ecG	1.35 ± 0.014	0.26 ± 0.005	98.9 ± 1.98	14 ± 0.16	30 ± 0.3
meG	0.51 ± 0.03	0.39 ± 0.040	75.5 ± 1.32	38 ± 1.0	11 ± 0.3
cvdG	0.073 ± 0.025	2.18 ± 0.53	37.7 ± 3.80	279 ± 88	1.6 ± 0.5

Upon meG exfoliation, it was assumed, that with enhanced exfoliation speed the number of stacked graphene sheets decreases even though the flake size might become smaller. The rotation speed was increased from 6,000 rpm to 9,000 rpm to exfoliate graphene mechanically. The enhanced number of edge-defects is emphasized by an increased value of $I_D/I_G = 1.19 \pm 0.02$ and broadened $FWHM_{2D} = (108 \pm 8.89)$ cm^{-1} shown in Figure 3.9. With increasing exfoliation speed the flake size decreased. Contrary to the former assumption, the 2D peak of meG$_{9k}$ is less intense compared to meG$_{6k}$ indicating

that with increased exfoliation speed the flakes rather break apart upon applied stress and flake collision than to become sufficiently delaminated.
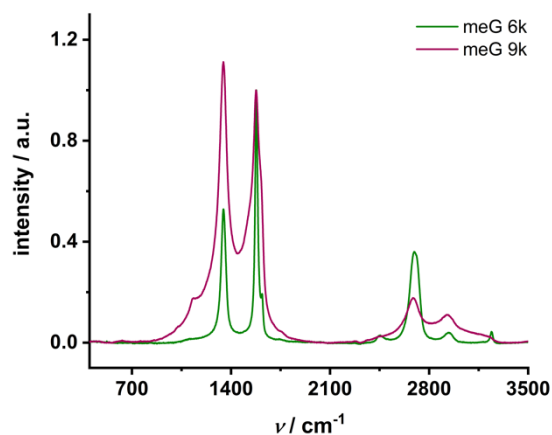

Figure 3.9: Raman spectra for mechanically exfoliated graphene normalized to its G-peaks yielded by an exfoliation speed of 6,000 rpm and 9,000 rpm, respectively. The spectra were recorded at 532 nm.

The coverage of the electrodes by the 2D carbon nanomaterials was characterized by Raman microscopy and an even distribution was found over large areas for all types (Figure 3.10).
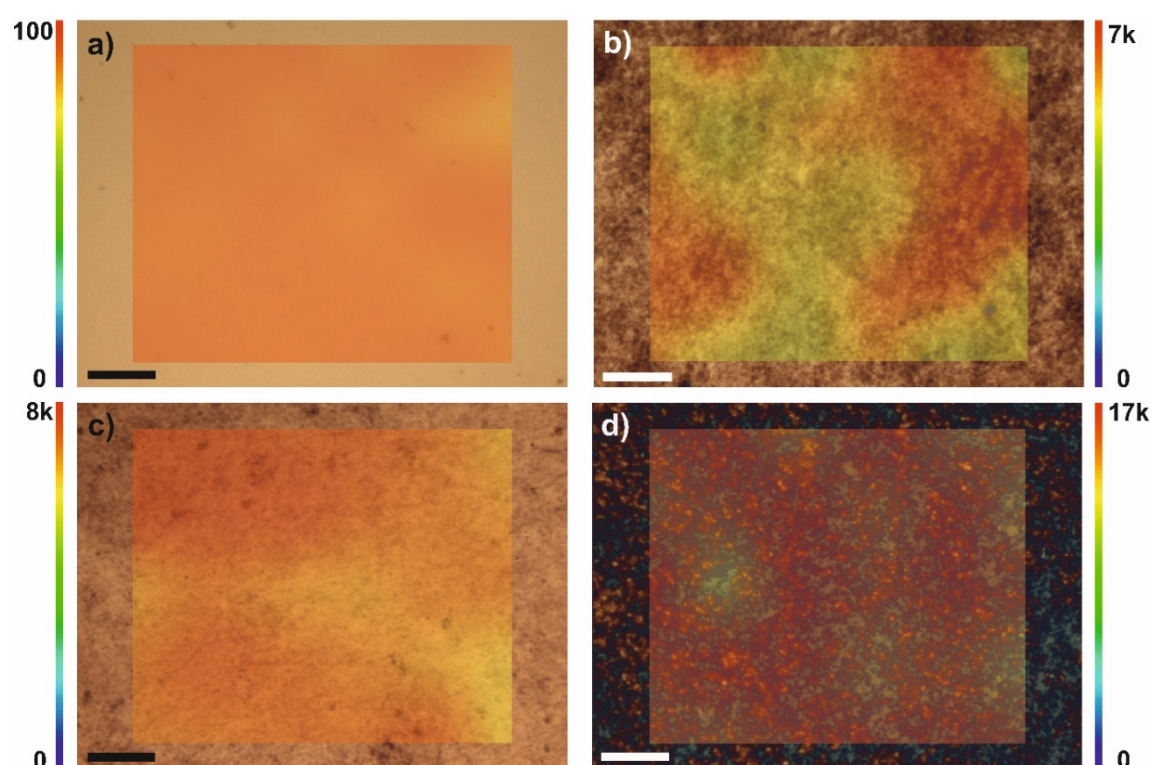
Figure 3.10: Microscopic image of a gold electrode modified with cvdG (a), meG (b), ecG (c) and rGO (d). A 2D intensity map of the G-peak for each material is blended over the microscopic images of the modified electrodes. The scale bars are 20 μm.

A comparison of the individual Raman spectra of the graphene modified electrodes demonstrate a successful transfer or deposition of all kind of materials without any residues or impurities left, neither from the precursors nor from any solvent used for the transfer (Figure 3.11).

Figure 3.11: Raman spectra of solvents and educts used for dispersion and deposition, intercalants and precursor materials.

3.3.6 Electrochemical Properties

The electroactive surface area of each electrode was determined from cyclic voltammetric measurements in the presence of 5 mM redox marker ($[Ru(NH_3)_6]Cl_3$ or $K_3[Fe(CN)_6]$) at various scan rates (Figure 3.12). The Randles-Sevcik equation (Equation 3.3) allows the calculatio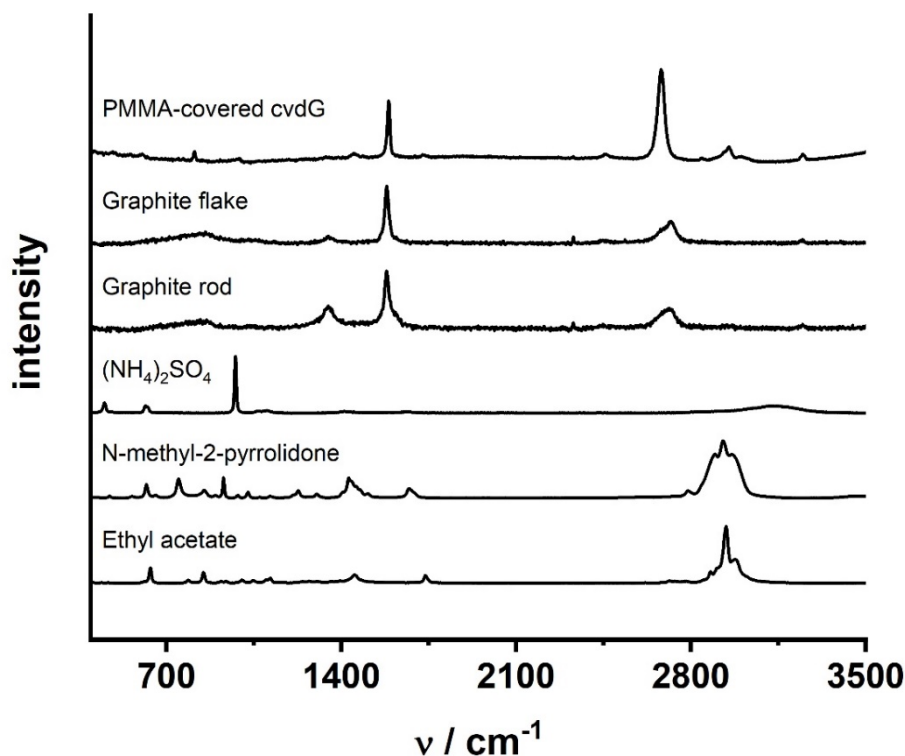n of the electrical active surface area investigating the peak current depending on the scan rate. The peak current is denoted as i_p, n is the number of transferred electrons during the redox reaction, F is the Faraday constant (96.485,33 C mol^{-1}), A is attributed to the electrical active surface area, c is the concentration of the redox marker (mol cm^{-3}), v corresponds to the scan rate (V s^{-1}), D is the diffusion coefficient ($D_{K_3[Fe(CN)_6]} = 6.7 \cdot 10^{-6}$ cm^2 s^{-1}, $D_{[Ru(NH_3)_6]Cl_3} = 5.7 \cdot 10^{-6}$ cm^2 s^{-1}) [38,39], and R attributes to the gas constant (8.314 J K^{-1} mol^{-1}).

$$i_p = 0.4463 \cdot n \cdot F \cdot A \cdot c \cdot \left(\frac{n \cdot F \cdot v \cdot D}{R \cdot T} \right)^{0.5} \tag{3.3}$$

The electrical active surface area of each type of graphene electrode to (6.1 ± 0.7) mm² for cvdG, (2.7 ± 0.6) mm² for meG, (9.0 ± 0.7) mm² for ecG, and (4.7 ± 1.7) mm² for rGO.
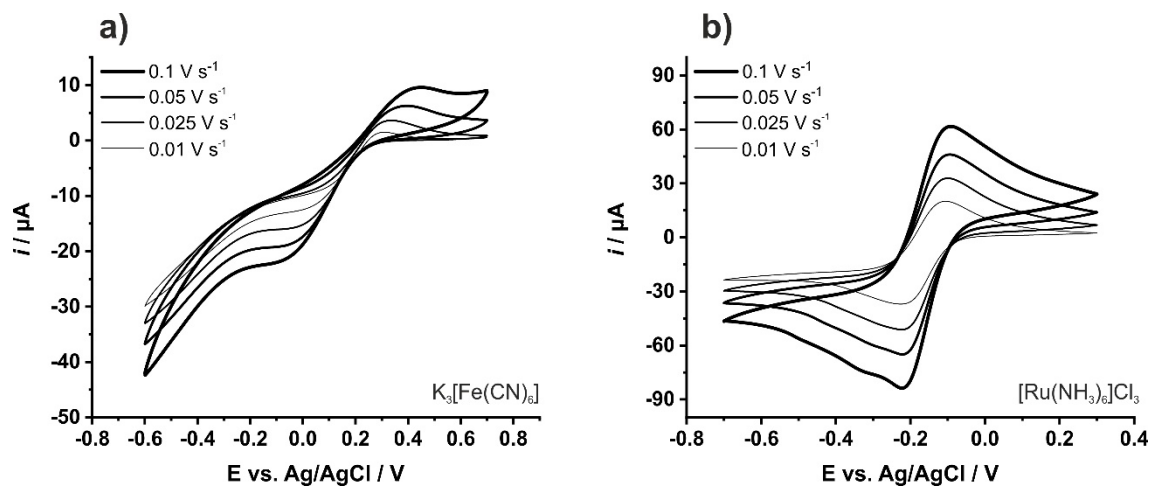
Figure 3.12: Cyclic voltammograms of a cvdG modified electrode in phosphate buffer (10 mM Na_2HPO_4 / NaH_2PO_4, 0.1 M NaCl, pH 7.4) containing either $K_3[Fe(CN)]_6$ (5 mM) (a) or $[Ru(NH_3)_6]Cl_3$ (5 mM) (b) vs. Ag/AgCl at alternating scan rates from (0.1 – 0.01) V s^{-1}.

The heterogeneous electron transfer (HET) between the redox probe and the graphene electrode surface was studied by cyclic voltammetry (Figure 3.13a and Figure 3.13b). The large peak separation of (547 ± 47) mV indicating a low HET for cvdG-modified electrodes is attributed to the low-defective nature of the material. In contrast, the carbon nanomaterials, identified by the Raman study to exhibit the most edge-planes or structural irregularities, show a superior behavior in electron transfer. From this result one can assume, that potential negatively charged analyte molecules preferably interact with the active sites of the carbon nanomaterial and not with the carbon atoms located in the basal plane. This can also be seen by the cyclic voltammograms shown in Figure 3.12 comparing differently charged redox markers. The positively charged hexammineruthenium exhibits an about six times higher peak intensity compared to the negatively charged hexacyanoferrate.

Figure 3.13: Cyclic voltammograms of cvdG (blue), meG (turquoise), ecG (orange) and rGO (red) modified electrodes in phosphate buffer (10 mM Na_2HPO_4 / $NaH_2P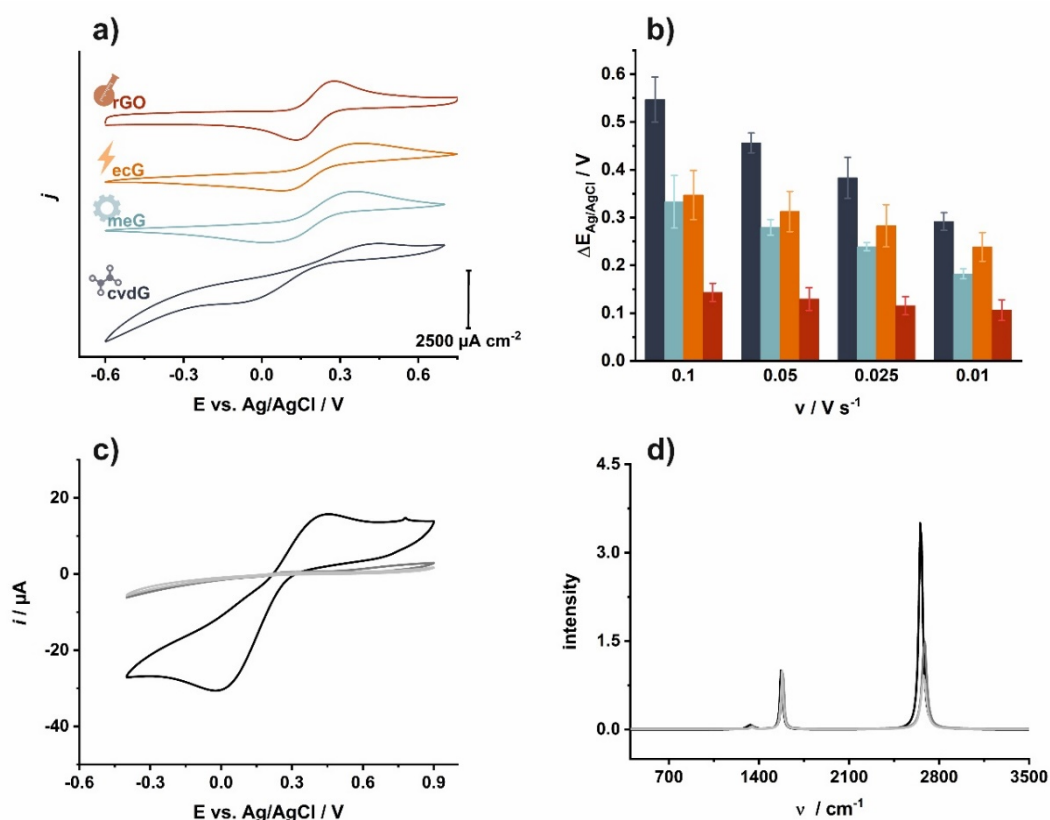O_4$, 0.1 M NaCl, pH 7.4) containing $K_3[Fe(CN)_6]$ (5 mM) vs. Ag/AgCl at a scan rate of 0.1 V s^{-1} (a). Bar charts reveal the peak potential separation of meG, ecG and rGO modified electrodes at scan rates from 0.1 – 0.01 V s^{-1} (b). Cyclic voltammograms of 1- (dark grey), 4- (grey) and 8-layers (light grey) cvdG modified electrodes in phosphate buffer (10 mM Na_2HPO_4 / NaH_2PO_4, 0.1 M NaCl, pH 7.4) containing $K_3[Fe(CN)_6]$ (5 mM) vs. Ag/AgCl at a scan rate of 0.1 V s^{-1} (c). Corresponding Raman spectra of the 1- (dark grey), 4-(grey) and 8-layers (light grey) cvdG modified electrodes showing a decrease of the 2D peak intensity upon increasing number of layers recorded at 532 nm (d).

The presence of defects, *i.e.* oxygen residues or vacancies enhances the electron transfer kinetics for graphene compounds of smaller flake size. Initially, it was expected for meG to combine a fast in-plane electron transport derived by an intact sp^2 hybridized carbon basal plane with electrochemical active edge planes. The interplay with the redox probe is quite satisfying revealed by a peak potential separation of (ΔE_{meG} = (333 ± 55) mV). The ecG-modified electrode exhibits a similar peak potential separation of (ΔE_{ecG} = (347 ± 51) mV) compared to meG. This can be attributed to the similar amount of charged functional groups, revealed by DLS, resulting in an improved interaction of electrode surface and redox probe. Still, the fastest HET is observed for the rGO modified electrode with a peak potential separation of 143 ± 19 mV, which is ascribed to the high

defect density ranging from edge planes to point defects within its carbon structure providing active defective sites. Besides improved analyte-electrode interaction, the fast in-plane electron transfer in rGO originates from electron hopping transport across the defective surface [40]. Reduced graphene oxide is close to the performance of unmodified gold electrodes as they exhibited a peak potential separation of (107 ± 8) mV. A carbon based heterostructure, derived by depositing rGO (2 µL, $\beta = 0.1$ mg mL^{-1}) onto a cvdG-modified electrode revealed a peak potential separation of 169 mV, therefore it is assumed that the redox process happens at the rGO surface, not on the underlying substrate, whether it is cvdG or gold. As control, cyclic voltammetry measurements were performed with an outer-sphere redox marker $Ru(NH_3)_6^{2+/3+}$, insensitive to the morphology of the electrode, to investigate whether the enhanced analyte-electrode interaction is ascribed predominantly to the morphology of the electrode or to the hydrophilicity of the defective materials. At a scan rate of 0.1 V s^{-1}, peak potential separations of (196 ± 71) mV were found for cvdG, (130 ± 38) mV for meG, (126 ± 18) mV for ecG and (118 ± 17) mV for rGO. Comparing the cyclic voltammograms of surface-sensitive $Fe(CN)_6^{3-/4-}$ with surface-insensitive $Ru(NH_3)_6^{2+/3+}$, the poor performance of cvdG, not interacting with the iron compound, is attributed to its missing defects. The peak potential separations are again narrower for materials, which distribute defects and are of smaller flake sizes. These findings relate to the investigations of Slate *et al.* upon the electrochemical properties of graphite paste and graphene paste electrodes with different flake sizes. Graphite paste and graphene paste electrodes examined electrochemically with an outer-sphere redox marker $Ru(NH_3)_6^{2+/3+}$ showed an enhanced HET for carbon materials of a smaller flake size. Electrochemical investigations using $Fe(CN)_6^{3-/4-}$ revealed that besides the dimensions of the flakes also functional groups play a role towards electrochemical reactivity [41].

The effect of the numbers of layers was investigated by cyclic voltammetry and Raman studies on multi-layer assemblies of low-defective cvdG. This type of graphene was chosen as the exact number of layers can be determined by the number of individually transferred cvdG flakes. The current flow decreased with an increased number of cvdG layers. This is also in correlation with the findings upon establishment of battery electrodes based on 2D materials [42]. Figure 3.13c shows cyclic voltammograms of

electrodes modified with one-, four- and eight-layers of cvdG. Raman spectroscopy verifies the increase of carbon layers by a decrease of the 2D peak and proves that no impurities during the transfer of the individual layer have been introduced (Figure 3.13d). The current decreases from 46 µA for the monolayer cvdG modified electrode to i = 1.2 µA and i = 0.5 µA for 4-layer- and 8-layer-cvdG electrodes, respectively. The blocking of the charge transfer by few-layer graphene might be attributed to an anisotropy in the charge transport in-plane and out-of-plane for sp^2 carbon layers. An analogy was found for graphite, which distributes an enhanced electrical resistance out-of-plane compared to the in-plane resistance [43].

Electrochemical impedance spectra have been used to obtain more information on the electrode-electrolyte interface, by fitting the spectra with a simple Randles equivalent circuit (Figure 3.14) (Table 3.2). It was revealed, that the double layer capacitance (C_{dl}) increases, whereas the charge-transfer resistance (R_{ct}) decreases from non-defective to defective carbon materials (Figure 3.15). The superior sp^2 hybridized carbon lattice of high-quality graphene ensures a fast in-plane charge transfer for cvdG. Nevertheless, in coherence with the findings of CV, the material interaction with the redox marker in the electrolyte is hindered resulting in a R_{ct} of (1.4 ± 0.1) kΩ cm^2. The values of R_{ct} decreases with the introduction of defects, *e.g.* edge-planes, which is shown for meG ($R_{ct} = (118 \pm 16)$ Ω cm^2) and ecG ($R_{ct} = (362 \pm 64)$ Ω cm^2). The R_{ct} for rGO is drastically decreased ($R_{ct} = (51 \pm 11)$ Ω cm^2) as it exhibits a highly defective structure, providing electrical active sites for the interaction of the electrode surface with the redox marker facilitating the charge transfer.
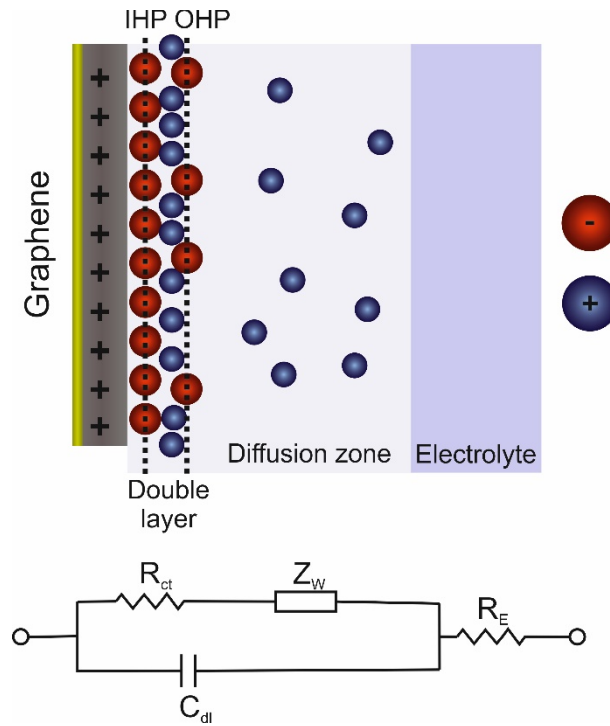
Figure 3.14: Randles equivalent circuit to model the electrochemical cell providing information on the resistance of the electrolyte (R_E), the charge transfer resistance (R_{ct}), the double layer capacity (C_{dl}) and the diffusion based Warburg impedance (Z_W). IHP stands for inner Helmholtz plane and OHP for outer Helmholtz plane.

The values of R_{ct} are either obtained by the intersection of the semicircle displayed in the Nyquist plot with the x-axis or by extrapolation of the plateau in the low-frequency segment of the Bode plot. The diffusion-controlled Warburg impedance cause the slope in the Nyquist plot as well as in the Bode plot. Equation 3.4 allows the calculation of the C_{dl} depending on the R_{ct} and the angular frequency at the maximum of the Nyquist plot.

$$C_{dl} = \frac{1}{R_{ct} \cdot 2\pi f_{max}}$$ (3.4)

Table 3.2: Electrochemical properties of graphene materials investigated by Electrochemical Impedance Spectroscopy. The measurements were recorded in phosphate buffer (10 mM Na_2HPO_4 / NaH_2PO_4, 0.1 M NaCl, pH 7.4) containing $K_3[Fe(CN)_6]$ (5 mM) (n = 3).

	R_{ct} [kΩ]	C_{dl} [µF]	C_{dl} A^{-1} [µF cm^{-2}]
cvdG	23.4 ± 1.5	0.45 ± 0.11	7.7 ± 2.6
meG	4.6 ± 1.4	0.8 ± 0.06	30 ± 10
ecG	4.0 ± 0.7	1.8 ± 1.5	20 ± 1.6
rGO	1.2 ± 0.6	8.1 ± 3.7	171 ± 17
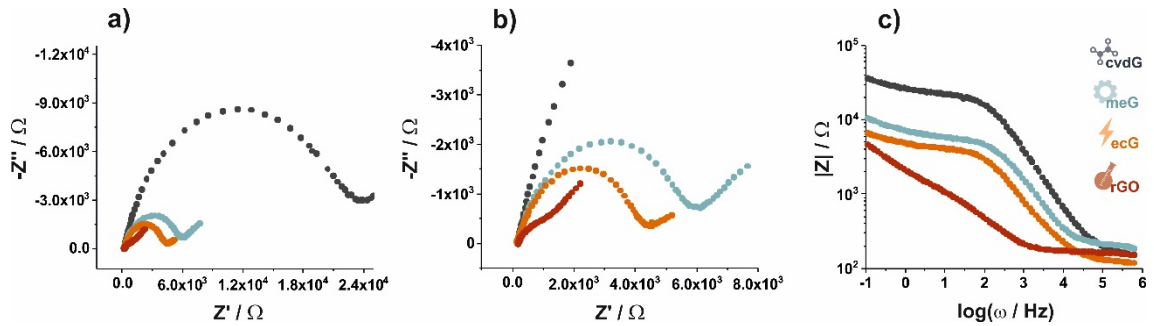
Figure 3.15: Electrochemical impedance spectroscopy for cvdG (blue), meG (turquoise), ecG (orange) and rGO (red) modified electrodes in phosphate buffer (10 mM Na$_2$HPO$_4$ / NaH$_2$PO$_4$, 0.1 M NaCl, pH 7.4) containing K$_3$[Fe(CN)$_6$] (5 mM) vs. Ag/AgCl (a, b). Corresponding Bode plot in (c).

In summary the Raman studies cluster the graphene materials when one looks at the I$_D$/I$_G$-ratio as a function of the FWHM of the 2D peak, in accordance to an increase in the structural disorder along the x-axis and the lattice disorder along the y-axis (Figure 3.16a). The data from electrochemical impedance spectroscopy also discriminate the individual types of graphene by plotting R$_{CT}$ as a function of the dielectric layer thickness (C$_{dl}$) A^{-1}. More defects and smaller flake sizes are in coincidence with a better ability to enable electrochemical reactions at the electrode surface (Figure 3.16b).
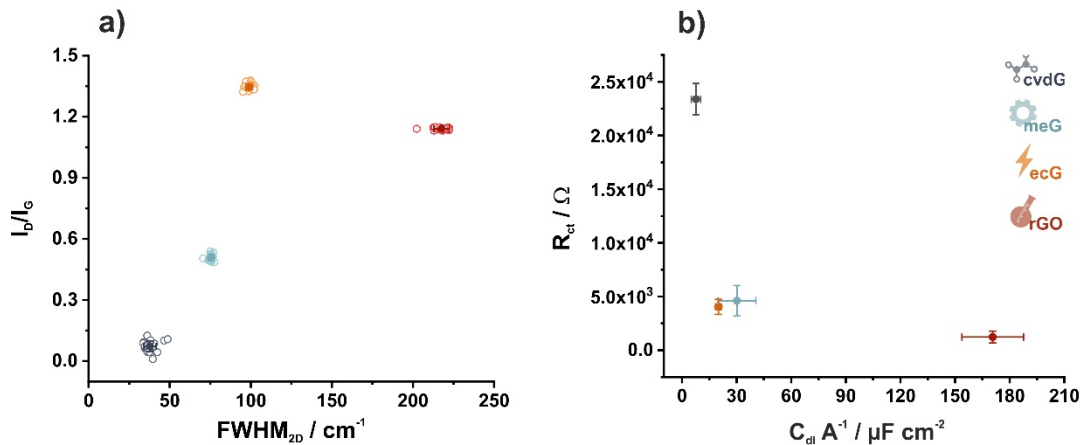
Figure 3.16: Correlation of the structural features of graphene revealed by statistical Raman analysis of 24 measurement points (a) and by electrochemical impedance spectroscopy of 3 individual electrodes of each type (b).

3.3.7 Amperometric Detection of Hydrogen Peroxide

The electrocatalytic behavior of the 2D carbon nanomaterial modified electrodes was studied by their reduction ability of H_2O_2 in 10 mM phosphate buffer at physiological pH of 7.4. Hydrogen peroxide gets physiosorbed at the graphene surface and reduced as following [44,45]. The cathodic current flow is of interest, as the reduction of H_2O_2 is an irreversible process [46]. The cathodic current is subtracted from the background current and set in relation to the signal of the blank. The lowest onset potential for the reduction process was found to be E = -0.2 V *vs*. Ag/AgCl. A change of the current was observed for 2D carbon nanomaterial modified electrodes. Figure 3.17 depicts the amperometric signal change during H_2O_2 addition with subsequently increasing concentration of H_2O_2 (0.125 mM – 4 mM) with the corresponding sensitivities for each graphene-modified electrode.
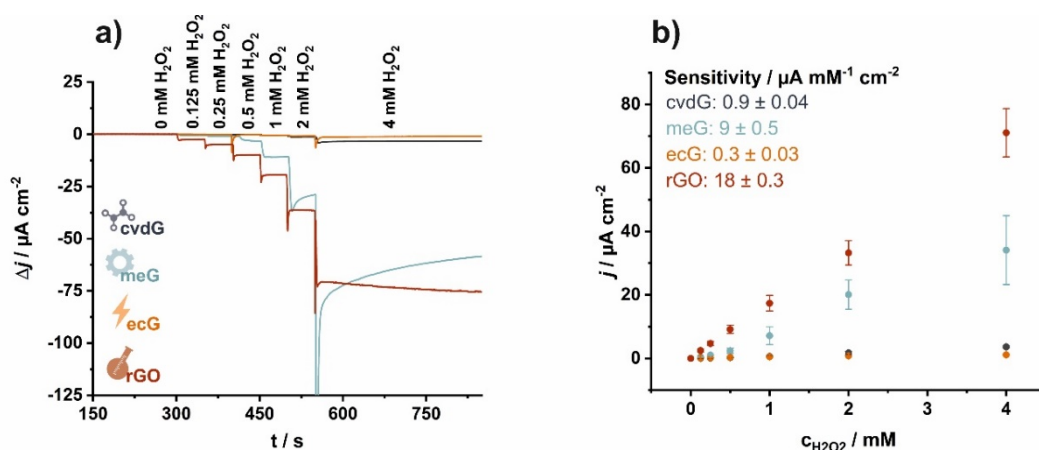
Figure 3.17: Time course of the current density changes of graphene modified electrodes in phosphate buffer (10 mM Na_2HPO_4 / NaH_2PO_4, 0.1 M NaCl, pH 7.4) containing H_2O_2 with increasing concentration from 0.25 mM to 4 mM at E = -0.2 V vs Ag/AgCl (a). The change of the current density as a function of the H_2O_2 concentration (n=3) (b).

Reduced graphene oxide modified electrodes and meG show the highest sensitivity towards H_2O_2 reduction. The sensitivity of cvdG-modified is almost three-times lower compared to the graphene derived by liquid exfoliation. The amperometric performance of ecG is decelerated, which can be attributed to a more vertically aligned structure, leading to a low diffusion of the analyte [42]. As revealed in the previous studies, oxygen moieties within the graphene structure can act as active sites in catalytic reactions [47].

Therefore, cvdG modified electrodes provide less reaction sites, resulting in a lower sensitivity. In contrast, rGO, the material with the most "deteriorated" carbon lattice, exhibits the highest signal change upon a concentration range of 0.125 – 4 mM H_2O_2. This is attributed to a sufficient interaction of the redox probe and an electron hopping based charge transfer across the defects. Mechanically exfoliated graphene modified electrodes exhibit a lower sensitivity towards H_2O_2. The flake sizes of meG are in the similar range as those of rGO, with planar arranged carbon sheets but less decorated by oxygen functionalities at the surface resulting in a lower sensitivity towards H_2O_2.

3.4   Conclusion

The advantage of liquid exfoliation processes is that graphene dispersions can be produced in large scale, either by chemical synthesis yielding defective carbon nanomaterials like rGO, by electrochemical exfoliation resulting in ecG or by applying shear forces to obtain meG. Upon the interest in 2D carbon materials, the field of preparation methods evolved. A high variety of graphene nanomaterials are on the market uncertain in their structure and characteristics, whether they can potentially contribute to a device's success or being the source of failure. Many different graphene materials were applied as sensor materials without significant indication what is the benefit of the used material compared to its counterparts. Therefore, an evaluation of the processing procedure of commonly used carbon materials, like cvdG, meG, ecG, and rGO, was performed. The variation in the chemical composition derived by the preparation is investigated upon its impact on the electrochemical properties and with regard to the electrode fabrication process, the morphology and wettability of the materials. The defects, *i.e.*, vacancies, edge sites etc., are evaluated *via* Raman spectroscopy, whereas the number of defects decreases in the order rGO, ecG, meG, and cvdG. In this study, it became apparent, that the choice of the material has an enormous influence on its electrochemical performance and that the selection is crucial for potential sensor applications. The electrode interface of graphene materials is all about the flake's size, defects and arrangement of the carbon layers on top of the substrate of choice, all affecting the chemical and physical characteristics. Reduced graphene oxide exhibits the fastest heterogeneous electron transfer between electrode surface and redox marker, coupled with a low intrinsic charge-transfer resistance derived by electron hopping within the layer. Additionally, the defective nature of the material exhibits active binding sites for potential analytes, as it showed an increased electrocatalytic activity towards H_2O_2 reduction. The rough surface of defective rGO increases the electric active area as well as improves the wettability of the nanostructured interface making it a highly desirable material for further applications implied in the field of electrochemical sensing in aqueous environment. In contrast, electrochemically derived graphene is characterized by defects, corrupting the electrical transport within the material. This result in a five-time higher R_{ct} compared to rGO and a slower heterogeneous electron transport. The

transferred cvdG, which retained its continuous sp² hybridized carbon lattice exhibits the highest R_{ct} compared to the other carbon nanomaterials. Yet, the lack of oxygen containing defects within the material pose a drawback in the sensing application performed in aqueous medium. In contrast, mechanically exfoliated graphene derived by shear force showed a doubled R_{ct} compared to rGO, as the exfoliated meG flakes, decorated with oxygen functionalities at its edges, form a coherent layer as electrode surface. The heterogeneous electron transfer is similar to ecG. Even though the defective rGO outperformed ecG, meG, and cvdG in terms of electrochemistry in aqueous medium, the benefits of the less-defective materials like cvdG and meG might be beneficial for other electrical applications. Therefore, it would be desired to get an even better understanding of the influence of the structure of the graphene deposited on solid substrates, e.g. by evaluating the exact chemical composition at the graphene electrolyte interface. First attempts by using XPS revealed that this is not an easy task as it is challenging to characterize the oxygen content accurately in such nano dimensions.

3.5 Experimental Section

3.5.1 Materials

1-Methyl-2-pyrrolidone (99 %) (NMP) was obtained from Honeywell (www.lab-honeywell.com). China flake graphite was purchased from K. W. Thielmann & Cie KG (www.kwthielmann.de). Graphite rods were obtained from Faber-Castell (www.faber-castell.de). Potassium hexacyanoferrate(III), potassium permanganate, iron(III) chloride, sodium nitrite, ammonia solution (30%$_{w/w}$), sodium hydroxide, sulfuric acid (96%$_{w/w}$), hydrogen peroxide (30%$_{w/w}$), sodium hydrogen phosphate, potassium chloride, MF-Millipore mixed cellulose ester membrane (13 mm diameter, 0.045 µm pore diameter), Omnipore polytetrafluoroethylene (PTFE) membrane (13 mm diameter, 0.1 µm pore diameter) were from Merck Millipore (www.merckmillipore.com). Hydrazine hydrate and Hexaammineruthenium(III)chlorid (98%) were purchased from Sigma-Aldrich (www.sigmaaldrich.com). All chemicals used were of analytical grade. Monolayer graphene on copper, deposited by chemical vapor deposition, were purchased from Graphenea (www.graphenea.com).

3.5.2 Apparatus

Mechanical exfoliation of graphite was performed with an ULTRA-TURRAX T25 – S 25 N – 18G dispersion tool (IKA-Werke GmbH & Co KG, Staufen, Germany). Atomic force microscopy was recorded on a custom-designed microscope using qPlus sensors [48]. Raman microscopy was performed on a DXR Raman microscope (Thermo Fisher Scientific GmbH, Dreieich, Germany) at 532 nm laser excitation (8 mW) using a 50 µm slit. All electrochemical measurements were conducted with an electrochemical analyzer CHI650A (CH Instruments, Inc., Austin, TX, USA) using a three-electrode electrochemical cell with an Ag/AgCl reference electrode and a platinum wire counter electrode. The substrate of choice for electrode modification processes and all electrochemical measurements was a piece of silicon wafer (3 × 14 mm) covered by a SiO_2 layer. On top of this, gold was sputtered in an interdigitated layout, with a distance between the gold fingers of 150 µm and a total surface of 2.95 mm^2 covered by gold. A Ti layer was used for a better adhesion of the gold on the SiO_2. The interdigitated gold area was fully

covered by the 2D carbon nanomaterials and connected *via* two 7 mm long connection paths of gold to contact pads of a size of 1.2 mm^2. Contact angle measurements were performed using a DataPhysics OCA. 15EC device (DataPhysics Instruments GmbH, Filderstadt, Germany) with corresponding SCA 20 software (DataPhysics Instruments GmbH, Filderstadt, Germany).

3.5.3 Mechanical Exfoliation of Graphene

China flake graphite (5.1 g, β = 60 mg mL^{-1}) was suspended in N-Methyl-2-pyrrolidone (NMP) (85 mL). The suspension was exfoliated for 1 h at a speed of 6,000 rpm. The suspension was left to settle overnight. The supernatant was discarded, the sediment suspended in NMP (85 mL) and a second exfoliation step was performed. Unexfoliated material was removed by centrifugation at 1,000 g. The sediment was discarded. The mixture was centrifuged with subsequently increasing centrifugation steps and the final product was collected and dispersed in NMP after the centrifugation at 9,000 g [49]. Gravimetric investigation revealed β = (0.133 ± 0.0321) mg mL^{-1}.

3.5.4 Anodic Electrochemical Exfoliation of Graphene

In a two-electrode set-up consisting of two graphite rods, 0.1 M $(NH_4)_2SO_4$ was used as electrolyte [27]. A potential of 10 V was applied for 30 min under ice cooling. The exfoliated material was vacuum filtrated and washed thoroughly with H_2O to remove residual salts. The material was dispersed in NMP, sonicated for 4.5 h, and centrifuged analogue to meG. The final product was obtained after a centrifugation at 9,000 g (β = 0.95 ± 0.0218 mg mL^{-1}) [49].

3.5.5 Graphene Oxide and Reduced Graphene Oxide

Graphene oxide was prepared by a modified Hummer's method [50]. Graphite flakes (1 g) were mixed with $NaNO_3$ (0.75 g, 8.9 mmol) and conc. H_2SO_4 (75 mL). The mixture was stirred for 20 min followed by a cooling step in an ice bath and $KMnO_4$ (4.5 g, 28 mmol) was added and sonicated for 3 h. After stirring for 3 d at room temperature, H_2SO_4 (5%$_{w/v}$, 75 mL) was added. The slurry was refluxed for 3 h at 115 °C. A color change from light to

dark brown indicated the complete oxidation of graphene. H_2O_2 ($30\%_{w/v}$, 15 mL) was added to the mixture and stirred for 1 h at room temperature to remove excess $KMnO_4$ by formation of MnO_2. The suspension was centrifuged 7 minutes at 3,000 rcf before the supernatant was removed and the remaining graphene oxide was washed: four times with H_2SO_4 ($3\%_{w/v}$) containing H_2O_2, ($0.5\%_{w/v}$), three times with HCl ($3\%_{w/v}$) and three times with $H_2O_{millipore}$. For further purification, the suspension was dialyzed (pore size: 12 – 14 kDa) for 10 d, whereas $H_2O_{millipore}$ was changed twice a day (60 mL GO suspension per 5 L $H_2O_{millipore}$). Gravimetrically determined, the concentration of GO in water is 2.5 ± 0.1 mg mL^{-1} (n = 3). For the reduction of graphene oxide, GO-solution (7 mL, β = 0.5 mg mL^{-1}) was mixed with NH_3 ($32\%_{w/v}$, 31 µL). As reduction agent hydrazine hydrate ($98\%_{w/v}$, 5 µL) was added. After refluxing the mixture for 1.5 h the complete reduction was indicated by the color change from brown to black.

3.5.6 Electrode Modification

The microelectrodes consist of gold conductive paths evaporated onto a SiO_2/Si wafer. The conducting paths form a meander structure to increase the surface. The microelectrodes were cleaned in a mixture of H_2O_2 (30%) and conc. H_2SO_4 $(1:3)_{v/v}$ before usage.

3.5.6.1   Electrode Modification with Reduced Graphene Oxide

On top of the interdigitated gold structure, reduced graphene oxide dispersion (4 µL, β = 0.5 mg mL^{-1}) was drop coated and dried at 40 °C. These parameters have been chosen in order to completely cover the gold surface by the carbon nanomaterial. The rGO modified electrode was treated with a thermally annealing step (T = 300°C, t = 10 s) to increase the stability of the graphene layer on the electrode surface.

3.5.6.2   Electrode Modification with Mechanical Exfoliated Graphene

Ethyl acetate was added to a meG (9,000 g)/NMP dispersion ($(1:5)_{v/v}$) and filtered through a PTFE membrane (13 mm, 0.1 µm pore diameter) forming a grey coating on top of the membrane. The graphene-membrane is slowly immersed vertically into a water bath. A layer of graphene detaches from the membrane surface and floats on top of the water

surface. The graphene layer is fished with an electrode covering the gold structure. The meG-modified gold electrode is thermally treated (T = 300 °C, t = 60 s) to remove any residual solvent.

3.5.6.3   Electrode Modification with Electrochemically Exfoliated Graphene

After the addition of ethyl acetate to ecG(9,000 g)/NMP (1:2)$_{v/v}$, the graphene dispersion was injected onto a water surface. After spreading, the solvent evaporates and leaves a floating graphene film, which is fished with the interdigitated gold electrode. The ecG modified electrode is thermally treated (T = 300 °C, t = 60 s).

3.5.6.4   Electrode Modification with Chemical Vapor Deposited Graphene

A cvdG graphene layer (10 mm x 10 mm), sandwiched between a thin copper substrate and PMMA cover (Graphenea, San Sebastián, Spain), was cut into the desired size. The PMMA/ cvdG graphene/Cu layer was placed on an aqueous solution of FeCl$_3$ (400 mM) until the copper layer was etched away. The film was washed thoroughly with H$_2$O$_{millipore}$ and transferred on the substrate of choice. Afterwards the PMMA/ cvdG electrode setup is thermally treated (T = 80 °C, t = 30 s) to remove excess water and smoothen the surface of the film. The PMMA layer is dissolved by immersing the electrode composite in an acetone bath (t = 1 h).

3.5.7 Atomic Force Microscopy

Atomic force microscopy was recorded on a custom-designed microscope using qPlus sensors [49]. The qPlus sensor was equipped with sapphire tips oscillating at a constant amplitude of 500 pm. Topographic images of graphene surfaces were recorded by scanning across the surface, while keeping the frequency shift constant.

3.5.8 Scanning Electron Microscopy

Scanning electron microscopy imaging was performed on a Zeiss Auriga Gemini (Carl Zeiss Microscopy GmbH, Oberkochen, Germany) equipped with an InLens detector. The accelerating voltage was 1.5 kV with a working distance of 4.4 mm.

3.5.9 Raman Microscopy

Raman microscopy was performed using a 532 nm laser excitation with a power of 8 mW and a 50 µm slit. The Raman spectra and microscopic images were taken at a 100 times magnification with a MPlan N objective (100×/0.90 BD, Olympus SE & Co. KG, Hamburg, Germany). The acquisition time is 0.8 s and averaged over 40 measurements.

3.5.10 Dynamic Light Scattering and Zeta Potential

Dynamic light scattering, and Zeta potential measurements were performed using a Malvern Zetasizer Nanoseries. The samples were diluted $(1:9)_{v/v}$. The samples were equilibrated to 20 °C for 120 s prior to each measurement. The solvent is NMP/H_2O $(1:9)_{v/v}$ with a viscosity of η = 1.08 mPa s, a refractive index of n = 1.344 and a dielectric constant of ε = 73.33 F m^{-1}. DLS measurements were taken using a backscatter mode.

3.5.11 Contact Angle Measurements

Contact angle measurements were performed by a sessile drop method of phosphate buffer (0.2 µL, 10 mM Na_2HPO_4 / NaH_2PO_4, 0.1 M NaCl, pH 7.4) on the graphene substrates of choice using a DataPhysics OCA 15EC (DataPhysics Instruments GmbH, Filderstadt, Germany). The data analysis was performed with the SCA 20 software (DataPhysics Instruments GmbH, Filderstadt, Germany).

3.5.12 Electrochemical Investigations

All electrochemical measurements were conducted with an electrochemical analyzer CHI650A (CH Instruments, Inc., Austin, TX, USA) using a three-electrode electrochemical cell with an Ag/AgCl reference electrode and a platinum wire counter electrode. Before every measurement, the electrolytes, phosphate buffer (10 mM Na_2HPO_4 / NaH_2PO_4, 0.1 M NaCl, pH 7.4) (containing $K_3[Fe(CN)_6]$ (5 mM) or $[Ru(NH_3)_6]Cl_3$ (5 mM)) were degassed by argon for 10 min.

Cyclic voltammetric measurements were performed applying a potential range of -0.6 V – 0.8 V. Cyclic voltammetric measurements are recorded by scanning the potentials at a speed rate of 0.1 V·s^{-1}, 0.05 V·s^{-1}, 0.025 V·s^{-1} and 0.01 V·s^{-1}. A potential of E = 0.2 V

vs. Ag/AgCl with an amplitude of 10 mV was applied for electrochemical impedance spectroscopy with a frequency range of $1 \cdot 10^{-1} – 1 \cdot 10^{5}$ Hz.

The electrocatalytic activity of graphene was investigated by chronoamperometry. The reduction process of subsequently added H_2O_2 (0.125 mM, 0.25 mM, 0.5 mM, 1 mM, 2 mM and 4 mM) at a potential of -0.2 V at an interval of 50 s was determined.

3.6 References

[1] Anichini C, Czepa W, Pakulski D, Aliprandi A, Ciesielski A, Samorì P (2018) Chemical sensing with 2D materials. Chem. Soc. Rev. 47:4860–4908..

[2] Wongkaew N, Simsek M, Griesche C, Baeumner AJ (2019) Functional nanomaterials and nanostructures enhancing electrochemical biosensors and lab-on-a-chip performances: recent progress, applications, and future perspective. Chem. Rev. 119:120–194.

[3] Meng Z, Stolz RM, Mendecki L, Mirica KA (2019) Electrically-transduced chemical sensors based on two-dimensional nanomaterials. Chem. Rev. 119:478–598.

[4] Nine MJ, Cole MA, Tran DNH, Losic D (2015) Graphene: a multipurpose material for protective coatings. J. Mater. Chem. A 3:12580–12602.

[5] Grieshaber D, MacKenzie R, Vörös J, Reimhult E (2008) Electrochemical biosensors - sensor principles and architectures. Sensors 8:1400–1458.

[6] Zhu C, Yang G, Li H, Du D, Lin Y (2015) Electrochemical sensors and biosensors based on nanomaterials and nanostructures. Anal.Chem. 87:230–249.

[7] Chen D, Tang L, Li J (2010) Graphene-based materials in electrochemistry. Chem. Soc. Rev. 39:3157–3180.

[8] Georgakilas V, Otyepka M, Bourlinos AB, Chandra V, Kim N, Kemp KC, Hobza P, Zboril R, Kim KS (2012) Functionalization of graphene: covalent and non-covalent approaches, derivatives and applications. Chem. Rev. 112:6156–6214.

[9] Sha R, Puttapati SK, Srikanth VV, Badhulika S (2017) Ultra-sensitive phenol sensor based on overcoming surface fouling of reduced graphene oxide-zinc oxide composite eectrode. J. Electroanal. Chem. 785:26–32.

[10] Morales-Narváez E, Baptista-Pires L, Zamora-Gálvez A, Merkoçi A (2017) Graphene-based biosensors: going simple. Adv. Mater. 29

[11] Novoselov KS, Geim AK, Morozov SV, Jiang D, Zhang Y, Dubonos SV, Grigorieva IV, Firsov AA (2004) Electric field effect in atomically thin carbon films. Science 306:666–669.

[12] Fitzer E, Kochling K-H, Boehm HP, Marsh H (1995) Recommended terminology for the description of carbon as a solid (IUPAC Recommendations 1995). Pure Appl. Chem. 67:473–506.

[13] Buzaglo M, Ruse E, Levy I, Nadiv R, Reuveni G, Shtein M, Regev O (2017) Top-down, scalable graphene sheets production: it is all about the precipitate. Chem. Mater. 29:9998–10006.

[14] J. Tour JM (2014) Top-down versus bottom-up fabrication of graphene-based electronics. Chem. Mater. 26:163–171.

[15] Ambrosi A, Chua CK, Bonanni A, Pumera M (2014) Electrochemistry of graphene and related materials. Chem. Rev. 114:7150–7188.

[16] Ambrosi A, Chua CK, Latiff NM, Loo AH, Wong CHA, Eng AYS, Bonanni A, Pumera M (2016) Graphene and its electrochemistry - an update. Chem. So. Rev. 45:2458–2493.

[17] Pang J, Bachmatiuk A, Ibrahim I, Fu L, Placha D, Martynkova GS, Trzebicka B, Gemming T, Eckert J, Rümmeli MH (2016) CVD growth of 1D and 2D sp2 carbon nanomaterials. J. Mater. Sci. 51:640–667.

[18] Eigler S, Hof F, Enzelberger-Heim M, Grimm S, Müller P, Hirsch A (2014) Statistical raman microscopy and atomic force microscopy on heterogeneous graphene obtained after reduction of graphene oxide. J. Phys. Chem. C 118:7698–7704.

[19] Eigler S (2016) Controlled chemistry approach to the oxo-functionalization of graphene. Chemistry 22:7012–7027.

[20] Rümmeli MH, Gorantla S, Bachmatiuk A, Phieler J, Geißler N, Ibrahim I, Pang J, Eckert J (2013) On the role of vapor trapping for chemical vapor deposition (CVD) grown graphene over copper. Chem. Mater. 25:4861–4866.

[21] Yi M, Shen Z (2015) A review on mechanical exfoliation for the scalable production of graphene. J. Mater. Chem. A 3:11700–11715.

[22] Narayan R, Kim SO (2015) Surfactant mediated liquid phase exfoliation of graphene. Nano convergence 2:20.

[23] Coleman JN (2013) Liquid exfoliation of defect-free graphene. Acc. Chem. Res. 46:14–22.

[24] Paton KR, Varrla E, Backes C, Smith RJ, Khan U, O'Neill A, Boland C, Lotya M, Istrate OM, King P, Higgins T, Barwich S, May P, Puczkarski P, Ahmed I, Moebius M, Pettersson H, Long E, Coelho J, O'Brien SE, McGuire EK, Sanchez BM, Duesberg GS, McEvoy N, Pennycook TJ, Downing C, Crossley A, Nicolosi V, Coleman JN (2014) Scalable production of large quantities of defect-free few-layer graphene by shear exfoliation in liquids. Nat. Mater. 13:624–630.

[25] Johnson DW, Dobson BP, Coleman KS (2015) A manufacturing perspective on graphene dispersions. Curr. Opin. Colloid Interface Sci. 20:367–382.

[26] Parvez K, Li R, Puniredd SR, Hernandez Y, Hinkel F, Wang S, Feng X, Müllen K (2013) Electrochemically exfoliated graphene as solution-processable, highly conductive electrodes for organic electronics. ACS Nano 7:3598–3606.

[27] Parvez K, Wu Z-S, Li R, Liu X, Graf R, Feng X, Müllen K (2014) Exfoliation of graphite into graphene in aqueous solutions of inorganic salts. J. Am. Chem. Soc. 136:6083–6091.

[28] Orth ES, Ferreira JGL, Fonsaca JES, Blaskievicz SF, Domingues SH, Dasgupta A, Terrones M, Zarbin AJG (2016) pKa determination of graphene-like materials: Validating chemical functionalization. J. Colloid Interface Sci. 467:239–244.

[29] Viinikanoja A, Kauppila J, Damlin P, Mäkilä E, Leiro J, Ääritalo T, Lukkari J (2014) Interactions between graphene sheets and ionic molecules used for the shear-assisted exfoliation of natural graphite. Carbon 68:195–209.

[30] Suk JW, Kitt A, Magnuson CW, Hao Y, Ahmed S, An J, Swan AK, Goldberg BB, Ruoff RS (2011) Transfer of CVD-grown monolayer graphene onto arbitrary substrates. ACS Nano 5:6916–6924.

[31] Santiago-Rosanne M, Vignes-Adler M, Velarde MG (2001) On the Spreading of Partially Miscible Liquids. J. Colloid Interface Sci. 234:375–383.

[32] Ferrari AC, Basko DM (2013) Raman spectroscopy as a versatile tool for studying the properties of graphene. Nature Nanotechnol. 8:235–246.

[33] Malard LM, Pimenta MA, Dresselhaus G, Dresselhaus MS (2009) Raman spectroscopy in graphene. Phys. Rep. 473:51–87

[34] Halbig CE, Nacken TJ, Walter J, Damm C, Eigler S, Peukert W (2016) Quantitative investigation of the fragmentation process and defect density evolution of oxo-functionalized graphene due to ultrasonication and milling. Carbon 96:897–903.

[35] Ferrari AC, Robertson J (2001) Origin of the 1150−cm−1 Raman mode in nanocrystalline diamond. Phys. Rev. B 63:688.

[36] Cançado LG, Takai K, Enoki T, Endo M, Kim YA, Mizusaki H, Jorio A, Coelho LN, Magalhães-Paniago R, Pimenta MA (2006) General equation for the determination of the crystallite size La of nanographite by raman spectroscopy. Appl. Phys. Lett. 88:163106.

[37] Cançado LG, Jorio A, Ferreira EHM, Stavale F, Achete CA, Capaz RB, Moutinho MVO, Lombardo A, Kulmala TS, Ferrari AC (2011) Quantifying defects in graphene via raman spectroscopy at different excitation energies. Nano Lett. 11:3190–3196.

[38] Tang J, Jiang S, Liu Y, Zheng S, Bai L, Guo J, Wang J (2018) Electrochemical determination of dopamine and uric acid using a glassy carbon electrode modified with a composite consisting of a Co(Ⅱ)-based metalorganic framework (ZIF-67) and graphene oxide. Microchim. Acta 185:486.

[39] Liu F, Kolesov G, Parkinson BA (2014) Time of flight electrochemistry: diffusion coefficient measurements using interdigitated array (IDA) electrodes. J. Electrochem. Soc. 161:H3015-H3019.

[40] Gómez-Navarro C, Weitz RT, Bittner AM, Scolari M, Mews A, Burghard M, Kern K (2007) Electronic transport properties of individual chemically reduced graphene oxide sheets. Nano Lett. 7:3499–3503.

[41] Slate AJ, Brownson DAC, Abo Dena AS, Smith GC, Whitehead KA, Banks CE (2018) Exploring the electrochemical performance of graphite and graphene paste electrodes composed of varying lateral flake sizes. Phys. Chem. Chem. Phys. 20:20010–20022.

[42] Tian R, Breshears M, Horvath DV, Coleman JN (2020) The rate performance of two-dimensional material-based battery electrodes may not be as good as commonly believed. ACS Nano 14:3129–3140.

[43] Krishnan KS, Ganguli N (1939) Large anisotropy of the electrical conductivity of graphite. Nature 144:667.

[44] Wu P, Du P, Zhang H, Cai C (2013) Microscopic effects of the bonding configuration of nitrogen-doped graphene on its reactivity toward hydrogen peroxide reduction reaction. Phys. Chem. Chem. Phys. 15:6920–6928.

[45] Amirfakhri SJ, Binny D, Meunier J-L, Berk D (2014) Investigation of hydrogen peroxide reduction reaction on graphene and nitrogen doped graphene nanoflakes in neutral solution. J. Power Sources 257:356–363.

[46] Zhang T, Li C, Gu Y, Yan X, Zheng B, Li Y, Liu H, Lu N, Zhang Z, Feng G (2017) Fabrication of novel metal-free "graphene alloy" for the highly efficient electrocatalytic reduction of H2O2. Talanta 165:143–151.

[47] Navalon S, Dhakshinamoorthy A, Alvaro M, Garcia H (2014) Carbocatalysis by graphene-based materials. Chem. Rev. 114:6179–6212.

[48] Giessibl FJ (2019) The qPlus sensor, a powerful core for the atomic force microscope. Rev. Sci. Instrum. 90:11101.

[49] Backes C, Szydłowska BM, Harvey A, Yuan S, Vega-Mayoral V, Davies BR, Zhao P-L, Hanlon D, Santos EJG, Katsnelson MI, Blau WJ, Gadermaier C, Coleman JN (2016) Production of highly monolayer enriched dispersions of liquid-exfoliated nanosheets by liquid cascade centrifugation. ACS Nano 10:1589–1601.

[50] Zöpfl A, Lemberger M-M, König M, Ruhl G, Matysik F-M, Hirsch T (2014) Reduced graphene oxide and graphene composite materials for improved gas sensing at low temperature. Faraday discuss. 173:403–414.

4 Conclusion and Future Perspective

Carbon is the element in the periodic table, which exhibits the highest number of compounds, due to the capacious ability to bind to itself or to other elements. The resulting organic molecules cover a broad range of physicochemical properties, which can be controlled by sophisticated synthesis protocols. For a long time, the only known carbon allotropes have been graphite and diamond. In 1985, Kroto *et al.* discovered fullerenes, which can be thought of as a large spherical molecule of three-dimensional arranged carbon atoms [1], followed by one-dimensional *helical microtubules of graphitic carbon*, the so-called carbon nanotubes in 1991 [2]. The pioneers of Buckminster-fullerene earned the Nobel Prize in 1996, whereas the famous Kavli prize was awarded to Dr. Sumio Iijima for his contributions in the field of carbon nanotubes. Such ones might be somehow similar to a linear polymer, with a regular motif, which repeats in a principally endless sequence. The Nobel Prize in 2010 was awarded to Novoselov and Geim, who completed the family of so far highly awarded carbon allotropes by the mechanical exfoliation of graphite to two-dimensional graphene in 2004. Having found the last piece of the puzzle completed the ensemble of hexagonal bonded carbons, which exhibit three different topologies: Fullerene, carbon nanotube and graphene that are of the same building block – aligned hexagons of sp^2 hybridized carbon (Figure 4.1).
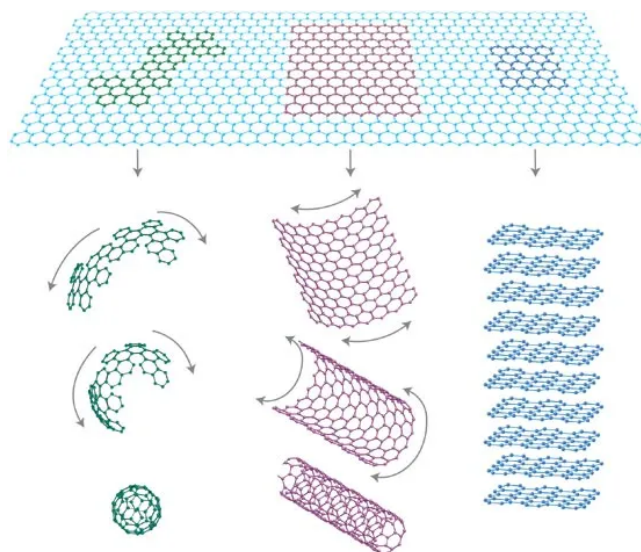
Figure 4.1: Graphene as a building block for all carbon materials of different dimensions, as it can be wrapped up in zero-dimensional fullerene, wrapped up in one-dimensional carbon nanotube or stacked into three-dimensional graphite. Reprinted with permission from Springer Nature Customer Service Centre GmbH: Nature Springer, Nature Materials, [3], (2007).

Pursuing the line of thought of molecules and polymers, the carbon family was extended by entering the class of nanomaterials with the planar arrangement of aromatic hexagons. As typical for materials, physical properties are engineered by introducing defects or dopants into a regular motif of 2D arranged carbon atoms. Motivated by the question, whether irregularities in the graphene lattice result to random changes in its characteristics or if the structure – feature coherence can be unraveled by thorough investigation; an emphasis of this work was put on different graphene fabrication techniques. The graphene compounds were studied towards their morphology and structural characteristics. Besides the optical investigations, especially the electrochemical behavior was of interest to observe the potential of graphene compounds to be integrated into sensing devices. Therefore, it was necessary to develop transfer protocols enabling the deposition of graphene layers of reproducible quality from a liquid dispersion to a solid support dealing as electrodes. A complementary study by different characterization methods revealed the correlation of structural features in the 2D nanomaterial and the intrinsic electrochemical behavior. With this, it was possible to demonstrate that amperometric detection principle prefers a defective graphene. It is supposed that the correlation between fabrication techniques, quality and physical

properties, demonstrated for the first time, allows to propose the ideal 2D carbon material for other transduction techniques in sensor development.

So far, graphene is aimed to be elevated from the laboratory level to commercialization. Therefore, research towards graphene synthesis strived to up-scale the production in a cost-effective way, balancing the ease of fabrication and quality of graphene [4,5]. Growth techniques are prominent for its ability to form sp^2-hybridized carbon lattices. The most critical issue is the transfer step required afterwards. Here, defects or impurities are introduced in a non-controllable way [6], arbitrarily changing the material's properties. More advanced in terms of simple equipment and low-cost production is the liquid exfoliation of graphite to graphene by chemical synthesis, application of shear forces or an electrical voltage [7-9]. Even though these preparation methods have the potential to be applied in large scale, the graphene flakes exhibit highly different structures, various numbers of stacked layers and are dispersed either in aqueous or organic solvents due to their hydrophilic or hydrophobic nature [8-12]. Up to now, many exfoliation protocols target the preparation of *non-defective* or *low-defective* graphene, implying that the structural irregularities within graphene pose a drawback. This should be reconsidered, as those structural features are not necessarily a bug, but rather a feature.

Graphene, in terms of a monolayer of sp^2 hybridized carbon atoms arranged in a honeycomb lattice of quasi-infinite size, barely is applied to any system. Even more, the state at which a carbon compound can be resembled as graphene is opaque. The International Organization for Standardization made a contribution to this and defined that the number of layers of single graphene sheets stacked above each other must not exceed ten layers to be still referred to as graphene [13]. This comes in quite handy, as most exfoliation techniques do not result in a one-atom thick layer. When having a closer look on research papers about two-dimensional carbon materials, beside the number of layers, another important classification becomes obvious dealing with quality and defects. Web of Science database counts about the same number of graphene related publications including either the term *high-quality* (465 hits) or *defective* (397 hits) in the title. These so-called *defects* refer to edge-planes of graphene flakes, covalently linked

functional groups, *e.g.* oxygen functionalities as well as structural irregularities like vacancies, holes and grain boundaries [14]. Stimulated by the exceptional physical properties of a single, pure graphene flake, many researchers aim to receive such a perfect 2D carbon material by developing synthesis methods as well as transfer protocols.

In terms of electrochemical sensors, graphene became popular as electrode material. In electrochemistry the benefits of graphene are acknowledged as high surface-to-volume ratio, inertness of the material, wide potential window and its stability against surface fouling [15-17]. It is of general question, whether and how the structural features, *e.g.* size, number of layers and defects, tailor the physical, especially electrochemical characteristics of the graphene compound. So far, many studies in amperometric sensing or in gas detection base on electrodes modified by graphene, where the carbon material was fabricated by various preparation techniques, without a thorough investigation of the effect of the material itself on the electrochemical properties.

Therefore, precise examinations upon the flake's morphology combined with an electrochemical study was performed for various two-dimensional carbon compounds (cvdG, meG, ecG, and rGO) in this work. It is revealed that the quality of graphene strongly depends on the preparation method [18]. Each material differs in its properties, *i.e.* number of stacked layers, flake size, defects densities. No uniform deposition protocol can be adapted for graphene dispersions. The aqueous dispersion of reduced graphene oxide, stabilized by negatively charged oxygen functionalities, was simply drop-coated forming a homogeneous film. Obstacles during the layer processing for NMP-dispersed graphene materials were faced as organic solvent stabilized carbon nanomaterials, meG and ecG, aggregate upon slow solvent evaporation. According to literature, with appropriated equipment, ink-jet printing can be a versatile tool to deposit NMP-dispersed materials onto the substrate of choice [19]. Deposition techniques like drop-coating under constant vibration and infrared illumination, spray- or spin-coating, caging between immiscible solvents did not yield in homogeneous carbon layers [20-22]. An alternative approach was developed in this work, based on vacuum filtrating of the graphene dispersion through a PTFE membrane, followed by stamping the

graphene/PTFE assembly onto the substrate of choice. Still a long deposition time of around 8 h is required to achieve a reproducible thin film, which should be object of optimization in further studies. After peeling-off the PTFE membrane, graphene remains as a thin film on the substrate. In contrast, a pre-deposition step of graphene, either on top of a PTFE membrane with subsequent delamination onto a water surface, or the direct deposition of graphene by mixing the NMP dispersion with ethyl acetate, spreading across the water surface resulted in a sufficient graphene layer formation. Despite the progress to deposit graphene on substrates without the formation of structural defects, aggregates and inhomogeneous layers, this still is one of the most challenging steps in device manufacturing. A major success is the option to create carbon structures directly on non-conductive substrates, which makes the post-production transfer obsolete. Laser-induced carbonization of a polyimide foil or alternative polymers realizes the direct scribing of carbon structures [23,24]. Customized patterns can be printed resulting in a porous graphene structure with enhanced surface area on a flexible substrate. This technique will become a versatile method for manufacturing cheap, miniaturized carbon-based electrodes for sensing applications utilizing the benefits of graphene motifs of such electrode surfaces. Studies on an aptamer-based electrochemical thrombin sensor revealed laser-induced graphene as highly potent material for electrochemical application [18]. The detection principle based on the shielding of the electrode surface upon exposure to thrombin. Examinations on the intrinsic electrocatalytic activity of laser-induced graphene itself are of interest to implement it as electrochemical sensor material for signal amplification. This production technique might be a step forward for the design of flexible devices implemented in the field of health care applications [25].

As the interest towards detailed material characterization upon the impact on sensor applications was not thriving so far, examination protocols tailored to each material were set up to investigate its structure and electrochemical behavior. Lateral dimensions of graphene flakes are examined *via* electron microscopy and dynamic light scattering. An empirical model for interpreting Raman spectra of graphene materials was already reported to determine the numbers of stacked layers [26]. This kind of evaluation is barely applied by other researchers as less is reported in literature. The equations suffer by the

fact that they need to be adapted to the individual experimental conditions such as type of devices, which have been used. Up to now, graphene flakes are classified as monolayer, few- or multilayered compounds. Furthermore, the lack of information towards the characteristics of a provided graphene material lead to confusions. An example is the statement, that no defects would be introduced into the carbon lattice *via* mechanical exfoliation [7,9,26,27]. Nevertheless, the processing parameters pose a significant influence on the materials characteristics, as it was observed for graphene derived by shear exfoliation with increased exfoliation speed. Apart from that, a class-spanning comparative study of the most promising graphene materials was not conducted so far. Reports are known, studying materials changed in their preparation technique, *i.e.* graphene oxide derived by various synthesis approaches compared to conventional graphene oxide, electrochemical exfoliation based on different intercalating species or liquid phase exfoliation performed using either a kitchen blender or derived by ultrasonication [9,28,29].

In this study, optical investigations based on atomic force microscopy, scanning electron microscopy, Raman spectroscopy revealed cvdG to exhibit the lowest number of defects, providing a large, monolayer of carbon. A completely defect-free cvdG is hardly obtained as already the growth processes induce structural defect variations in formed layers, like wrinkles or grain boundaries with differently oriented sp^2 hybridized domains as depicted in Figure 4.2 [30,31].
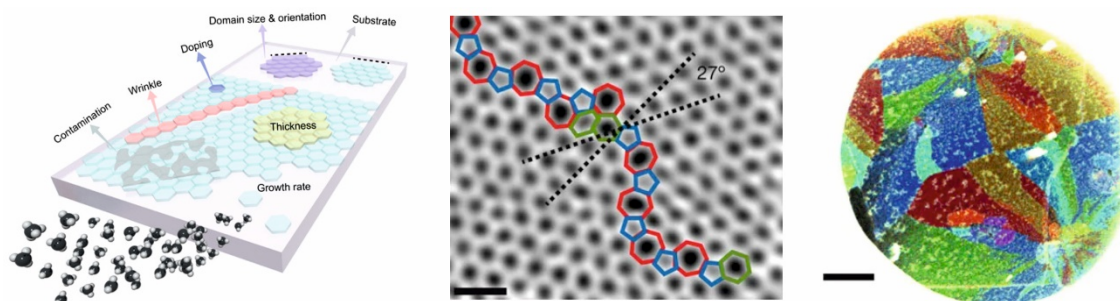
Figure 4.2: Scheme of CVD grown carbon lattice dependent on the growth rate, exhibiting structural disorders like wrinkle formation, atom doping, variation in thickness upon bi- to multilayer formation, differently oriented cvdG domains. Reprinted with permission from [30]. Copyright (2018) American Chemical Society. High-resolution TEM image of one grain boundary with the pentagons (blue), heptagons (red), and distorted hexagons (green). False color overlay of a dark field TEM of cvdG indicating shapes and lattice orientations of various grains. Reprinted by permission from [31]. Copyright (2011) Nature Springer.

Mechanically and electrochemical exfoliated graphene result in few-layered carbon compounds with a moderate number of defects within its structure. Reduced graphene oxide exposes the highest number of defects within the structure, which is attributed to the harsh synthesis conditions to oxidize graphite. A clustering of graphene materials according to their preparation method can be found by sophisticated Raman analysis investigating intensity ratios and the width of characteristic bands. All carbon materials, except ecG, cluster according to the number of layers and the structural defects and follow a linear trend as to be expected for the respective materials.

Electrochemical studies based on cyclic voltammetry and electrochemical impedance spectroscopy show a faster heterogeneous electron transfer and lower charge transfer resistance between the redox marker $Fe(CN)_6^{3-/4-}$ and the defective graphene derivatives, rGO, meG, and ecG compared to the low-defective cvdG. Chemical vapor deposited graphene barely interacts with the surface-sensitive redox marker. In contrast, reduced graphene oxide provides a faster electron transfer rate and lower charge transfer resistance compared to the materials with a lower number of defects. The charge transfer resistance, compared to cvdG, is decreased by a factor of about 20. The many electrochemical active oxygen groups within rGO preferably interacted with the redox marker. The electrocatalytic ability to reduce H_2O_2 amperometrically behaved similarly. Defects present within the nanomaterial can be claimed as electrical active sites, as they preferably interact with potential analytes [32]. The fundamental research on the electrochemical behavior of carbon-based nanomaterials proves defective materials more sensitive towards potential analytes due to active groups, potentially interacting with the analyte of choice. To get an even better understanding, it would be interesting to investigate the chemical composition of such materials after the transfer onto a substrate, *e.g.* in terms of carbon-to-oxygen ratios. Up to now, there is no single method, which gives a precise access of this value. Whereas elemental analysis requires a lot of sample material, X-ray photoelectron scattering would be a substitute to provide information about the elemental composition of the deposited material of choice. Nevertheless, the technique is hardly applicable towards the investigation of a monolayer or few-layer compound as influences of the substrate or adsorbing contaminants distort the results. During this work, a first try to study graphene modified electrodes by XPS

was made. Yet, it became clear that a great deal of work lies ahead to establish a method to retrieve reliable values. The largest difficulty is the exclusion of sources of errors derived by oxygen from the substrate or by impurities during the transfer or by the storage of the material. In many other methods, oxygen can only be identified indirectly. Therefore, it is recommended to develop a protocol for an instrumental analysis method which does not only resemble the C:O ratio but also the type of the chemical binding. One can imagine developing a fragmentation technique, breaking apart individual flakes into small pieces, separated and identified by chromatography and mass spectrometry.

From the correlations obtained so far, the prediction, that defective materials, are highly suitable for electrochemical sensing is demonstrated by the amperometric reduction ability of H_2O_2. To select materials more proactive towards customized application requirements, general metrics based on the association of the cost-effective techniques like Raman spectroscopy, cyclic voltammetry and electrochemical impedance spectroscopy, are recommended. The obtained knowledge regarding the structure - physicochemistry *via* statistical Raman spectroscopy, it is of advantage to monitor synthesis and exfoliation proceedings at early stages, especially beneficial when preparation protocols were modified, *e.g.* to introduce structural features.

One of the next approaches, which should be tackled by a proper choice of 2D carbon materials, is the design of *nanozymes*, which describe nanomaterials that exhibit enzyme-mimicking characteristics. Nanozymes are believed to find its way into sensor applications, potentially enhancing the sensitivity and selectivity towards an analyte of choice [33]. The design of heterostructures moved from enzymes towards metallic nanoparticles, *i.e.* based on iron, vanadium, noble metals, or carbon-based catalysts as they are less prone to an activity loss, are long time stable, mass-producible and can be handled under harsh conditions [34] Graphene could deal as promising material for the deposition of artificial functionalities. It exhibits intrinsic electrocatalytic activities and the defects serve as nucleating sites triggering particle deposition and growth [22,35,36]. Additionally, the widely distributed sp^2 hybridized system allows the non-covalent interaction of graphene with other carbon allotropes, like fullerenes, carbon nanotubes as well as carbon species, like porphyrins, retaining the intrinsic properties of graphene

as sensor material [38]. Natural enzymes are replaced effectively regarding catalytic reactions, but there is still room for improvement. It is not surprising, that the strategy of "trial-and-error" in terms of nanozyme-design is pursued. The structure-activity relation of nanozymes as well as distinct catalytic reaction has to be evaluated experimentally as well as computational. With this knowledge, correlations between size and shape of the materials with regard to catalytic activity could be established [37].

Popular became the "trial-and-error"-attempt regarding the design of sensor materials. The choice of graphene materials seems often rather random, as it is common sense, that, unlike in the electronics' sector, no high-quality materials are demanding for sensor applications. Therefore, carbon-based nanomaterials were not examined thoroughly in terms of physicochemical properties affecting the sensing performance [38]. All materials within the pool of graphene compounds have found its way to the implementation as recognition element in both, optical and electrochemical sensors. Complementary to that, as revealed in this study, it is necessary, to characterize each material before implementation as the highly diverse chemical structure of materials have an impact on the physical properties. The understanding of the correlation between the amount and nature of defects of the nanomaterial with the resulting physical behavior shall be adapted towards directed material design by defect engineering.

When graphene is understood as a class of materials with various content of oxygen, instead of a perfect two-dimensional, all sp^2 hybridized carbon crystal, its physicochemical properties could span a wide range comparable to the class of polymers. This can already be seen in the field of chemical and biosensors where those materials are not only applicable in electrochemical sensing but also in optical sensors, as well as a combination of both approaches like electrochemiluminescence (ECL). Indium tin oxide is often used as transparent electrode material, yet it is more brittle and tend to surface degradation upon application of a high voltage. Flexible, robust and transparent graphene materials might be attractive as substitute [39]. In conventional ECL sensors, the detection principle base on the application of a voltage exciting an electroactive species, which emit light upon relaxation determined by a detector such as *e.g.* a photomultiplier tube. The choice of material is not trivial as ECL is a multiplex sensing

tool. Without a doubt, LIG wins the game of electrode fabrication compared to the other materials, as defined electrode patterns of a carbon structure are printed onto a flexible substrate. Furthermore, it exhibits a large, porous structure, which is easily functionalized (non-)covalently potentially enhancing the sensitivity and selectivity regarding assay applications. A structural alternative would be rGO, which forms a dense, rough surface. The intrinsic electrocatalytic activity of graphene is potentially capable to decrease the excitation potential for luminophores like tris(bipyridine)ruthenium(II) chloride (Ru(bpy)$_2$Cl$_2$) (+1.5 V on gold electrodes using Ag/AgCl as reference electrode) [40]. Investigations on the electrocatalytic activity of the material should be conducted and compared to the examined defective graphene materials, *e.g.* meG and rGO. As ECL sensors coupled to an optical detector rely on the intensity of the emitted luminescence it is mandatory not to minimize the luminescence intensity by sensor layers, which exhibit high fluorescence quenching behavior. To return to the principal point of the paramount importance of characterization, no comparative study is found on the various derived graphene compounds regarding their fluorescence quenching behavior, except for GO and rGO [41]. The material with the lowest quenching behavior would be highly suitable for implementation as ECL sensor layer. An interesting alternative approach would be the replacement of the optical detector by a bipotentiostat, simplifying the sensor set-up. Two electrodes are patterned in an interdigitated layout, *e.g.* by laser-induced carbonization. One working electrode applies the voltage for ECL excitation, whereas the resistance change of the second working electrode upon light irradiation is recorded. Direct band-gap engineering (narrower than 1.91 eV for Ru(bpy)$_2^{2+}$ or 2.92 eV for luminol emission, respectively) of the material enables electrons to be excited from the valence band to the conduction band resulting in an electrical current or in a change of the resistance of the semiconducting material. A decrease of the emitted light intensity becomes obsolete regarding quenching effects, as this read-out base on the material's uptake of the photon energy emitted by the luminophore.

Common motivation for graphene used in sensor applications is the adsorption capability of potential analytes due to π-stacking, the reduction of the thickness of the receptor layer by replacing the surface assembled monolayer of thiol-linkers on gold substrates as well as protection from corrosion [42,43]. When applied in the field of

optical analysis, graphene, again, is mostly used by trial and error. But it offers much more than that: It was mentioned beforehand, that the physicochemistry of graphene materials is tuned by direct introduction of defects within the material. Also, the creation of heterostructures based on graphene with a metallic substrate can lead to tailored physical properties, due to the synergy of both materials. This is observed in surface-sensitive optical analytical techniques, like surface plasmon resonance (SPR) and surface-enhanced Raman spectroscopy (SERS). Intentionally, both techniques rely on the excitation of coherent oscillations of electrons in the conduction band of a thin metal film in the presence of an electromagnetic field. Those charge density oscillations are referred to as surface plasmon polaritons (SPP). The design of SPP band-gap structures allows the control of optical properties by modulation of the physical properties of the material. The deposition of a graphene layer onto a metallic surface induces a charge transfer, shifting the Fermi level of graphene, tuning its band gap. Designing nanostructures within the metallic support lead to localized surface plasmons (*hot electrons*), which are confined to the nanostructure resulting in an immense enhancement of the electromagnetic field. This allows the establishment of low-light intense active photonic devices [44]. The tunability of the fluorescence quenching behavior of graphene materials, due to band gap modulation by creation of heterostructures or surface modifications would be of interest. Either to reduce background fluorescence specifically or establish read-out techniques based on photon-energy consumption of a potential analyte resulting in turn-off fluorescence sensors. Surface-enhanced Raman spectroscopy, a powerful sensing technique to identify smallest concentrations of molecules would benefit of the fluorescence quenching effect of graphene, as background fluorescence potentially overlaps low-yield Raman signals [45]. Biotechnology forsakes the uptake of nanoparticles, *e.g.* used for theranostics or drug delivery within the cell, which attracted a lot of attention. It is of interest, how the uptake mechanisms work, where the nanomaterials are accumulated within the cell or how they are excreted. A versatile tool to track the cellular uptake of lanthanide-based upconversion nanoparticles (UCNPs) is SERS. Simple Raman spectroscopy is hardly applied to determine single UCNPs in a cell, due to the concentration dependent signal response. By combination of graphene with a metallic substrate, enhanced surface

plasmon effects can be generated improving the Raman scattering effect. Even more, tuning the band gap of the graphene compound towards the energy of the incident excitation laser, the Raman scattering effect would be ultimately enhanced, capable of single particle detection. Interferences would not be expected, as the graphene derived Raman peaks (> 1350 cm^{-1}) do not overlap with those of UCNPs (250 - 375 cm^{-1}) [46]. These were just a few possible concepts to implement carbon nanostructures in sensor systems taking advantage of their outstanding properties. With better understanding of the correlation between chemical structure and relating physical properties, a new class of purposely tailored two-dimensional materials can be established, versatile for sensing applications.

The massive effort on graphene has revealed that it has the potential to launch the achievement of advanced technology. In principle, graphene would be all set to be elevated from the laboratory to the industry, yet a very basic but fundamental building block limits the graphene application. The attempts to characterize the material thoroughly in these large dimensions, providing a correlation towards the structural and resulting physical features are still at its infants.

Graphene materials are not supplied with an intense structural analysis, albeit it is essential to reveal the flake size, the number of staked layers and the oxygen content, even more the elemental composition of the carbon-based nanomaterial, as these are the key factors influencing the physical and chemical characteristics. Generally, the two-dimensional carbon material seems to be, to put it in an exaggerated description, omnipotent as depicted in Figure 4.3, which reveals potential graphene applications for commercialization based on the structural variations of the carbon nanomaterial [47].
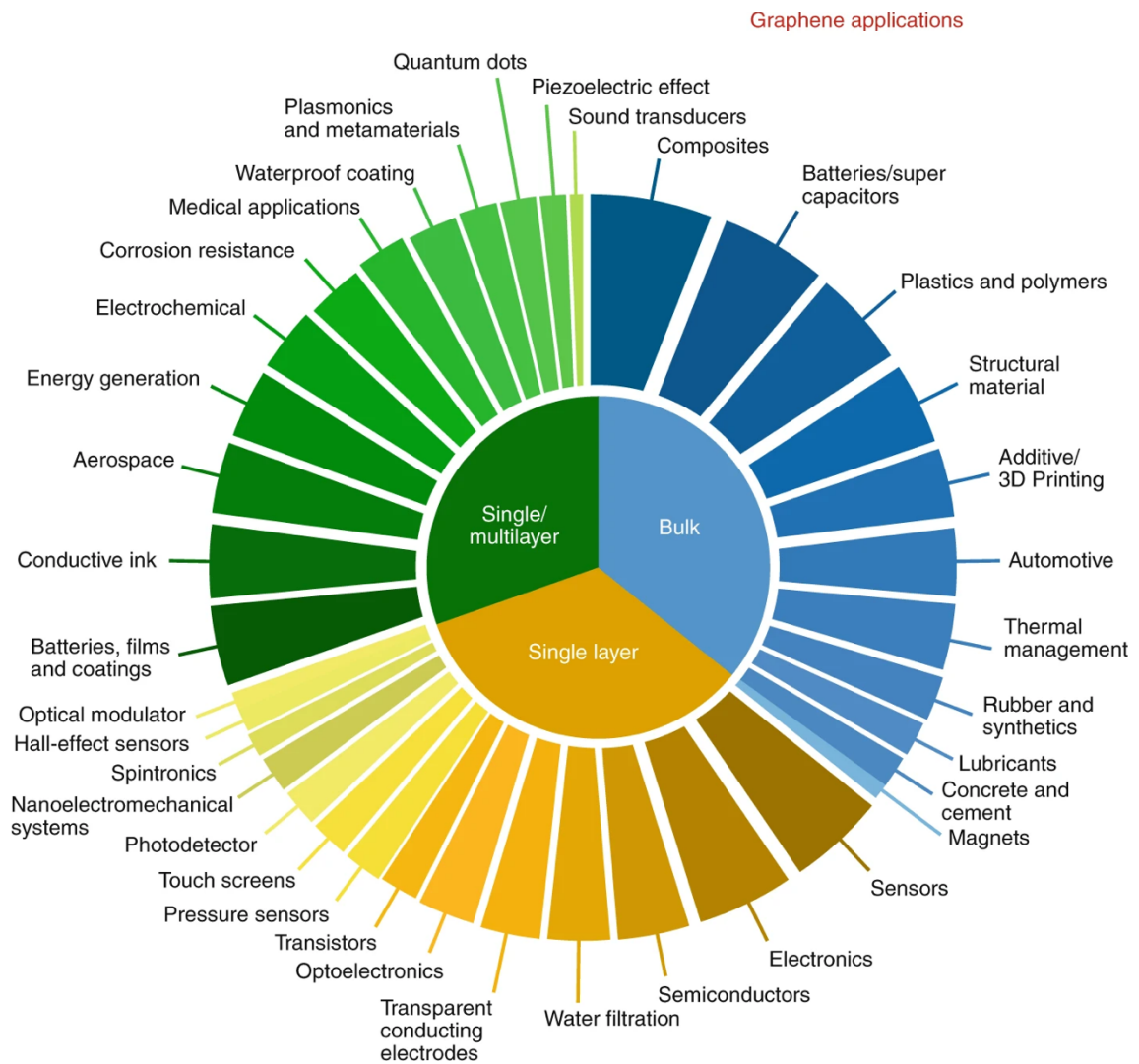
Figure 4.3: The relative quantity of bulk, single- or multilayer graphene in various applications. Reprinted with permission from [47], Copyright (2019), Springer Nature.

It is still surprising that there are not more than a few niche products on the market [48]. In principle, the graphene material of choice could be selected within a pool of offered nanomaterials upon the special requirements towards an intended device implementation. With 142 graphene manufacturers distributed over 27 countries, the graphene supply lacks a clear communication between customer and vendors until now. By achieving the precise examination of graphene compounds, which can be fully correlated to the resulting physical properties of graphene including the potential to directly modify the material by explicit introduction of defects, not as a bug, but as a feature, the rise of graphene will have ended, as it would have reached its goal.

4.1   References

[1]   Kroto HW, Heath JR, O'Brien SC, Curl RF, Smalley RE (1985) C60: Buckminsterfullerene. Nature 318:162–163.

[2]   Iijima S (1991) Helical microtubules of graphitic carbon. Nature 354:56–58.

[3]   Geim AK, Novoselov KS (2007) The rise of graphene. Nature Mat. 6:183–191.

[4]   Lin L, Peng H, Liu Z (2019) Synthesis challenges for graphene industry. Nature Mat. 18:520–524.

[5]   Reiss T, Hjelt K, Ferrari AC (2019) Graphene is on track to deliver on its promises. Nature Nanotechnol. 14:907–910.

[6]   Chen Y, Gong X-L, Gai J-G (2016) Progress and challenges in transfer of large-area graphene films. Adv. Sci. 3:1500343.

[7]   Coleman JN (2013) Liquid exfoliation of defect-free graphene. Acc. Chem. Res. 46:14–22.

[8]   Pei S, Cheng H-M (2012) The reduction of graphene oxide. Carbon 50:3210–3228.

[9]   Ambrosi A, Pumera M (2016) Electrochemically exfoliated graphene and graphene oxide for energy storage and electrochemistry applications. Chemistry 22:153–159.

[10] Backes C, Higgins TM, Kelly A, Boland C, Harvey A, Hanlon D, Coleman JN (2017) Guidelines for exfoliation, characterization and processing of layered materials produced by liquid exfoliation. Chem. Mater. 29:243–255.

[11] Konkena B, Vasudevan S (2012) Understanding aqueous dispersibility of graphene oxide and reduced graphene oxide through pKa measurements. J. Phys. Chem. Lett. 3:867–872.

[12] Amiri A, Naraghi M, Ahmadi G, Soleymaniha M, Shanbedi M (2018) A review on liquid-phase exfoliation for scalable production of pure graphene, wrinkled, crumpled and functionalized graphene and challenges. FlatChem 8:40–71.

[13] Fitzer E, Kochling K-H, Boehm HP, Marsh H (1995) Recommended terminology for the description of carbon as a solid (IUPAC Recommendations 1995). Pure Appl. Chem. 67:473–506.

[14] Eftekhari A, Garcia H (2017) The necessity of structural irregularities for the chemical applications of graphene. Mater. Today Chem. 4:1–16.

[15] Zhou M, Zhai Y, Dong S (2009) Electrochemical sensing and biosensing platform based on chemically reduced graphene oxide. Anal. Chem. 81:5603–5613.

[16] Mani V, Periasamy AP, Chen S-M (2012) Highly selective amperometric nitrite sensor based on chemically reduced graphene oxide modified electrode. Electrochem. Commun. 17:75–78.

[17] Hersey M, Berger SN, Holmes J, West A, Hashemi P (2019) Recent developments in carbon sensors for at-source electroanalysis. Anal. Chem. 91:27–43.

[18] Fenzl C, Nayak P, Hirsch T, Wolfbeis OS, Alshareef HN, Baeumner AJ (2017) Laser-scribed graphene electrodes for aptamer-based biosensing. ACS Sens. 2:616–620.

[19] Torrisi F, Hasan T, Wu W, Sun Z, Lombardo A, Kulmala TS, Hsieh G-W, Jung S, Bonaccorso F, Paul PJ, Chu D, Ferrari AC (2012) Inkjet-printed graphene electronics. ACS Nano 6:2992–3006.

[20] Belyaeva LA, Fu W, Arjmandi-Tash H, Schneider GF (2016) Molecular caging of graphene with cyclohexane: transfer and electrical transport. ACS Cent. Sci. 2:904–909.

[21] Hu L, Gruner G, Jenkins J, Kim C-J (2009) Flash dry deposition of nanoscale material thin films. J. Mater. Chem. 19:5845.

[22] Zöpfl A, Lemberger M-M, König M, Ruhl G, Matysik F-M, Hirsch T (2014) Reduced graphene oxide and graphene composite materials for improved gas sensing at low temperature. Faraday Discuss. 173:403–414.

[23] Wongkaew N, Simsek M, Arumugam P, Behrent A, Berchmans S, Baeumner AJ (2019) A robust strategy enabling addressable porous 3D carbon-based functional nanomaterials in miniaturized systems. Nanoscale 11:3674–3680.

[24] Wongkaew N, Simsek M, Griesche C, Baeumner AJ (2019) Functional nanomaterials and nanostructures enhancing electrochemical biosensors and lab-on-a-chip performances: recent progress, applications, and future perspective. Chem. Rev. 119:120–194.

[25] Qiao Y, Li X, Hirtz T, Deng G, Wei Y, Li M, Ji S, Wu Q, Jian J, Wu F, Shen Y, Tian H, Yang Y, Ren T-L (2019) Graphene-based wearable sensors. Nanoscale 11:18923–18945.

[26] Backes C, Paton KR, Hanlon D, Yuan S, Katsnelson MI, Houston J, Smith RJ, McCloskey D, Donegan JF, Coleman JN (2016) Spectroscopic metrics allow in situ measurement of mean size and thickness of liquid-exfoliated few-layer graphene nanosheets. Nanoscale 8:4311–4323.

[27] Paton KR, Varrla E, Backes C, Smith RJ, Khan U, O'Neill A, Boland C, Lotya M, Istrate OM, King P, Higgins T, Barwich S, May P, Puczkarski P, Ahmed I, Moebius M, Pettersson H, Long E, Coelho J, O'Brien SE, McGuire EK, Sanchez BM, Duesberg GS, McEvoy N, Pennycook TJ, Downing C, Crossley A, Nicolosi V, Coleman JN (2014) Scalable production of large quantities of defect-free few-layer graphene by shear exfoliation in liquids. Nature Mat. 13:624–630.

[28] Yadav N, Lochab B (2019) A comparative study of graphene oxide: Hummers, intermediate and improved method. FlatChem 13:40–49.

[29] Varrla E, Paton KR, Backes C, Harvey A, Smith RJ, McCauley J, Coleman JN (2014) Turbulence-assisted shear exfoliation of graphene using household detergent and a kitchen blender. Nanoscale 6:11810–11819.

[30] Lin L, Deng B, Sun J, Peng H, Liu Z (2018) Bridging the gap between reality and ideal in chemical vapor deposition growth of graphene. Chem. Rev. 118:9281–9343.

[31] Huang PY, Ruiz-Vargas CS, van der Zande AM, Whitney WS, Levendorf MP, Kevek JW, Garg S, Alden JS, Hustedt CJ, Zhu Y, Park J, McEuen PL, Muller DA (2011) Grains and grain boundaries in single-layer graphene atomic patchwork quilts. Nature 469:389–392.

[32] Zhang Y, Hao H, Wang L (2016) Effect of morphology and defect density on electron transfer of electrochemically reduced graphene oxide. Appl. Surf. Sci. 390:385–392.

[33] Liang M, Yan X (2019) Nanozymes: from new concepts, mechanisms, and standards to applications. Acc. Chem Res. 52:2190–2200.

[34] Huang Y, Ren J, Qu X (2019) Nanozymes: classification, catalytic mechanisms, activity regulation, and applications. Chem. Rev. 119:4357–4412.

[35] Sundaram RS, Gómez-Navarro C, Balasubramanian K, Burghard M, Kern K (2008) Electrochemical modification of graphene. Adv. Mater. 20:3050–3053.

[36] Georgakilas V, Tiwari JN, Kemp KC, Perman JA, Bourlinos AB, Kim KS, Zboril R (2016) Noncovalent functionalization of graphene and graphene oxide for energy materials, biosensing, catalytic, and biomedical applications. Chem. Rev. 116:5464–5519.

[37] Wu J, Wang X, Wang Q, Lou Z, Li S, Zhu Y, Qin L, Wei H (2019) Nanomaterials with enzyme-like characteristics (nanozymes): next-generation artificial enzymes (II). Chem. Soc. Rev. 48:1004–1076.

[38] Ferrari AC, Bonaccorso F, Fal'ko V, Novoselov KS, Roche S, Bøggild P, Borini S, Koppens FHL, Palermo V, Pugno N, Garrido JA, Sordan R, Bianco A, Ballerini L, Prato M, Lidorikis E, Kivioja J, Marinelli C, Ryhänen T, Morpurgo A, Coleman JN, Nicolosi V, Colombo L, Fert A, Garcia-Hernandez M, Bachtold A, Schneider GF, Guinea F, Dekker C, Barbone M, Sun Z, Galiotis C, Grigorenko AN, Konstantatos G, Kis A, Katsnelson M, Vandersypen L, Loiseau A, Morandi V, Neumaier D, Treossi E, Pellegrini V, Polini M, Tredicucci A, Williams GM, Hong BH, Ahn J-H, Kim JM, Zirath H, van Wees BJ, van der Zant H, Occhipinti L, Di Matteo A, Kinloch IA, Seyller T, Quesnel E, Feng X, Teo K, Rupesinghe N, Hakonen P, Neil SRT, Tannock Q, Löfwander T, Kinaret J (2015) Science and technology roadmap for graphene, related two-dimensional crystals, and hybrid systems. Nanoscale 7:4598–4810.

[39] Chang H, Wu H (2013) Graphene-based nanomaterials: synthesis, properties, and optical and optoelectronic applications. Adv. Funct. Mater. 23:1984–1997.

[40] Mayer M, Takegami S, Neumeier M, Rink S, Jacobi von Wangelin A, Schulte S, Vollmer M, Griesbeck AG, Duerkop A, Baeumner AJ (2018) Electrochemiluminescence bioassays with a water-soluble luminol derivative can outperform fluorescence assays. Angew. Chem. Int. Ed. 57:408–411.

[41] Kim J, Cote LJ, Kim F, Huang J (2010) Visualizing graphene based sheets by fluorescence quenching microscopy. J. Am. Chem. Soc. 132:260–267.

[42] Choi SH, Kim YL, Byun KM (2011) Graphene-on-silver substrates for sensitive surface plasmon resonance imaging biosensors. Opt. Express 19:458–466.

[43] Zeng S, Baillargeat D, Ho H-P, Yong K-T (2014) Nanomaterials enhanced surface plasmon resonance for biological and chemical sensing applications. Chem. Soc. Rev. 43:3426–3452.

[44] Zayats AV, Smolyaninov II (2003) Near-field photonics: surface plasmon polaritons and localized surface plasmons. Appl. Phys. Lett. 5:S16-S50.

[45] Lai H, Xu F, Zhang Y, Wang L (2018) Recent progress on graphene-based substrates for surface-enhanced Raman scattering applications. J. Mater. Chem. B 6:4008–4028.

[46] Wiesholler LM, Genslein C, Schroter A, Hirsch T (2018) Plasmonic enhancement of NIR to UV upconversion by a nanoengineered interface consisting of NaYF4:Yb,Tm nanoparticles and a gold nanotriangle array for optical detection of vitamin B12 in serum. Anal Chem. 90:14247–14254.

[47] Barkan T (2019) Graphene: the hype versus commercial reality. Nature Nanotechnol. 14:904–906.

[48] Kong W, Kum H, Bae S-H, Shim J, Kim H, Kong L, Meng Y, Wang K, Kim C, Kim J (2019) Path towards graphene commercialization from lab to market. Nature Nanotechnol. 14:927–938.

Summary

This thesis addresses the potential of various graphene materials to be implemented as an electrochemical sensor depending on its surface characteristics.

Chapter 1 reviews the most common synthesis protocols to derive graphene materials, either by growth or delamination of graphite. The following section describes state-of-the-art functionalization routines to modify the surface either non-covalently by physical adsorption or π-stacking or by the covalent introduction of functional groups. The variety of graphene allotropes is evaluated upon its applicability as recognition layer in electrochemical sensors. It is observed, that the structure of graphene highly influences the sensor's performance. Interestingly, among the pool of graphene materials, solely two representatives are frequently used as recognition layer. These are, low-defective cvdG and defective rGO. Little is reported on the exact contribution of the structural features and the layer morphology of the applied materials with regard to its sensing behavior.

Chapter 3 describes the impact of the chemical structure and surface morphology of processed graphene layers on their electrochemical performance. Various graphene allotropes derived either chemically, electrochemically or mechanically are exfoliated in liquid. The dispersed graphene flakes were examined beforehand by dynamic light scattering and Zeta potential, revealing a diversity in flake size and surface charge. Layer processing is complex as each graphene allotrope required an alternative transfer procedure to establish coherent graphene films. The surface morphology was investigated by SEM and AFM revealing rough layers for small flake compounds as reduced graphene oxide and mechanically exfoliated graphene, whereas the electrochemically exfoliated and vapor grown graphene distributed smooth surfaces. The defect distribution of each graphene compound was examined by Raman spectroscopy observing an increase in the material quality in the order rGO < ecG < meG < cvdG. Electrochemical investigations conducted by cyclic voltammetry and electrochemical impedance spectroscopy revealed defective, rough graphene compounds to exhibit a high electron transfer rate and a low charge transfer resistance in presence of a redox

marker. The charge transfer resistance of rGO is 20 times decreased compared to low-defective cvdG. Reduced graphene outperformed the other materials in terms of electrocatalytic reduction of hydrogen peroxide. It is shown that the interplay of structural characteristics and surface morphology of the processed recognition layers highly affects the electrochemical performance in aqueous medium. Still, a full characterization of the processed material is challenging, due to the small dimensions.

Chapter 4 describes the challenges on graphene synthesis, processing and the lack of characterization. The main results of the synthesis, transfer techniques, optical and electrochemical investigations are summarized. The synthesis of graphene, its processing and the analysis need to be further investigated. An improvement of standardized characterization techniques might potentially enable a correlation between the structural features and the physical properties, which results in tailoring of the material towards the required needs. Future perspectives are envisioned integrating graphene in optical and electrochemical sensor systems.

Zusammenfassung

Die vorliegende Arbeit beschäftigt sich mit dem Einfluss verschiedener Graphenmaterialien hinsichtlich deren Grenzflächeneigenschaften zur Verwendung in elektrochemischen Sensoren.

Kapitel 1 stellt einen Übersichtsartikel dar, der die gängigsten Synthesemethoden von Graphen zusammenfasst. Diese basieren entweder auf einem Bottom-up- oder Top-down-Ansatz. Anschließend werden Funktionalisierungsmethoden vorgestellt, welche das Graphen entweder nicht-kovalent, über Physisorption, sowie π-Wechselwirkung, oder kovalent durch Bindung funktioneller Gruppen modifizieren. Die unterschiedlich hergestellten Graphenmaterialien und deren Anwendbarkeit als elektrochemisches Sensormaterial wird kritisch zusammengefasst. Diese Literaturstudie legt nahe, dass die Art des verwendeten Graphens einen großen Einfluss auf das Sensorverhalten hat. Es überrascht, dass trotz der vielen unterschiedlichen Graphenmaterialien im Wesentlichen nur zwei Vertreter als Sensormaterial benutzt wurden: Diese sind entweder das defektarme cvdG oder das defektreiche rGO. Jedoch bleibt unklar, wie genau sich die strukturellen Eigenschaften und Beschaffenheit der Elektrodengrenzfläche auf das Sensorverhalten auswirken.

Kapitel 3 beschreibt die Ergebnisse einer Studie, die den Einfluss der chemischen Struktur und Oberflächenmorphologie prozessierter Graphenfilme auf ihre elektrochemischen Eigenschaften untersucht. Unterschiedliche Graphenmaterialien wurden hierzu chemisch, elektrochemisch oder mechanisch hergestellt und in flüssigem Medium dispergiert. Dynamische Lichtstreuung und elektrophoretische Mobilitätsstudien der Graphendispersionen ergaben, dass sich die Materialien hinsichtlich Flockengröße sowie Oberflächenladungen unterscheiden. Die Prozessierbarkeit eines einheitlichen Graphenfilms erwies sich als schwierig und erforderte die Entwicklung individueller Transfermethoden. Für Materialien mit kleiner Flockengröße, wie rGO und meG erhält man relativ raue Oberflächen. Auf der anderen Seite war es möglich, für cvdG und ecG glatte Graphenoberflächen abzuscheiden. Untersuchungen der Filme durch Ramanspektroskopie zeigt eine steigende Defektverteilung für rGO<ecG<meG<cvdG.

Cyclovoltammetrie und elektrochemische Impedanzspektroskopie in Gegenwart eines Redoxmarkers bestätigte, dass raue, defektreiche Graphenoberflächen eine erhöhte Elektronentransferrate sowie einen verminderten Ladungstransferwiderstand aufweisen. Der Ladungswiderstand von rGO ist um den Faktor 20 geringer als von defektreichem cvdG. Desweiteren übertraf rGO die übrigen Materialien hinsichtlich der elektrokatalytischen Reduktion von Wasserstoffperoxid. Das Zusammenspiel von strukturellen Eigenschaften und der Oberflächenbeschaffenheit der Graphenfilme hat einen großen Einfluss auf die Elektrochemie in wässrigem Medium. Zur vollständigen Charakterisierung, insbesondere der exakten lokalen chemischen Zusammensetzung des Materials, fehlt aktuell eine geeignete Methode, die die entsprechende Auflösung erreicht.

Kapitel 4 beschreibt die Schwierigkeiten der Graphenherstellung und Prozessierbarkeit sowie fehlende Standardcharakterisierungmethoden. Es werden die Resultate der Graphensynthese, Transfertechniken sowie optischen und elektrochemischen Untersuchungen zusammengefasst. Die Synthese von Graphen, die Prozessierbarkeit und vollständige Analyse gilt es weiter voranzutreiben. Entsprechende Vorschläge wurden aufgezeigt. Das Erstellen einer Standardcharakterisierungsmethode oder –abfolge könnte das Bindeglied zwischen den Erkenntnissen struktureller Beschaffenheit und daraus resultierender physikalischer Eigenschaften sein. Dies würde es erlauben, Graphenmaterialien maßgeschneidert hinsichtlich einer potentiellen Anwendung herzustellen. Weitere Konzepte werden in Aussicht gestellt, in welchen Graphen seinen Beitrag in optischen sowie elektrochemischen Sensoren zu leisten vermag.

Curriculum Vitae

Persönliche Daten

Name	Eva-Maria Kirchner
Adresse	Mälzereiweg 21, 93053 Regensburg
Geburtsdatum	19.05.1991
Geburtsort	Regensburg
Familienstand	ledig
Staatsangehörigkeit	deutsch

Hochschulausbildung

Feb 2016 – Jul 2020	**Promotionsstudium Chemie** an der Universität Regensburg Thema: *„Electroanalysis and Raman Spectroscopy of Graphene-Modified Electrodes Influenced by the Synthesis and Transfer of the Two-Dimensional Nanomaterial "*, Institut für Analytische Chemie, Chemo- und Biosensorik (Dr. Thomas Hirsch, Prof. Antje J. Bäumner)
Okt 2013 – Dez 2015	**Masterstudium Chemie** an der Universität Regensburg Hauptfach: Analytische Chemie, 1. Nebenfach: Organische Chemie, 2. Nebenfach: Medizinische Chemie Abschlussthema: *„Studies of Graphene for Electrochemical Sensor Applications"*, Institut für Analytische Chemie, Chemo- und Biosensorik (Dr. Thomas Hirsch, Prof. Antje J. Bäumner)

Okt 2010 – Juli 2013   **Bachelorstudium Chemie** an der Universität Regensburg
                              Abschlussthema**:** *„Synthesis of coumarin-based Chalcones"*,

                              Institut für Organische Chemie (Dr. Sabine Amslinger)

Sep 2001 – Jun. 2010   **Allgemeine Hochschulreife** am Gymnasium Parsberg

Weiterbildungen

Juni 2019	Projektmanagement (Fr. Dr. Ingrid Zeitlhöfler, Regensburg)
Februar/März 2019	Bewerbungstraining kompakt (Falkenberg Seminare, Regensburg)
Februar 2019	Ich, die Führungskraft (Carpe verba!)
August 2018 (Dublin)	Liquid Phase Exfoliation 10th Anniversary Workshop
Juli 2018	BWL für Ingenieure (Strategische Partnerschaft Sensorik Regensburg)
April 2017	HPLC Seminar (Agilent, Regensburg)
Juli 2015	Qualitätsmanagement in der Analytischen Chemie (Universität Regensburg, Regensburg)

Auszeichnungen

2020	Mitglied im Komitee des GDCh Doktorandenseminar (Potsdam)
2018	Reisestipendium der GDCh (Dresden)
2017	Reisestipendium Graphene 2017 (Barcelona)

Wissenschaftliche Vorträge

2019 – **Euroanalysis 2019**, Istanbul, Türkei

Electrochemical sensors based on 2D carbon materials: impact of the fabrication

method on the performance

2019 – **Doktorandenkolloquium ChemPharm**, Regensburg, Deutschland

Impact of the Fabrication Method of Graphene on the Electrochemical Performance in

Sensing Applications

2018 – **Graphene 2018**, Dresden, Deutschland

Impact of the Fabrication Method of Graphene on the Electrochemical Performance in Sensing Applications

2017 – **Internal Workshop GRK 1570**, Rattenberg, Deutschland

Graphene as Electrode Material for Electrochemical Sensing

2017 – **11. Interdisziplinäres Doktorandenseminar**, Berlin, Deutschland

Mechanical Exfoliated Graphene for Non-Enzymatic Detection of Glucose

Poster Präsentationen

2017 – **Graphene 2017**, Barcelona, Spanien

Mechanical Exfoliated Graphene for Non-enzymatic Detection of Glucose

2016 – **Graphene 2016**, Genua, Italien

Studies of Graphene as Electrode Material for Sensor Applications

Publikationen

Kirchner EM, Hirsch T, (2020) Control of the Graphene Electrode by the Synthesis and Transfer of the 2D Carbon Material, Adv. Mater. Interfaces, *submitted*.

Kirchner EM, Hirsch T, (2020) Recent Developments in Carbon-Based Two-Dimensional Materials: Synthesis and Modification Aspects for Electrochemical Sensors, Microchim. Acta, 187, 441, doi: 10.1007/s00604-020-04415-3.

Genslein C, Hausler P, **Kirchner EM**, Bierl R, Baeumner AJ, Hirsch T, (2017) Detection of small molecules with surface plasmon resonance by synergistic plasmonic effects of nanostructured surfaces and graphene, SPIE BiOS. International Society for Optics and Photonics, 100800F-100800F-7, doi: 10.1117/12.2252256.

C. Genslein C, P. Hausler P, **E.-M. Kirchner EM**, R. Bierl R, A. J. Baeumner AJ, T. Hirsch T, (2016) Graphene-enhanced plasmonic nanohole arrays for environmental sensing in aqueous samples, Beilstein J. Nanotechnol., 7: 1564-1573, doi:10.3762/bjnano.7.150.

Eidesstattliche Erklärung

Ich erkläre hiermit an Eides statt, dass ich die vorliegende Arbeit ohne unzulässige Hilfe Dritter und ohne Benutzung anderer als der angegebenen Hilfsmittel angefertigt habe; die aus anderen Quellen direkt oder indirekt übernommenen Daten und Konzepte sind unter Angabe des Literaturzitats gekennzeichnet.

Weitere Personen waren an der inhaltlich-materiellen Herstellung der vorliegenden Arbeit nicht beteiligt. Insbesondere habe ich hierfür nicht die entgeltliche Hilfe eines Promotionsberaters oder anderer Personen in Anspruch genommen. Niemand hat von mir weder unmittelbar noch mittelbar geldwerte Leistungen für Arbeiten erhalten, die im Zusammenhang mit dem Inhalt der vorgelegten Dissertation stehen.

Die Arbeit wurde bisher weder im In- noch im Ausland in gleicher oder ähnlicher Form einer anderen Prüfungsbehörde vorgelegt.

Ort, Datum   Unterschrift